APPLICATION SPECIFIC NANOANTENNAS AND NANOPHOTONIC DEVICES

Thesis submitted by

RITIKA RANGA

In Partial Fulfilment of the Requirements for the Degree of

DOCTOR OF PHILOSOPHY

Under the Supervision of

Dr. YOGITA KALRA

&

Dr. KAMAL KISHOR

Department of Applied Physics, Delhi Technological University

Delhi, India

December-2023

Dedicated to my parents who are always there to support and motivate me.

DELHI TECHNOLOGICAL UNIVERSITY
(Govt. of National Capital Territory of Delhi)
Shahbad Daulatpur, Main Bawana Road,
Delhi 110042, India

CERTIFICATE

This is to certify that the Ph.D. thesis entitled "**Application specific nanoantennas and nanophotonic devices**" submitted to the Delhi Technological University, Delhi for the award of the Doctor of Philosophy is based on the original research work carried out by me under the supervision of Dr. Yogita Kalra and Dr. Kamal Kishor, Department of Applied Physics, Delhi Technological University, Delhi, India. It is further certified that the work embodied in this thesis has, neither partially nor fully submitted to any other university or institution for the award of any degree or diploma.

Ritika Ranga
Candidate
(2K17/PhD/AP/05)

This is to certify that the above statement made by the candidate is correct to the best of our knowledge.

Dr. Yogita Kalra
(Supervisor)
Assistant Professor
Department of Applied Physics
Delhi Technological University

Dr. Kamal Kishor
(Supervisor)
Assistant Professor
Department of Applied Physics
Delhi Technological University

Prof. A.S. Rao
(Head of the Department)
Department of Applied Physics
Delhi Technological University

ACKNOWLEDGEMENTS

This thesis have been accomplished with the help of many people for whom, I am very pleased to pay my gratitude.

First of all, I express my utmost gratitude to my supervisors Dr. Yogita Kalra and Dr. Kamal Kishor for their proficient supervision and provided me peaceful and research oriented environment. I am grateful to them for their intellectual advice, prolific discussions, various suggestions, logical criticism and continuous support and motivation given to me during the period of my research. All these valuable things will definitely help me for further continuing my research.

I express respect towards the Honorable Vice-Chancellor, Delhi Technological University and Head of the Department, Applied Physics, Delhi Technological University for providing me worthy infrastructure for carrying my research work. I am further thankful to the SRC and DRC members for their valuable suggestions.

My sincere thanks to my seniors Dr. Nishant Shankhwar, Dr. Reena Dalal, whose suggestions and discussions helped me carrying out my research work. I am thankful for my labmates Mr Ankush Dewan, Mr. Ankit, Ms Varanam Sherawat, Ms Vishakha Sharma, Mr Lokesh Ahlawat, who created positive, calm, helpful and assiduous environment in the laboratory. I am also thankful for all my friends Ms. Jenia Dhankhar, Dr. Pooja Rohilla, Ms. Suman Dahiya, Dr. Ritika Khatri, Dr. Mukesh Kumar Sahu, and Dr. Prateek Sharma who always motivates me.

Further, I am grateful to my respected and loving parents, for their love, support and encouragement. My caring and loving brother, who is always ready to help me. My humble thanks to my husband Mr. Akash Deep, who is a sincere, punctual and workaholic person who always inspires and motivates me. I am also thankful to my respected parents-in-law whose blessings always remain over me. My sisters-in-law and brothers-in-law are also cooperative for me. I am indebted to all my family members for their moral support.

I acknowledge the initiatives and support from the establishment of TIFAC-Centre of Relevance and Excellence in Fiber Optics and Optical Communication at Delhi Technological University (Formerly Delhi College of Engineering) Delhi, through the Mission REACH program of Technology Vision-2020 of the Government of India.

I am also thankful to the optical societies SPIE and OSA who gave me chance to enhance my network of research. They also provided me funding for attending workshops and conferences.

Date: **(Ritika Ranga)**

Place: Delhi

ABSTRACT

Recently, nanoantennas have become one of the most fascinating technologies in the field of optics and photonics. Nanoantennas have been found capable of producing strong enhanced and highly localized light fields. Existing research on them has shown their considerable applications in diverse fields such as the near-field optical microscopy, spectroscopy, chemical, bio-sensing, and optical devices. Thus the useful results prompt us to implement a more systematic and further exploration on nanoantennas of some specific configurations of interest.

Nanoantennas are known for converting electromagnetic energy into confined field. Electric field enhancement and radiation efficiency are the important parameters for measurement of harvesting efficiency of nanoantenna. In this thesis, different structures of nanoantennas have been designed to enhance and confine the electric field, when it interacts with electromagnetic radiation in the optical region. A petal shaped nanoantenna has been designed and studied for radiation efficiency and harvesting efficiency. Various geometrical parameters, such as the length, the width, the height and the gap of the nanoantenna have been varied to find their effect on the radiation efficiency and the harvesting efficiency. Additionally, the significance of the material of the nanoantenna has also been studied by choosing four different types of materials, and their corresponding radiation efficiency, harvesting efficiency and electric field enhancement have been reported. Other than this, flower shaped nanoantenna, arrow shaped nanoantenna, tapered cone shaped nanoantenna have been designed for the same application.

Further, novel designs of nanoantennas for the enhancement of magnetic field in the near infrared region have been modelled. The designed nanoantennas have been thoroughly analysed by varying various geometrical parameters to find their effect on magnetic field enhancement. Also, different materials have been considered for the nanoantenna, to investigate the significance of the choice of the material effect on magnetic field enhancement. The proposed structures can prove to be a good alternative for the enhancement of magnetic field as compared to the various paramagnetic and ferromagnetic materials, having weak magnetic properties in the optical regime.

Plasmonics is widely used for converting electromagnetic radiation into energy and confining electromagnetic radiation below the diffraction limit. However, the ultra narrowband and high electromagnetic field cannot be obtained simultaneously because of resistive loss and radiation damping in the metals. In this thesis, a metallic ultra-narrow band perfect absorber

has been proposed consisting of an array of four squares on a silver layer. The structure shows more than 99% absorption and full width at half maxima less than 2 nm at resonance wavelength. The absorption mechanism has been revealed by calculating electric and magnetic field profiles. The dependence of the structure on the geometrical parameters has been studied and the structure has thus been optimized at 692 nm i.e. in the visible range of frequency. The proposed structure is then investigated for sensing application. The structure shows high sensitivity of 680 nm/RIU in the visible range of wavelength and a high figure of merit of 348.72.

In previous years optical trapping of nanoparticles such as magnetic nanoparticles, proteins, λ-DNA, gold nanoparticles, polystyrene and silica beads catches researcher's attention. Plasmonic nanoantenna due to its ability to enhance electric field in subwavelength region are widely used for optical trapping. For ideal trapping high trapping stiffness is required along with using a low intensity power Laser, so that there will low heat generation and no damage occurred to delicate nanoparticles. In this thesis, an attempt to design a nanoantenna which can trap nanoparticle of order tens of nanometre with high trapping stiffness using low power Laser has been done so that nanoparticle can easily be trapped without getting damaged.

LIST OF PUBLICATIONS

Publications in Refereed International Journals (Thesis)

[1] **Ritika Ranga,** Yogita Kalra, and Kamal Kishor. "Petal shaped nanoantenna for solar energy harvesting." Journal of Optics 22.3, 035001 (2020).

[2] **Ritika Ranga**, Yogita Kalra, and Kamal Kishor. "Design of hourglass nanoantenna for magnetic field enhancement." Optics Communications 481, 126511 (2021).

[3] **Ritika Ranga**, Yogita Kalra, Kamal Kishor and Nishant Shankhwar. “Nanoantenna as perfect absorber and refractive index sensor” The European Physical Journal D 77.3, 42 (2023).

Publications in Refereed International Conferences and workshops (Thesis)

[1] **Ritika Ranga**, Parul Goyal, Yogita Kalra, "Field enhancement in a tapered cone dipole nanoantenna", Proceedings of IEEE International Conference on Photonics & High Speed Optical Networks (ICPHON 2018), 12-13 April 2018, S. A. Engineering College, Chennai, India.

[2] **Ritika Ranga**, Nishant Shankhwar, and Yogita Kalra. "Design and Analysis of Broadband Square Spiral Shaped Nanoantenna" Frontiers in Optics, Optical Society of America, 2018.

[3] **Ritika Ranga**, Nishant Shankhwar, Yogita Kalra, and Kamal Kishor "Design of hexameric flower shaped nanoantenna for energy harvesting" In AIP Conference Proceedings, vol. 2136, no. 1, p. 030005. AIP Publishing, 2019.

[4] **Ritika Ranga**, Yogita Kalra, and Kamal Kishor "Design of arrow-shaped nanoantenna for electric field enhancement" In Plasmonics: Design, Materials, Fabrication, Characterization, and Applications XVII, vol. 11082, p. 1108229. International Society for Optics and Photonics, 2019.

[5] **Ritika Ranga**, Nishant Shankhwar, Yogita Kalra, and Kamal Kishor "Design of nanoantenna for magnetic field enhancement" Plasmonics: Design, Materials, Fabrication, Characterization, and Applications XVIII. Vol. 11462. SPIE, 2020.

Publications in Refereed International Conferences and workshops (Outside Thesis)

[1] Nishant Shankhwar, **Ritika Ranga**, Yogita Kalra, and Ravindra Kumar Sinha. "Controlling the radiation pattern of a microstrip patch antenna using a checkerboard patterned metasurface" In AIP Conference Proceedings, vol. 2136, no. 1, p. 030003. AIP Publishing LLC, 2019.

[2] Nishant Shankhwar, **Ritika Ranga**, Yogita Kalra, and Ravindra Kumar Sinha "Dielectric ring based metamaterial perfect reflector" In Metamaterials, Metadevices, and Metasystems 2019, vol. 11080, pp. 156-159. SPIE, 2019.

CONTENTS

3. Nanoantenna as magnetic device in infrared frequency region

4. Nanoantenna as Perfect absorber and Refractive Index Sensor

5. Nanoantennas as Optical Tweezer

6. Concluding Remarks and Future Scope 107

LIST OF FIGURES

LIST OF TABLES

LIST OF ABBREVIATIONS

- PV: Photovoltaic
- NIR:Near-infrared
- PML: Perfectly Matched Layer
- EM: Electro Magnetic
- EF: Electric Field
- MF: Magnetic Field
- FEM: Finite Element Method
- RIU: Refractive Index Unit
- FWHM : Full Width At Half Maxima
- FOM : Figure of Merit
- MDM : Metal-Dielectric-Metal

CHAPTER-1

CHAPTER-1

INTRODUCTION

1.1 Introduction

Antenna is the one of the common devices used in our daily life applications. Antennas are everywhere, when it comes to transmitting or receiving signals. Talking to someone who is miles away from us or listening to a radio station from miles away while driving in car is possible because of antenna. It can be found on roofs to provide signal to television, in power towers, in cars to catch radio channels and in many more things. There are different types of antennas based on their shape, size and mode of operation, providing different types of radiation pattern, directivity, gain, and radiation efficiency. Significant advancements in their design have occurred since Marconi invented wireless telegraphy at the turn of the 19^{th} century. There has been a great demand for wireless devices that can function at different frequency bands has increased over the past few decades with the rapid development of electronics and wireless communications. Examples of wireless devices include satellite communications, Bluetooth devices, mobile telecommunications systems, and wireless local area networks. However, a number of communication devices, such as cell phones, require the antennas that can be contained in a very small dimensional footprint. These two requirements have led to extensive research for designing complex and compact antenna structures for radio frequency and microwave applications. Antennas can be as small as to fit in cell phones to as big as a football stadium for receiving signals from deep space.

An antenna is a device made up of conductive material that is used in a wireless communication system. It converts electric current into electromagnetic radio waves and vice versa [1-4]. Signal produced is transmitted to space by a transmitter antenna which then travels to travel through the space as electromagnetic waves. Similarly, at the receiver end, antenna is required to convert electromagnetic (EM) signal into electric signal. Thus, an antenna can be used as a transmitter, a receiver, a modulator and an impedance matching device.

When an oscillating current passes through an antenna electric field is generated due to the accumulation of charges and magnetic field is generated due to the flow of current, thereby generating electromagnetic radiation, which then travels through the space. Mechanism of generating electromagnetic wave by the antenna is illustrated in figure 1.1.

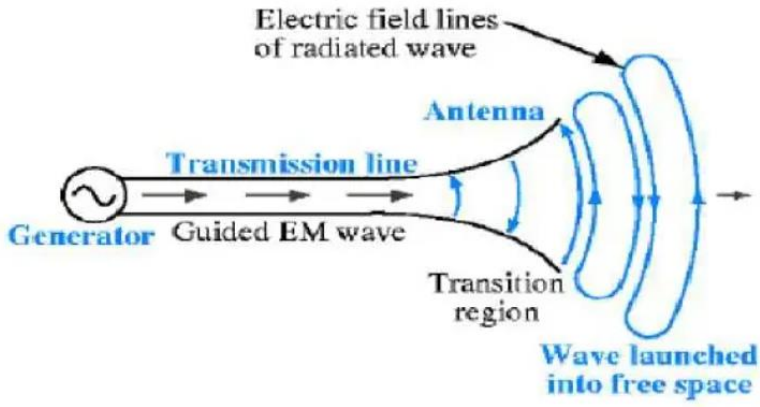

Figure 1.1 Antenna as a transition device [3].

At the receiver end, this electromagnetic wave signal is converted into electric current. Thus, an antenna converts current into electromagnetic signal and vice-versa. Take an example of listening to a radio channel in vehicle from a radio station far away. Transmitter converts sound into electric current, this current flows to the radio tower and electromagnetic radio waves are generated by the antenna connected into the tower due to continuous change in the current received. These waves are then transmitted into the space. The receiver on other end detects these radio waves and converted into electric current by the antenna, which are again converted

into the sound signal transmitted by the radio station. In case of internet packets of data are transmitted by antenna relayed between computer and Wi-Fi router. The signal is transmitted very fast at the speed of light.

Over the past few decades, there has been a constant need for antennas due to their great assistance in communications such as in radio, television, radar and space exploration, sensing and many more applications [1-4]. Numerous theories have been developed to examine their characteristics, and a great deal of research has been done to enhance their designs and performances. Numerous beneficial applications for classic antennas have been shown by the current research. Some of the common applications of antennas are shown in figure 1.2.

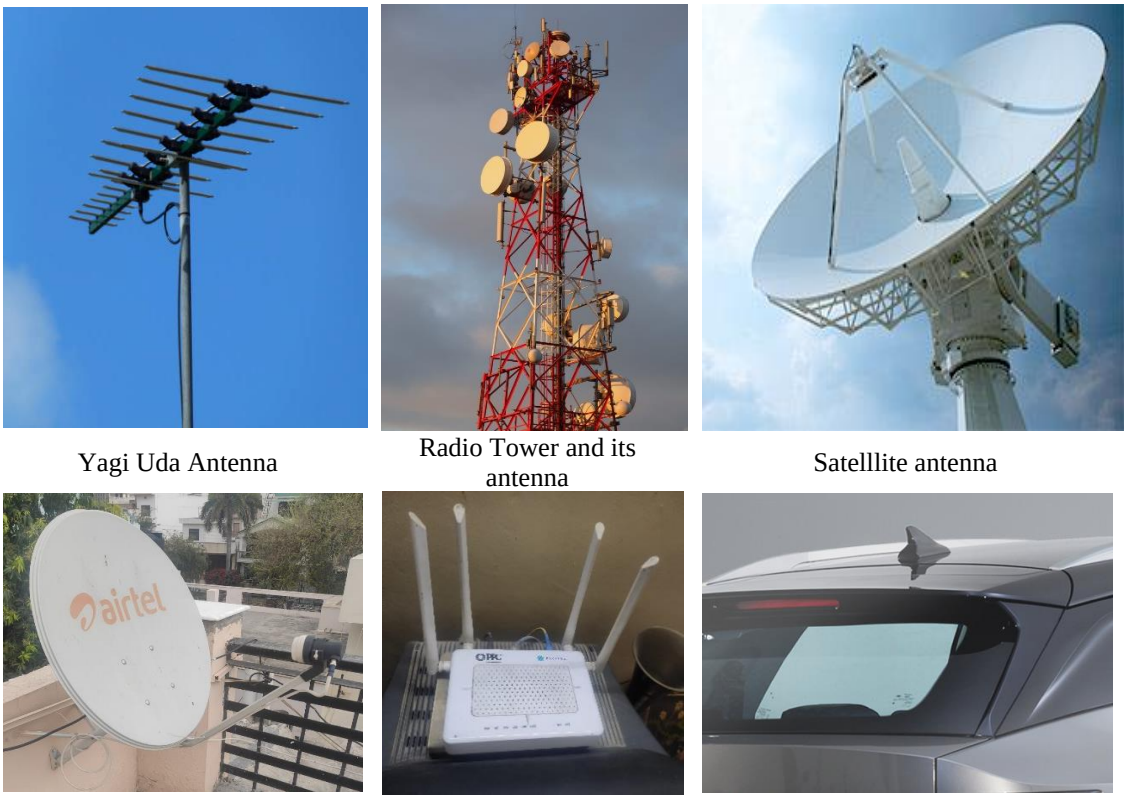

Yagi Uda Antenna | Radio Tower and its antenna | Satelllite antenna

Dish antenna for TV signals | Antenna in Wi-Fi Router | Car antenna

1

Figure 1.2 Different applications of antenna

[1]Image: https://getquicktech.com.au/blog/tricks-to-get-the-best-possible-reception-with-your-antenna, https://study.com/learn/lesson/antenna-types-function.html , https://www.viasat.com/products/satellite-antennas https://wuling.id/en/blog/autotips/8-functions-of-car-shark-fin-antenna

The majority of widely used antennas find applications in the radio and microwave frequencies, especially for wireless communications. In another context, the optical analogue of the well-known RF/microwave antennas, known as plasmonic nanoantennas, have attracted a lot of attention due to recent advancements in nanoscale optical systems. In case of a nanoantenna, electromagnetic radiation is converted into confined energy and vice versa. It covers broad range of the spectrum utilising visible and infrared region. As these nanoantennas work in optical frequency region i.e. visible and near infrared region, they are called as optical nanoantennas [5, 6]. There are two significant differences in the operational properties of these metallic nanoantennas from the conventional RF/microwave antennas, which should be considered while designing nanoantenna. When it comes to optical wavelengths, the conventional law that metals behave like perfect electrical conductors no longer holds true. Rather, they begin to show dielectric properties. At this high frequency regime, electric field can pass through metals, and compared to microwave frequencies, the Ohmic losses become substantial. Second, the formation of surface plasmon polaritons (SPP) at metallic and dielectric interfaces are confined in the nanoscale region [7, 8]. That is why, the response of the optical plasmonic nanoantenna structures significantly differs from that of their microwave analogues. One of the significant differences is the strong field confinement in the subwavelength nanogap region due to the generation of localised surface plasmons, in case of metallic nanoantennas. This region of the nanogap can serve as the nanoantenna system's feeding or receiving point [9]. These qualities have garnered a lot of attention recently because of the implications they have for both fundamental research and technical applications.

One of most significant accomplishments of science is the ability to manipulate and guide the light. It has an impact on daily life in a variety of ways, including the advancement of optical fibers, spectrometers, telescopes, and microscopes. These instruments rely on the reflection, refraction, and diffraction of light by optical components like mirrors, lenses, or

gratings. All these instruments has a low resolution power due to diffraction limit which is related to wavelength of light. This diffraction limit originates from the fact that it is impossible to focus the light to a spot smaller than half of its wavelength [10]. However, this limitation can be overcome with the use of nanoantennas. For laser light in visible range, maximum resolution of 250 - 350 nm can be achieved, however, nanoantennas can confine field in a very small region ~ 20 nm which is significantly below the diffraction limit []. The subwavelength confinement of light can be very useful in various applications such as in near field scanning optical microscopy (NSOM) [11, 12], surface enhanced Raman scattering (SERS) [13-15, 43], spectroscopy [16,17], data storage [18], optical circuits [19-21], fabrication techniques etc. [22]. Nanoantennas are also ideally suited for biological applications because of their ability to detect marker emission from cells with sub-diffraction limit resolution and able to kill cancer cells via resistive heating of resonant nanoparticle. In the coming section, we will discuss about the basic parameters of nanoantennas, different types of nanoantennas, their working and applications.

1.2 Types of nanoantennas

In 1928, E.H. Synge first suggested that nanoparticle can be used to confine electric field. Later in 1985, John Wessel first used a plasmonic nanoparticle as an antenna [23]. The functioning and mechanism of redistribution of electromagnetic energy into space via absorption, scattering, confined field etc. strongly depends on the constituting material of the nanoantenna [24]. On the basis of constituting material, nanoantennas can be mainly classified into three types namely metallic, dielectric and hybrid nanoantennas.

1.2.1 Metallic nanoantennas

Metallic nanoantennas are most commonly used nanostructure made up of metals. Metallic nanoantennas are also known as plasmonic nanoantennas, as localised surface plasmons are generated in this type of nanoantennas which are responsible for stronger field confinement. A

detailed mechanism of localised surface plasmon (LSP) will be discussed in sec 1.4. Some of the common designs of the plasmonic nanoantennas are depicted in figure 1.3 and discussed further. As mentioned above, a single metallic nanoparticle has ability to enhance the electromagnetic field strength in its vicinity due to excitation of plasmon resonances, therefore, capable of operating as a receiving nanoantenna. A simplest design of the nanoantennas is a single structure known as a monopole (fig 1.3 (a)) [25-27]. Owing to a fewer number of geometrical parameters, monopoles are suitable, when a large size antenna array is required. In these type of NAs, the electric field is confined near its vicinity, when an electromagnetic wave impinges on it. The resonant wavelength depends on the size, shape, and material of the nanoantenna. Another design of the nanoantenna is a dimer or dipole nanoantennas (fig. 1.3(b)) [22-31]. In these types of nanoantennas, field is confined in the gap region between two arms of nanoantennas. Figure 1.4 shows the intensity enhancement by monopole and dipole nanoantenna. It is clear from the figure that field enhancement in case of dipole nanoantenna is remarkably greater when compared to the monopole nanoantenna. This is because surface plasmons couple strongly in the gap region, hence, stronger electric field is generated at the centre. Surface plasmons tend to accumulate more at the tips than at the flat surface. Furthermore, the electric field enhancement in the gap becomes more promising as the gap size is reduced. Keeping that in mind, dipole nanoantennas have been modified into another more promising design known as the Bowtie nanoantenna [32-34], whose geometry is shown in figure 1.3 (c). The comparison of electric field enhancements between a two-wire and a bow-tie antenna for same total length, gap and radius of curvature is shown in figure 1.5. Since bowtie antennas are the two-dimensional equivalent of biconical antennas, it is believed that they will have a relatively wide bandwidth. Additionally, due to their stronger lightning-rod effect at the apex, bowtie antennas are thought to have a higher field enhancement in the gap than two-wire antennas. However, for the same total length, gap and radius of curvature

between a two-wire and a bow-tie antenna, the two-wire antenna exhibits the largest resonant field enhancement. This is because the larger volume of the bow-tie structure leads to more losses, thereby lowering the quality factor. Some research works have proposed the use of a layer of bowtie nanoantenna array as a substrate of solar cells, due is its broad bandwidth in order to enhance absorption of sunlight, thereby increasing the efficiency of the solar cell [35,36] .

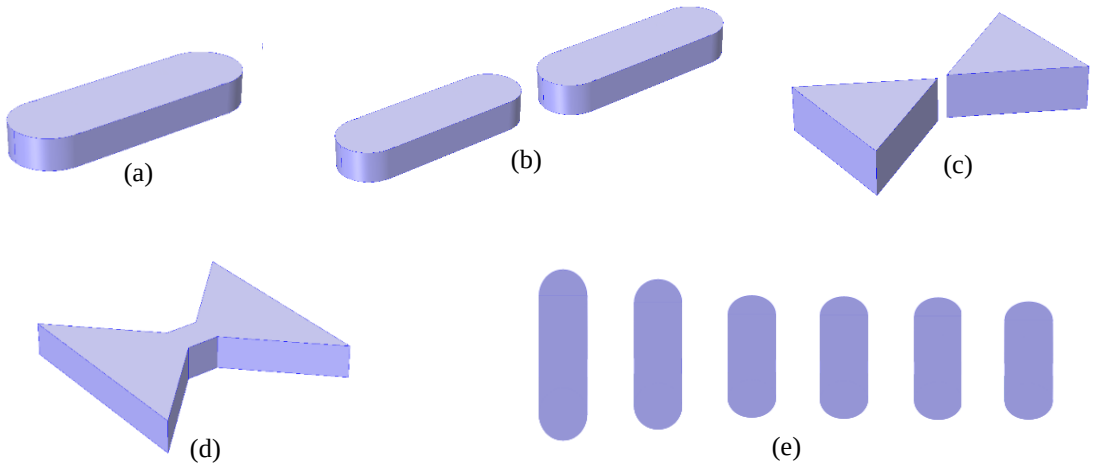

Figure 1.3 Schematic of various designs of nanoantenna (a) monopole nanoantenna, (b) dipole nanoantenna, (c) bowtie nanoantenna, (d) diabolo nanoantenna and (e) Yagi Uda nanoantenna.

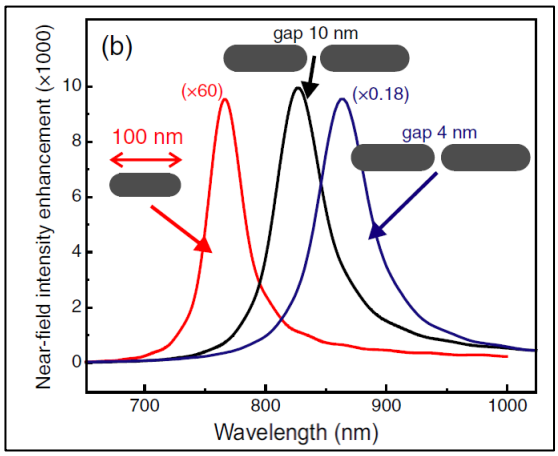

Figure 1.4 FDTD simulation results for near-field spectra for 100 nm long single and two wire Au nanoantennas (red circles: single-wire antenna; black solid squares: 10 nm gap two-wire antenna; blue empty squares: 4 nm gap two-wire antenna) antennas [34]

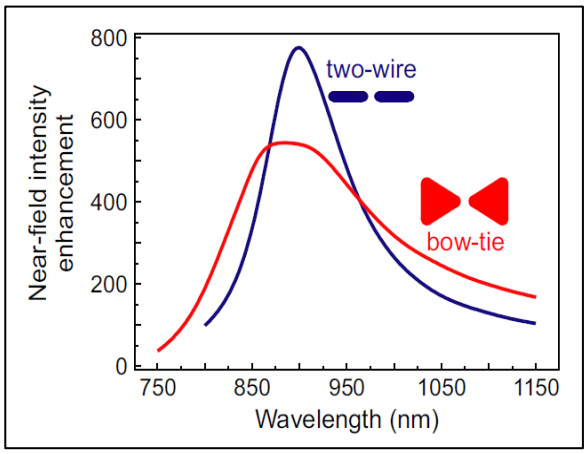

Figure 1.5 FDTD simulated near-field spectra in the middle of the gap for a two-wire and a bow-tie antenna on a glass substrate with the same total length, same gap size and same radius of curvature at the apex. The reduced field enhancement for the bow-tie structure is clearly observable on resonance [34]

It is worth mentioning that the conversion of energy is not limited to generation of electric field only but also extends to magnetic field. In 2011, authors in ref [37] proposed a diabolo nanoantenna in which two arms of a bowtie were connected through a bridge. The geometry of diabolo nanoantenna is shown in figure 1.3 (d). The name “diabolo” is given as the geometry of the nanoantenna resembles with the toy diabolo. High magnetic field was observed around the central bridge of the diabolo nanoantenna, which can be used for various applications in the optical frequency regime

It is well-known that for reception of TV signals from remote stations can be achieved by a special type of highly directive antenna, called the Yagi-Uda antenna. Interestingly its optical analogue has also been designed and studied for special application in nanophotonics which require high directivity. Yagi-Uda Nanoantenna was proposed to obtain narrow emission pattern. It consists of one reflector and one or several directors. Typical geometry of Yagi-Uda nanoantenna is shown in figure 1.3 (e). First experimental validation was done by Curto et al. [38] showing the possibility of obtaining narrow directivity diagram.

Work done on designing of nanoantennas is not limited to simple designs but more complicated geometries have also been proposed [39-45]. More than field confinement and increasing directivity, plasmonic nanoantennas have been utilised in absorption of energy. A layer of plasmonic nanoantenna is laid over the photovoltaic cells, so that they can absorb maximum energy from the sunlight and convert it into useful electric energy.

Only the major drawback of using plasmonic nanoantenna is that energy gets dissipated by the metal in the form of heat. The presence of ohmic losses in the metals degrades the performance of nanoantenna. Attempt to reduce these loses in antenna by creating frackels in the nanoantenna such as Sierpinskito nanoantenna has been done but fabrication of these types

of nanoantenna is very complex [46]. Dielectric nanoantennas are then introduced to cope up with these challenges.

1.2.2 Dielectric nanoantennas

Although metallic nanoantennas have been remarkably successful in a variety of applications, they have considerable limitation attached to them in terms of resistive or ohmic loss. To get rid of the resistive losses associated with metals, a specifically new class of all-dielectric nanoantennas have evolved in the past one and a half decade. Dielectric nanoantennas are made up of materials transparent to optical frequency. They are basically made up of semiconductor materials that are transparent to optical frequency. The working of dielectric nanoantennas is fundamentally based on the concept of Mie resonance. Hence, materials of high refractive index are chosen for their designs such as silicon (Si, $\varepsilon = 16$), germanium (Ge, $\varepsilon = 20$), aluminium antimonide (AlSb, $\varepsilon = 12$), aluminium arsenide (AlAs, $\varepsilon = 10$) etc. Most of the dielectric nanoantennas are spherical, made up of Silicon designed to operate in near the IR spectrum (~1500 nm) [47-49]. There are two main advantages of using these types of nanoantenna- first is the reduction of heat losses, and second is the achieving high electric field and magnetic field simultaneously. A substantial work to increase the directivity of nanoantennas has been performed and reported. These nanoantennas basically consist of a single or a group of dielectric microspheres, and based on their design peculiarities can be categorized as Whispering gallery nanoantennas, Huygens elements and Yagi-Uda nanoantenna.

Whispering gallery nanoantennas: They are so called because the electromagnetic solutions of the particles are of the form of standing waves, similar to the case of standing wave of sound (called whispering-gallery waves) created in the large circular halls, where words spoken in any part of the hall can be heard in any other part. These nanoantennas have high directional

ability and good at concentrating the radiation in a narrow beam increasing the intensity at the reception point manifolds [50, 51].

Huygens elements: A Huygens element basically consists of the particle of high refractive index or relative permittivity. Silicon (ε=16) and germanium ((ε=20)) are most common candidates for their design. The speciality of these antennas is the fact that upon excitation they can exhibit both magnetic and electric dipole resonance in the desired ranges of wavelength. The advantage of the Huygens elements is their high directionality. Moreover, it is capable of toggling the direction of radiation between either of the two main directions (referred to as forward and backward) [52, 53].

Yagi-Uda nanoantenna: This design is actually an enhanced version of Huygen elements design in which five microspheres of specific sized are placed in straight line with a specific gap between them. Similar to the RF counterpart, various elements of a Yagi-Uda nanoantenna have specific roles as the reflector and the directors, and the distance between them is also strategically choosen according to the desired wavelength of operation. Due to collective performance of more than one dielectric sphere the resultant directivity of the Yagi-Uda antenna is enhanced 3-4 times than that of a single Huygens element. [48, 49, 52].

In addition to spherical design of dielectric nanoantennas various designs of nanoantennas such as nanocylinders [54], nanoellipses [55, 57], split-ring [56] etc. Dielectric nano-dimers, a dielectric analogue of plasmonic dipole nanoantenna, have also been shown to achieve high field enhancement [58]. Despite several properties being comparable to the plasmonic counterparts and having a great advantage of being free from ohmic loss, dielectric nanoantennas have some serious limitations as well. It has been commonly observed that, the Purcell factor of dielectric nanoantennas is substantially smaller as compared to plasmonic nanoantennas. Furthermore, the confinement of field is lesser due a significant penetration of

electric field into the dielectric material region, which on the other hand is negligibly small in metals.

1.2.3 Hybrid metal-dielectric nanoantennas

Hybrid nanoantenna is a combination of both plasmonic and dielectric nanoantenna. This type of nanoantenna overcomes the shortcomings of plasmonic and dielectric nanoantennas. In this type of design, the plasmonic (i.e. metallic) nanoparticles can be used to enhance the radiation emitted by an nanoscale emitter and the dielectric particles serving as Huygens elements can redirect the radiation in a particular direction in the form of a narrow beam. In this way, both type of elements, serve their specific purposes based on their specialities [59-62].

1.3 Nanoantenna Parameters

Various parameters are associated to nanoantennas in order to critically evaluate their performance and efficiency for various applications.

1.3.1 Radiation Power

Radiation power is defined as the total power radiated by the nanoantennas in the far field region. It is calculated as the surface integral of the Poynting vector.

$$P_{rad} = \int P_{av}.\, ds = \frac{1}{2}\int Re[E \times H^{*}].\, ds \qquad (1.1)$$

Where P_{rad} is the radiation power, P_{av} is the average Pointing vector, E is the electric field, H is the magnetic field and ds is the surface element.

1.3.2 Radiation Pattern

Radiation pattern is the 2D graphical representation of the radiated power or field pattern along the different axes or planes. Radiated power or field pattern are normalised to maximum at a fixed distance from the nanoantenna. The radiation pattern can be described as isotropic, omni-directional and directional as shown in figure 1.6 (a), (b) and (c) respectively. If the field

distribution or radiation power radiated by the antenna in the far- field region is same in all directions i.e. the radiation pattern is spherical in shape, then the pattern is said to be isotropic. No nanoantenna shows this type of pattern and this type of pattern is considered only for references. If the field distribution or radiation power radiated by nanoantenna is equally distributed in only one plane while null in another plane, then the pattern is said to be omnidirectional. If the nanoantenna radiates energy more in a particular direction rather than any other direction, then the pattern is said to be directional.

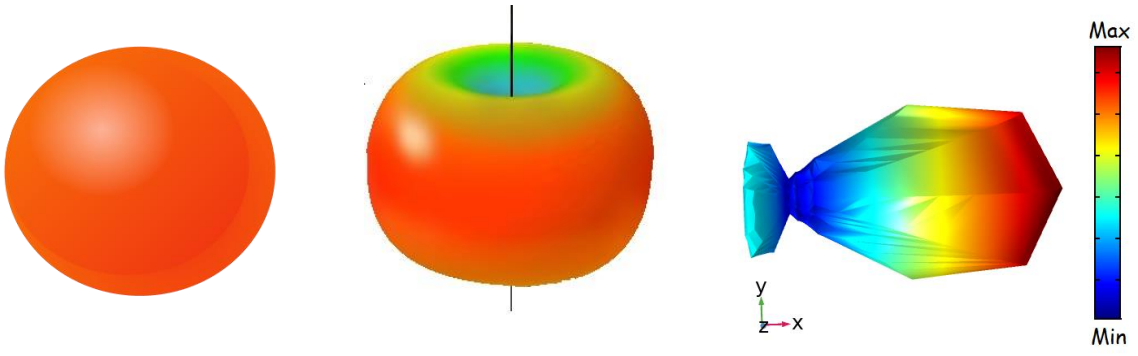

(a) Isotropic (b) Omni-directional (c) Directional

Figure 1.6 Different types of radiation Pattern exhibited by nanoantenna.

1.3.3 Field region

When a nanoantenna transmits electromagnetic waves, electric field distribution exists from the close proximity of the antenna surface to infinite distance away from it. The field region is mainly divided into two zones – the near field and the far field domain. Near field can be defined as the region in the vicinity of nanoantennas. It refers to a region that lies within the distance less than the resonance wavelength from the nanoantenna surface (*near-field, d* <λ). Far field region is defined as the region of space that occurs at a distance very far from the nanoantennas or very large compared to the resonance wavelength (*far-field, d* >>λ).

1.3.4 Directivity

The directivity is the measure of ability of nanoantenna to concentrate power in a particular direction. The directivity (D) in a given direction is the ratio of power intensity U (θ, φ) along that direction (θ, φ) to the radiation intensity averaged over all directions.

$$D = 4\pi \frac{U(\theta,\varphi)}{P_{rad}} \tag{1.2}$$

Considering the space around the antenna at unit distance, average power is given by $P_{rad}/4\pi$, where P_{rad} is the total radiated output power. In other words, it is the ratio of the radiation intensity received at a given point in a particular direction from the directional antenna to the intensity that would have been received at the same point from an isotropic antenna.

If direction is not defined, then the direction in which power is maximum is considered for calculating the directivity. Further its P_{max} is the maximum power intensity radiated by the nanoantenna, then the directivity is given by

$$D = 4\pi \frac{P_{max}}{P_{rad}} \tag{1.3}$$

Gain

Gain is defined as the power radiated in a particular direction relative to the total input power. Mathematically, gain (G) is represented as

$$G = 4\pi \frac{P_{max}}{P_{in}} \tag{1.4}$$

1.3.5 Resonance frequency

Resonance frequency is the frequency where the interaction between incident electromagnetic light and nanoantenna are maximum. Optical properties such as field confinement, power radiated or scattered are maximum at this frequency. In general, the optical properties such as the field confinement, power radiated or scattered are maximized at this frequency.

1.3.6 Band width

The nanoantenna shows optical properties not only at resonance frequency but over a range of frequencies around it. The range of frequencies throughout which the performance of nanoantennas with respect to any characteristic can be observed is defined as the bandwidth for that particular nanoantenna. Some nanoantennas operate in single band while some operate in dual or triple band. In this bandwidth, the radiation properties of nanoantennas such as field confinement, scattered power, are highly noticeable whereas outside the bandwidth these properties reduce significantly.

1.3.7 Radiation efficiency

When power is supplied to a nanoantenna, some part of it is undergoes dissipation loss in its material while rest gets radiated to space. The radiation efficiency, denoted by η_{rad}, is defined as the ratio of the power radiated by the nanoantenna to the total power supplied to it. Mathematically,

$$\eta_{rad} = \frac{P_{rad}}{P_{rad}+P_{ab}} \tag{1.5}$$

where, P_{rad} is power radiated by the nanoantenna and P_{ab} is the power absorbed by its material.

1.3.8 Purcell factor

A quantum emitter in free space undergoes spontaneous transition from high energy states to lower energy allowed states by emitting photons. Such transition occur due to interaction of the quantum emitter with environment and the subsequent radiation is called *spontaneous radiation.* E. M. Purcell showed that if a quantum emitter is present inside a resonant device instead of the free space, its rate of spontaneous radiation can be substantially increased. This effect is called *Purcell effect* and the ratio of the rate of spontaneous radiation in a particular heterogenous system γ (e.g., in a nanoantenna), to the rate of spontaneous radiation in free space γ_0 is called Purcell factor F_P, given as

$$F_P = \frac{\gamma}{\gamma_0} = \frac{P_{tot}}{P_0}$$

where, P_{tot} is total power radiation by the emitter in a heterogeneous system and P_0 is the total power radiated by it when in free space.

1.4 Localized surface plasmon resonance (LSPR)

Localised surface plasmons occur when the metal size is very small in comparison with the wavelength of the light. At visible and near-infrared frequency metals exhibit dielectric properties and allow electromagnetic radiations to slightly penetrate into them (skin depth ~ 50 nm). At the metal surface, when electromagnetic radiation of suitable frequency is incident, surface plasmons are formed. These surface plasmons produce electric field on the metal surface. All metals have freely available electrons, which are responsible for its conductivity. These electrons oscillate with external electromagnetic wave incident on it with a suitable propagation vector. In case of nanoparticles, the charge cloud moves throughout the material. The charges accumulate at the opposite extremes of the nanoparticle and tend to oscillate with the frequency of incident light. These plasmons are localized and are thus called the *localised surface plasmons* (LSP). Electromagnetic field is generated at the nanoparticle-dielectric surface, due to formation of LSP, decays away from in the dielectric region. When the frequency of external light falling on nanoparticle matches with the natural frequency of vibration of system the resonance occurs showing maximum amplitude of vibration. This situation is called *localized surface plasmon resonance* (LSPR) [see figure 1.7]. The localised surface plasmon resonance depends on the refractive index of the material, refracted index of the surrounding environment, and size and shape of the plasmonic nanoparticle.

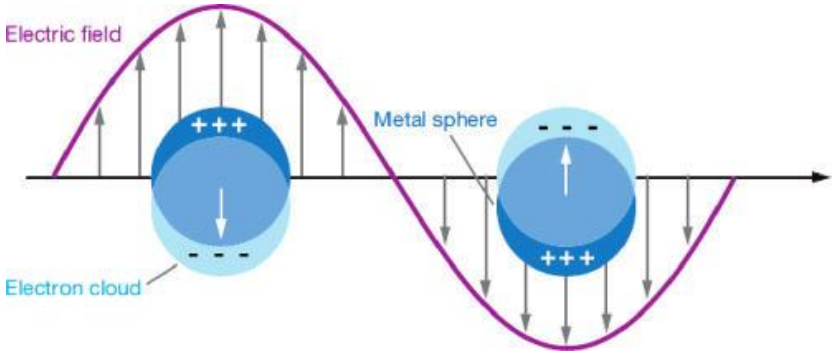

Figure 1.7 Localised Surface Plasmon Resonance in nanosphere [63].

Aspect ratio is the relationship length/width of the nanoparticle. Aspect ratio of the nanoparticles is one of the factors on which resonance wavelength depends [64]. To understand the concept let us consider metallic nanotubes placed in two different orientations as shown in figures 1.8 (a) and (b) respectively i.e. the longitudinal and the transverse position. In the longitudinal position LSP concentrate in a narrow region compared to the transverse position where they spread across the length of the rod. Also, there is different resonance wavelength for the nanotubes of the same size but different orientation as they have different aspect ratio. Further, as the aspect ratio increases, there is red-shift in the resonance wavelength. This shift is much larger for the nanoantenna when placed longitudinally as compared to the transverse orientation with the electric field.

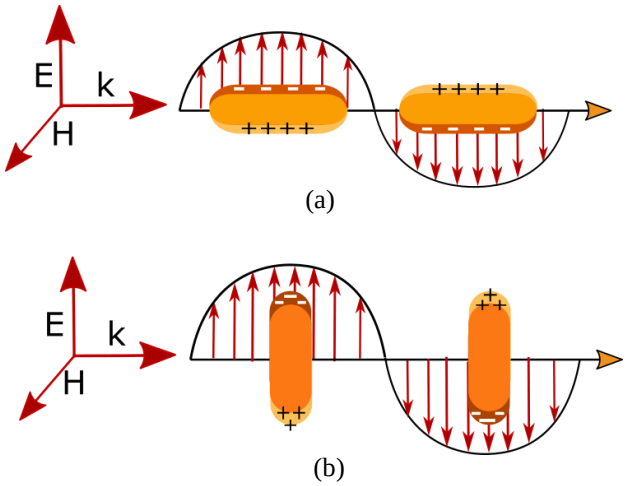

Figure 1.8 Plasmon in nanoparticle (a) longitudinal position, (b) transverse position.

1.5 Computational Method

A common technique for numerically solving differential equations that appear in engineering and mathematical modelling is the finite element method (FEM). The Finite Element Method (FEM) is a versatile numerical technique that discretizes the domain of the problem into small elements. This method entails meshing or segmenting of complicated device geometries into a finite number of subdomains or regions called finite elements. The finite element methods can be implemented in various ways for analysing vector wave, such as FEM using longitudinal electromagnetic field components (Ez and Hz), FEM using transverse electromagnetic field components and FEM using the three electric or magnetic field components. The typical properties of interests including scattering, S11 parameter, S21 parameter, electromagnetic potential, energy flow, power flow can be solved using above method. In the present thesis, FEM simulations have been carried out to study various optical properties of nanoantennas using COMSOL Multiphysics software by COMSOL at Delhi Technological University, Delhi.

The various designs of nanoantennas described in this thesis have been modelled and examined using the aforementioned computational and numerical method. Also, MATLAB by Mathworks is used for the calculation of various parameters such as calculating radiation efficiency and harvesting efficiency etc at Delhi Technological University, Delhi.

.

1.6 The Main objectives of this thesis

The main objectives of this thesis are

1. To design and analyze design of nanoantennas for utilization in solar energy harvesting by enhancing electric field and radiation efficiency.

2. To design and analyze nanoantenna to obtain high magnetic field in the optical frequency region.
3. To design and analyze nanoantenna as refractive index sensor for sensing applications in the visible region.
4. To utilize nanoantenna for trapping nanoparticle by means of trapping force applied on it generated by the nanoantenna.

1.7 Overview of the thesis

This thesis comprises of six chapters. The 1st chapter discusses the basic idea and importance of using optical nanoantennas. It discusses about the fundamental concepts of nanoantennas including operation principle and main characteristics of optical nanoantennas. Different types of nanoantennas, their designs, working and applications have been discussed. After that, working principal of plasmonic nanoantenna and modelling technique has been discussed.

In the chapter 2, various designs of plasmonic nanoantenna have been modelled. Various designs of nanoantennas namely petal-shaped nanoantenna, arrow-shaped nanoantenna, hexameric flower-shaped nanoantenna, tapered-cone dipole nanoantenna have been proposed and their optical properties such as electric field enhancement, radiation efficiency and harvesting efficiency have been calculated. The chapter emphasizes on solar energy harvesting using electric field enhancement property of nanoantennas. Various geometrical parameters of the nanoantennas have been varied to find their effect on the radiation efficiency and the harvesting efficiency. Additionally, the significance of the material of the nanoantenna has also been studied by choosing four different types of materials and their corresponding radiation efficiency, harvesting efficiency and electric field enhancement have been reported.

Chapter 3 focusses on the magnetic field enhancement by nanoantennas. Two designs of nanoantenna have been presented in this chapter - the hourglass nanoantenna, and the rhombic

nanoantenna. The design of hourglass nanoantenna has been thoroughly analysed by varying various geometrical parameters to find their effect on magnetic field enhancement. Also, different materials have been considered for the nanoantenna, to investigate the effect of the choice of material on magnetic field enhancement. Mechanism to achieve high magnetic field by the designed nanoantenna has clearly been discussed. Another design of the nanoantenna which shows magnetic field enhancement consists of the two rhombus with the sides of length *L*, a central square with sides of length *G*, and height or thickness of structure *H*. The structure has also been studied for the enhancement of the magnetic field by varying geometrical parameters.

In chapter 4, a metallic ultra-narrow band perfect absorber has been proposed consisting of an array of four squares on a silver layer. The structure shows more than 99% absorption and FWHM less than 2 nm at resonance wavelength. The absorption mechanism has been revealed by calculating electric and magnetic field profiles. The dependence of the structure on the geometrical parameters has been studied and the structure has thus been optimized at 692 nm i.e. in the visible range of frequency. The proposed structure is then investigated for sensing application. The structure shows high sensitivity of 680 nm/RIU in the visible range of wavelength and a high figure of merit of 348.72. The proposed design holds great potential for sensing and near-field optics.

In chapter 5, nanoantenna design has been utilized for optical trapping application by means of generating high electric field. The structure consists of semi cones each supposed to be cut into halves through axis passing through the centre of the cones, facing each other at the tips. The nanoantenna is placed on the glass substrate and surrounded by water from above. The dielectric nanoparticle which is to be trapped is immersed in the water. The design is optimized such that low input power of laser is sufficient to generate high field at the hot spot. The design nanoantenna can trap a dielectric particle of size as small as 20 nm in the gap region. Forces

along y-axis and z-axis have been calculated by integrating Maxwell stress tensor over the surface of nanoparticle.

Chapter 6 includes summary of the thesis work and the future research scope by utilizing the current thesis work.

References

[1] Silver, S. (Ed.). (1984). *Microwave antenna theory and design* (No. 19). Iet.

[2] Olmon, R. L., & Raschke, M. B. (2012). Antenna–load interactions at optical frequencies: impedance matching to quantum systems. *Nanotechnology*, *23*(44), 444001.

[3] Balanis, C. A., & Polycarpou, A. C. (2003). Antennas. *Wiley Encyclopedia of Telecommunications*.

[4] Huang, Y. (2021). *Antennas: from theory to practice*. John Wiley & Sons.

[5] Bharadwaj, P., Deutsch, B., & Novotny, L. (2009). Optical antennas. *Advances in Optics and Photonics*, *1*(3), 438-483.

[6] Novotny, L., & Van Hulst, N. (2011). Antennas for light. *Nature photonics*, *5*(2), 83-90.

[7] Barnes, W. L., Dereux, A., & Ebbesen, T. W. (2003). Surface plasmon subwavelength optics. *Nature*, *424*(6950), 824-830.

[8] Ozbay, E. (2006). Plasmonics: merging photonics and electronics at nanoscale dimensions. *Science*, *311*(5758), 189-193.

[9] Sundaramurthy, A., Crozier, K. B., Kino, G. S., Fromm, D. P., Schuck, P. J., & Moerner, W. E. (2005). Field enhancement and gap-dependent resonance in a system of two opposing tip-to-tip Au nanotriangles. *Physical Review B*, *72*(16), 165409.

[10] Weiss, S. (2000). Shattering the diffraction limit of light: A revolution in fluorescence microscopy? *Proceedings of the National Academy of Sciences*, *97*(16), 8747-8749.

[11] Vasconcelos, T. L., Archanjo, B. S., Oliveira, B. S., Valaski, R., Cordeiro, R. C., Medeiros, H. G., ... & Cançado, L. G. (2018). Plasmon-Tunable Tip Pyramids: Monopole Nanoantennas for Near-Field Scanning Optical Microscopy. *Advanced Optical Materials*, *6*(20), 1800528.

[12] Lereu, A. L., Passian, A., & Dumas, P. (2012). Near field optical microscopy: a brief review. *International journal of nanotechnology*, *9*(3-7), 488-501.

[13] Giannini, V., Fernández-Domínguez, A. I., Heck, S. C., & Maier, S. A. (2011). Plasmonic nanoantennas: fundamentals and their use in controlling the radiative properties of nanoemitters. *Chemical reviews*, *111*(6), 3888-3912.

[14] Hatab, N. A., Hsueh, C. H., Gaddis, A. L., Retterer, S. T., Li, J. H., Eres, G., ... & Gu, B. (2010). Free-standing optical gold bowtie nanoantenna with variable gap size for enhanced Raman spectroscopy. *Nano letters*, *10*(12), 4952-4955.

[15] Ahmed, A., & Gordon, R. (2011). Directivity enhanced Raman spectroscopy using nanoantennas. *Nano letters*, *11*(4), 1800-1803.

[16] Neubrech, F., Huck, C., Weber, K., Pucci, A., & Giessen, H. (2017). Surface-enhanced infrared spectroscopy using resonant nanoantennas. *Chemical reviews*, *117*(7), 5110-5145.

[17] Kusa, F., Morichika, I., Takegami, A., & Ashihara, S. (2017). Enhanced ultrafast infrared spectroscopy using coupled nanoantenna arrays. *Optics Express*, *25*(11), 12896-12907.

[18] Wang, H., Chong, C. T., & Shi, L. (2009, May). Optical antennas and their potential applications to 10 terabit/in 2 recording. In *2009 Optical Data Storage Topical Meeting* (pp. 16-18). IEEE.

[19] Huang, J. S., Voronine, D. V., Tuchscherer, P., Brixner, T., & Hecht, B. (2009). Deterministic spatiotemporal control of optical fields in nanoantennas and plasmonic circuits. *Physical Review B*, *79*(19), 195441.

[20] Huang, J. S., Feichtner, T., Biagioni, P., & Hecht, B. (2009). Impedance matching and emission properties of nanoantennas in an optical nanocircuit. *Nano letters*, *9*(5), 1897-1902.

[21] Brongersma, M. L. (2008). Engineering optical nanoantennas. *Nature Photonics*, *2*(5), 270-272.

[22] Biagioni, P., Huang, J. S., & Hecht, B. (2012). Nanoantennas for visible and infrared radiation. *Reports on Progress in Physics*, *75*(2), 024402.

[23] Wessel, J. (1985). Surface-enhanced optical microscopy. *JOSA B*, *2*(9), 1538-1541.

[24] Haes, A. J., & Van Duyne, R. P. (2002). A nanoscale optical biosensor: sensitivity and selectivity of an approach based on the localized surface plasmon resonance spectroscopy of triangular silver nanoparticles. *Journal of the American Chemical Society*, *124*(35), 10596-10604.

[25] Acar, H., Coenen, T., Polman, A., & Kuipers, L. K. (2012). Dispersive ground plane core–shell type optical monopole antennas fabricated with electron beam induced deposition. *ACS nano*, *6*(9), 8226-8232.

[26] Zhou, R., Ding, J., Arigong, B., Lin, Y., & Zhang, H. (2013). Design of a new broadband monopole optical nano-antenna. *Journal of Applied Physics*, *114*(18), 184305.

[27] Vasconcelos, T. L., Archanjo, B. S., Oliveira, B. S., Valaski, R., Cordeiro, R. C., Medeiros, H. G., ... & Cançado, L. G. (2018). Plasmon-Tunable Tip Pyramids:

Monopole Nanoantennas for Near-Field Scanning Optical Microscopy. *Advanced Optical Materials*, *6*(20), 1800528.

[28] Wissert, M. D., Schell, A. W., Ilin, K. S., Siegel, M., & Eisler, H. J. (2009). Nanoengineering and characterization of gold dipole nanoantennas with enhanced integrated scattering properties. *Nanotechnology*, *20*(42), 425203.

[29] Razzari, L., Toma, A., Shalaby, M., Clerici, M., Zaccaria, R. P., Liberale, C., ... & Di Fabrizio, E. (2011). Extremely large extinction efficiency and field enhancement in terahertz resonant dipole nanoantennas. *Optics express*, *19*(27), 26088-26094.

[30] Andryieuski, A., Malureanu, R., Biagi, G., Holmgaard, T., & Lavrinenko, A. (2012). Compact dipole nanoantenna coupler to plasmonic slot waveguide. *Optics letters*, *37*(6), 1124-1126.

[31] Ren, X., Wei, E. I., & Choy, W. C. (2013). Tuning optical responses of metallic dipole nanoantenna using graphene. *Optics express*, *21*(26), 31824-31829.

[32] Chen, H., Bhuiya, A. M., Liu, R., Wasserman, D. M., & Toussaint Jr, K. C. (2014). Design, fabrication, and characterization of near-IR gold bowtie nanoantenna arrays. *The Journal of Physical Chemistry C*, *118*(35), 20553-20558.

[33] Fromm, D. P., Sundaramurthy, A., Schuck, P. J., Kino, G., & Moerner, W. E. (2004). Gap-dependent optical coupling of single "bowtie" nanoantennas resonant in the visible. *Nano letters*, *4*(5), 957-961.

[34] Schuck, P. J., Fromm, D. P., Sundaramurthy, A., Kino, G. S., & Moerner, W. E. (2005). Improving the mismatch between light and nanoscale objects with gold bowtie nanoantennas. *Physical review letters*, *94*(1), 017402.

[35] Duarte, F., Torres, J. P. N., Baptista, A., & Marques Lameirinhas, R. A. (2021). Optical nanoantennas for photovoltaic applications. *Nanomaterials*, *11*(2), 422.

[36] Gallo, M., Mescia, L., Losito, O., Bozzetti, M., & Prudenzano, F. (2012). Design of optical antenna for solar energy collection. *Energy*, *39*(1), 27-32.

[37] Grosjean, T., Mivelle, M., Baida, F. I., Burr, G. W., & Fischer, U. C. (2011, May). Nanoantennas for enhancing and confining the magnetic optical field. In *Metamaterials VI* (Vol. 8070, pp. 23-27). SPIE.

[38] Dregely, D., Taubert, R., Dorfmüller, J., Vogelgesang, R., Kern, K., & Giessen, H. (2011). 3D optical Yagi–Uda nanoantenna array. *Nature communications*, *2*(1), 267.

[39] Lee, H., You, S., Pikhitsa, P. V., Kim, J., Kwon, S., Woo, C. G., & Choi, M. (2011). Three-dimensional assembly of nanoparticles from charged aerosols. *Nano letters*, *11*(1), 119-124.

[40] Bachman, K. A., Peltzer, J. J., Flammer, P. D., Furtak, T. E., Collins, R. T., & Hollingsworth, R. E. (2012). Spiral plasmonic nanoantennas as circular polarization transmission filters. *Optics express*, *20*(2), 1308-1319.

[41] Yahyaoui, A., Elsharabasy, A., Yousaf, J., & Rmili, H. (2020). Numerical analysis of MIM-based log-spiral rectennas for efficient infrared energy harvesting. *Sensors*, *20*(24), 7023.

[42] Liu, G., Zhao, C., Jiang, J., Gao, Z., & Gu, J. (2023). Structural Design and Optimization of Optical Nano-Antenna Based on Bridge Structure. *Progress In Electromagnetics Research M*, *117*, 95-104.

[43] Zhang, X., Zhang, Q., Yuan, Y., Liu, J., & Liu, X. (2020). Ultra-directional forward scattering by a high refractive index dielectric T-shaped nanoantenna in the visible. *Physics Letters A*, *384*(27), 126696.

[44] Hadadi, T., Naser-Moghadasi, M., Arezoomand, A. S., & Zarrabi, F. B. (2016). Sub wavelength plasmonic nano-antenna with modified ring structure for multi resonance application and circular polarization. *Optical and Quantum Electronics*, *48*, 1-9.

[45] Brown, L. V., Yang, X., Zhao, K., Zheng, B. Y., Nordlander, P., & Halas, N. J. (2015). Fan-shaped gold nanoantennas above reflective substrates for surface-enhanced infrared absorption (SEIRA). *Nano letters*, *15*(2), 1272-1280.

[46] Li, N., Lai, Y., Lam, S. H., Bai, H., Shao, L., & Wang, J. (2021). Directional control of light with nanoantennas. *Advanced Optical Materials*, *9*(1), 2001081.

[47] Rosa, L., Sun, K., & Juodkazis, S. (2011). Sierpin´ ski fractal plasmonic nanoantennas. *physica status solidi (RRL)–Rapid Research Letters*, *5*(5-6), 175-177.

[48] Krasnok, A. E., Simovski, C. R., Belov, P. A., & Kivshar, Y. S. (2014). Superdirective dielectric nanoantennas. *Nanoscale*, *6*(13), 7354-7361.

[49] Krasnok, A. E., Miroshnichenko, A. E., Belov, P. A., & Kivshar, Y. S. (2012). All-dielectric optical nanoantennas. *Optics Express*, *20*(18), 20599-20604.

[50] Gérard, D., Devilez, A., Aouani, H., Stout, B., Bonod, N., Wenger, J., ... & Rigneault, H. (2009). Efficient excitation and collection of single-molecule fluorescence close to a dielectric microsphere. *JOSA B*, *26*(7), 1473-1478.

[51] Gu, F., Zhang, L., Zhu, Y., & Zeng, H. (2015). Free-space coupling of nanoantennas and whispering-gallery microcavities with narrowed linewidth and enhanced sensitivity. *Laser & Photonics Reviews*, *9*(6), 682-688.

[52] Krasnok, A. E., Miroshnichenko, A. E., Belov, P. A., & Kivshar, Y. S. (2011). Huygens optical elements and Yagi—Uda nanoantennas based on dielectric nanoparticles. *JETP letters*, *94*, 593-598.

[53] Ollanik, A. J., Smith, J. A., Belue, M. J., & Escarra, M. D. (2018). High-efficiency all-dielectric Huygens metasurfaces from the ultraviolet to the infrared. *ACS photonics*, *5*(4), 1351-1358.

[54] Devi, I., Dalal, R., Kalra, Y., & Sinha, R. K. (2016). Modeling and design of all-dielectric cylindrical nanoantennas. *Journal of nanophotonics*, *10*(4), 046011-046011.

[55] Sinev, I., Komissarenko, F., Iorsh, I., Permyakov, D., Samusev, A., & Bogdanov, A. (2020). Steering of guided light with dielectric nanoantennas. *ACS Photonics*, *7*(3), 680-686.

[56] Samadi, M., Abshari, F., Algorri, J. F., Roldán-Varona, P., Rodríguez-Cobo, L., López-Higuera, J. M., ... & Dell'Olio, F. (2022, February). All-dielectric metasurface based on complementary split-ring resonators for refractive index sensing. In *Photonics* (Vol. 9, No. 3, p. 130). MDPI.

[57] Reena, R., Kalra, Y., Kumar, A., & Sinha, R. K. (2016). Tunable unidirectional scattering of ellipsoidal single nanoparticle. *Journal of Applied Physics*, *119*(24).

[58] Baranov, D. G., Makarov, S. V., Krasnok, A. E., Belov, P. A., & Alù, A. (2016). Tuning of near-and far-field properties of all-dielectric dimer nanoantennas via ultrafast electron-hole plasma photoexcitation. *Laser & Photonics Reviews*, *10*(6), 1009-1015.

[59] Sun, S., Li, M., Du, Q., Png, C. E., & Bai, P. (2017). Metal–dielectric hybrid dimer nanoantenna: Coupling between surface plasmons and dielectric resonances for fluorescence enhancement. *The Journal of Physical Chemistry C*, *121*(23), 12871-12884.

[60] Devilez, A., Stout, B., & Bonod, N. (2010). Compact metallo-dielectric optical antenna for ultra directional and enhanced radiative emission. *ACS nano*, *4*(6), 3390-3396.

[61] Rusak, E., Staude, I., Decker, M., Sautter, J., Miroshnichenko, A. E., Powell, D. A., ... & Kivshar, Y. S. (2014). Hybrid nanoantennas for directional emission enhancement. *Applied Physics Letters*, *105*(22), 221109.

[62] Lepeshov, S. I., Krasnok, A. E., Belov, P. A., & Miroshnichenko, A. E. (2019). Hybrid nanophotonics. Physics-Uspekhi, 61(11), 1035.

[63] Willets, K. A., & Van Duyne, R. P. (2007). Localized surface plasmon resonance spectroscopy and sensing. *Annu. Rev. Phys. Chem.*, *58*, 267-297.

[64] Cao, J., Sun, T., & Grattan, K. T. (2014). Gold nanorod-based localized surface plasmon resonance biosensors: A review. *Sensors and actuators B: Chemical*, *195*, 332-351.

CHAPTER-2

CHAPTER-2

NANOANTENNAS FOR ELECTRIC FIELD ENHANCEMENT*

2.1 Introduction

As discussed in the previous chapter, nanoantennas can be classified into plasmonic, dielectric and hybrid nanoantennas [1-3] of which plasmonic nanoantennas can convert localized energy into confined electric field due to localised surface plasmon resonance [4-6]. These localised surface plasmons overlap more in the gap between the two arms of the nanoantenna contributing to high electric field confinement. In this chapter, this property has been utilised for the designing of the nanoantenna to obtain high electric field which further can be used for various applications such as in the field of solar energy harvesting [10-12], optical sensors [13], surface-enhanced Raman spectroscopy [14, 15], optical data storage and optical circuits [16,17]

*****Part of the results reported in this chapter has been published in the journal/conference proceedings

1. "Petal shaped nanoantenna for solar energy harvesting." Journal of Optics 22.3, 035001 (2020).

2. "Design of hexameric flower shaped nanoantenna for energy harvesting" In AIP Conference Proceedings, vol. 2136, no. 1, p. 030005. AIP Publishing, 2019.

3. "Design of arrow-shaped nanoantenna for electric field enhancement" In Plasmonics: Design, Materials, Fabrication, Characterization, and Applications XVII, vol. 11082, p. 1108229. International Society for Optics and Photonics, 2019.

4. "Field enhancement in a tapered cone dipole nanoantenna", Proceedings of IEEE International Conference on Photonics & High Speed Optical Networks (ICPHON 2018), 12-13 April 2018, S. A. Engineering College, Chennai, India.

and many more. Bailey et al. had proposed the concept of rectenna in which antenna can be coupled to a rectifier/ diode to convert induced ac power into dc power [18]. In some notable experimental works, the performance of the nanoantennas has been experimentally tested by calculating the extinction coefficient and electric field enhancement [19-23]. One of the application of nanoantennas in solar energy harvesting has been discussed thoroughly in this chapter. Various designs of nanoantennas namely Petal shaped nanoantenna, Hexameric flower shaped nanoantenna, Arrow shaped nanoantenna, and Tapered cone dipole shaped nanoantenna have been proposed and discussed thoroughly for solar energy harvesting application.

Energy from the sun is the most abundant and freely available energy on the earth's surface. From years photovoltaic (PV) solar cells have been used for solar energy harvesting but there are certain limitations in their use. One of them is their low efficiency. Single PV cell has a conversion efficiency of approximately 29% and multi-junction cells have a conversion efficiency of 46% approximately [27]. The reason for this is low efficiency is that when light strikes on a PV solar cell, photons having energy higher than the bandgap of the semiconductor are absorbed. The rest of the energy is converted into heat rather than being converted into useful electrical energy. Hence, only a small region of the spectrum is utilized. The efficiency is also affected by input light, surface area, weather conditions, and the polarization of light [7-9]. One of the promising alternatives of a solar cell can be a nanoantenna that converts electromagnetic light into electrical power over a large bandwidth of the solar spectrum.

In this chapter, the solar energy harvesting capability has been investigated by computing radiation efficiency and field enhancement in the optical spectrum. The performance of nanoantenna for energy harvesting largely depends upon the radiation efficiency and electric field generated inside the feed gap of the nanoantenna. Hence, the effects of geometrical as well as material parameters on these two characteristics have been discussed extensively. The rest of the chapter has been divided into two sections. Section 2.2 discusses the design of petal

shaped nanoantenna which is further divided into several sub sections that discuss the design of the proposed structure in terms of geometrical parameters, the modelling technique, and the analyses of the results obtained. Section 2.3 presents the various other designs of nanoantenna namely Hexameric flower shaped nanoantenna, Arrow shaped nanoantenna, Tapered cone dipole shaped nanoantenna for field enhancement. Finally, the chapter is concluded in section 2.4.

2.2 Petal shaped nanoantennas

2.2.1 The fundamental principle

The designed petal shaped nanoantenna is a structural intermediate of dipole and dimer nanoantenna design. It has been referred to as petal shaped nanoantenna on the account of its petal shaped arms. Figure 2.1 shows the schematic design of the proposed nanoantenna indicating the significant geometrical parameters, i.e. antenna arm length *l*, width *w*, height *h* and gap between the two arms *g*. The proposed structure has been analyzed with respect to all the above-mentioned geometrical parameters. Further, the performance of the nanoantenna has been analysed for different materials such as gold (Au), silver (Ag), copper (Cu) and aluminium (Al). The data for the permittivity of materials have been adapted from Johnson and Christy [24].

The interest in the optical spectrum is inspired by the fact that most of the solar radiation is concentrated in this region, with its peak value at approximately 500 nm. According to Planck's law of black body radiation, power radiated by a black body as a function of wavelength and temperature is given by

$$P(\lambda, T) = \frac{2hc^2}{\lambda^5} \frac{1}{e^{\frac{hc}{\lambda kT}} - 1} \tag{2.1}$$

where, h is the Planck's constant, k is Boltzmann constant and T is the absolute temperature of the black body, λ is the wavelength and c is the speed of light in free space. Figure 2.2 shows the solar spectrum i.e. normalized intensity vs wavelength curve computed according to Planck's law by considering sun as a black body with the surface temperature equal to 5777 K. It can be noticed from the figure 2.2 that the spectral peak occurs at 500 nm which corresponds to the maximum irradiance.

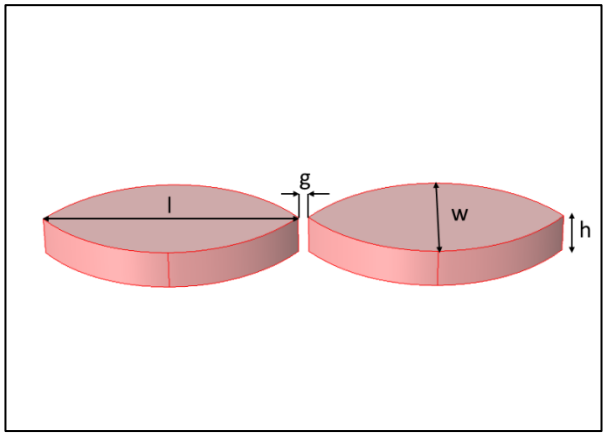

Figure 2.1 Design of the petal shaped nanoantenna

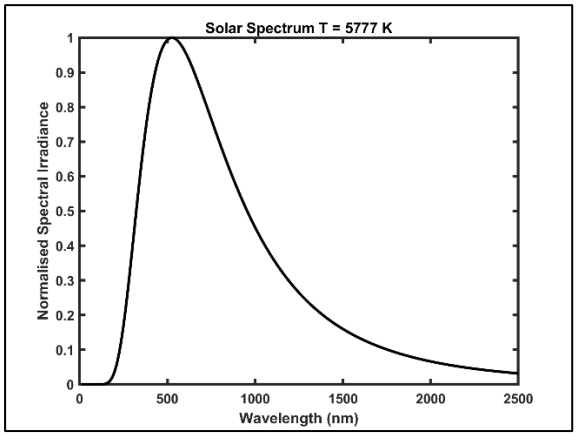

Figure 2.2 Solar energy spectrum

When the light falls on the nanoantenna, some part of the energy is re-radiated and some is absorbed. The two most important factors on which the performance of the nanoantenna in solar energy harvesting applications depends are radiation efficiency and electric field enhancement. The radiation efficiency, denoted by η_{rad}, is defined as the ratio of the power radiated by the nanoantenna to the total incident power [1]. Mathematically,

$$\eta_{rad} = \frac{P_{rad}}{P_{rad}+P_{ab}} \tag{2.2}$$

where, P_{rad} is the power radiated by the nanoantenna and P_{ab} is the power absorbed by it. P_{rad} can be controlled by varying the size, hence, the effective surface area of the nanoantenna. More is the effective surface area, greater is the light gathering capability of the nanoantenna, and hence, greater is the radiation efficiency. Radiation efficiency is important because

harvested power will increase accordingly. However, the total harvested power depends not only on the radiation efficiency but also on the spectral irradiance through the spectrum. Hence, combining Planck's law with radiation efficiency, the harvesting efficiency of the nanoantenna (η_{total}) is defined as

$$\eta_{total} = \frac{\int_0^\infty P(\lambda)\eta_{rad}d\lambda}{\int_0^\infty P(\lambda)d\lambda} \tag{2.3}$$

The harvesting efficiency is the direct measure of usable output power extracted from radiation falling on the nanoantenna.

2.2.2 Design and its advantage

The peculiarity of the petal shape is that it, being an intermediate structure, has partial characteristics of both – dimer as well as dipole nanoantennas. Figure 2.3 (a) shows the designs of three types of nanoantennas. The figure 2.3 (b) and 2.3 (c) clearly indicate that the best field enhancement but lowest radiation efficiency among the three is achieved in the dipole nanoantenna and whereas the disc-shaped nanoantenna shows best radiation efficiency and lowest electric field enhancement. Interestingly, the proposed petal shaped structure exhibits fairly high field enhancement and radiation efficiency.

The high field enhancement is attributed to the pointedness of the structure in the gap region, while high radiation efficiency is attributed to the large surface area offered to the incident radiation. The dipole nanoantenna design has the most pointed edge in the gap region but offers the least surface area to the incident radiation and, hence, it provides maximum enhancement but minimum radiation efficiency. On the other extreme end, the disc structure has a round edge but offers maximum surface area, hence, it has the lowest enhancement but maximum efficiency. The petal shaped nanoantenna, being an intermediate design, has pointed edges in the gap region and has greater surface area than a dipole. Consequently, its results lie in

between the other two and it offers good field enhancement and radiation efficiency. This discourse proves that the proposed structure is a better candidate than the other two.

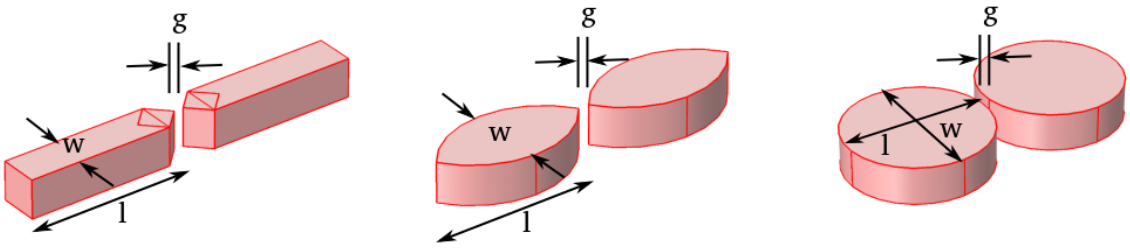

Dipole shaped
l = 120 nm, w = 40 nm

Petal shaped
l = 150 nm, w = l/2

Disc shaped
l = 137.5 nm, w=l

(a)

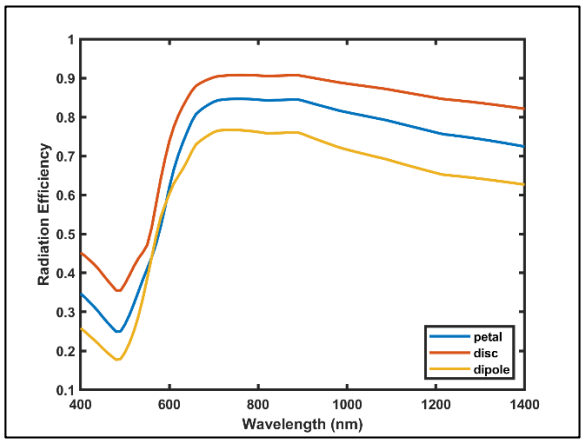

(b)

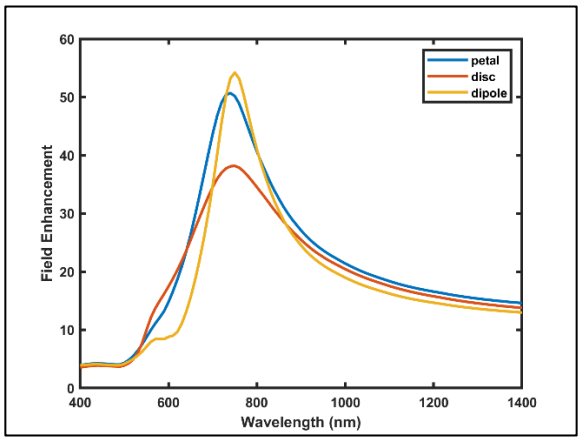

(c)

Figure 2.3 Comparison of the proposed design with dipole and disc-shaped nanoantennas (a) geometry, (b) Variation of radiation efficiency with wavelength, (c) Variation of Electric field enhancement with wavelength.

The proposed nanoantenna has been designed and analyzed using finite element method (FEM) based COMSOL Multiphysics software. Plane polarised light, polarised along x-axis is allowed to fall on the nanoantenna with electric field along the direction of length 'l' of the nanoantenna. In all the computations, non-uniform meshing has been used. While an extra-fine mesh, with a minimum element size of 1.5 nm and maximum element size of 35 nm, has been used for modelling of nanoantenna. The thickness of the PML has been kept 150 nm. Value for permittivity for gold and other material has been taken from experimental data provided by Johnson and Christy [24].

2.2.3 Results and Discussion

2.2.3.1 Effect of length *l*

Length of the nanoantenna is the main factor on which the resonant wavelength depends. The structure can be tuned to operate at different wavelengths, simply by changing the length *l*. In order to study the effect of length, the radiation efficiency and field enhancement have been calculated for different sizes of the nanoantenna. The length has been varied from 100 nm to 250 nm, keeping $w=l/2$, h=40 nm and g=10 nm, in all the cases.

Figure 2.4(a) shows the variation of radiation efficiency with respect to wavelength for different lengths of the antenna arm. An increase in length results in an increase in effective surface area available for the reception of incident radiation. Hence as the length increases the radiation efficiency (or radiation gathering capability) increases, as seen in figure 2.4(a). Further, the increase in length causes a prominent redshift in the field enhancement peak as shown in figure 2.4(b). This is a direct consequence of the redshift in the localized surface plasmon resonance on increasing the dimension parallel to the incident electric field. Maier (2007) gives a detailed account of the plasmon resonance of metallic nanoparticles by presenting polarizability as a function of particle size and its dielectric constant [4]. Thus, the designed nanoantenna can be tuned to different wavelengths by simply varying the length 'l' of the nanoantenna. For a conventional dipole antenna, the resonant wavelength is twice its length, but at the nanoscale, this relation does not hold good.

Harvesting efficiency has also been calculated for different values of length 'l' of petal shaped nanoantenna using equation 2.3. The output values of harvesting efficiency for different values of length *l* of petal shaped nanoantenna are listed in table 2.1. As harvesting efficiency depends on the radiation efficiency, greater the radiation efficiency greater is the harvesting efficiency. Maximum harvesting efficiency obtained is 0.7458 which corresponds to the 250 nm length of the nanoantenna.

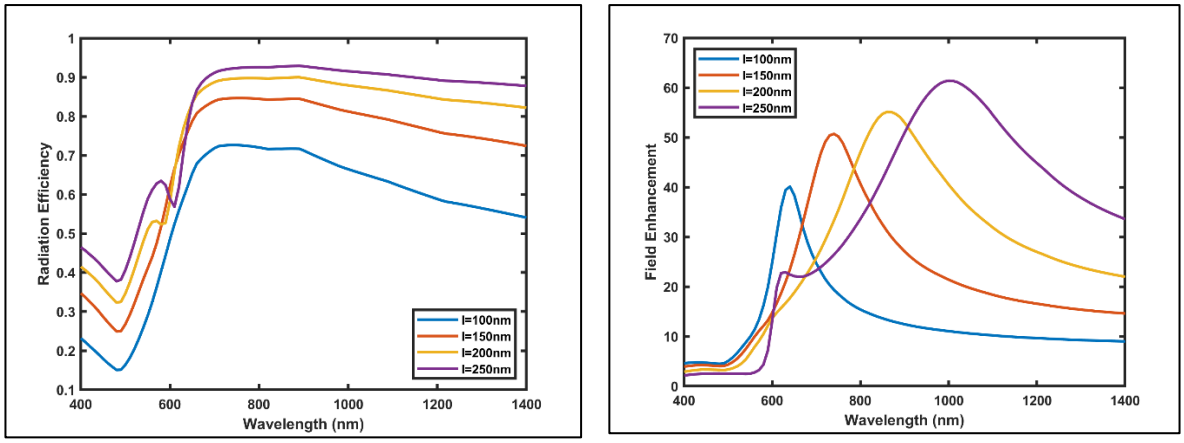

(a) (b)

Figure 2.4 (a) Variation of radiation efficiency and (b) electric field enhancement with wavelength for different length *l* of the petal shaped nanoantennas.

TABLE 2.1. Harvesting efficiency for different values of length *l* of the petal shaped nanoantenna

Length (*l*)	**100nm**	**150nm**	**200nm**	**250nm**
Harvesting Efficiency	0.5175	0.6484	0.7088	0.7458

2.2.3.2 Effect of width *w*

Besides length, width *w* is also an important parameter which needs contemplation. Variation in width alters the pointedness of the structure hence directly affects the field enhancement. Effect of width has been studied by setting different values, i.e. $w = l, l/2, l/3, l/4, l/5$, keeping *l* constant at 150 nm. When $w = l$, the structure is simply disc-shaped, whereas, for $w = l/5$ the antenna arms become so thin that it resembles a dipole nanoantenna. Consequently, when $w = l$, maximum radiation efficiency (>90%) and minimum field enhancement (~40) is achieved, whereas, for $w = l/5$, the radiation efficiency is minimum (<70%) and field enhancement is maximum (~85 times), as shown in figure 2.5 (a) and (b). For all other intermediate values of *w*, the radiation efficiency and field enhancement lie between the above-mentioned extremities and the structure remains petal shaped.

This analysis exhibits the trend that as the width of the nanoantenna is reduced, keeping the length constant, radiation efficiency decreases due to a reduction in effective surface area, but field enhancement increases because of the improvement in pointedness (i.e. reduction of tip angle) of the arm. Sharp corners are always the site of near field enhancement due to the lightning rod effect, as explained in rigorous detail by Liao and Wokaun [25]. Hence as the aspect ratio (length/width) becomes more skewed, the corners become sharper and the field at the tip becomes more enhanced [25, 26].

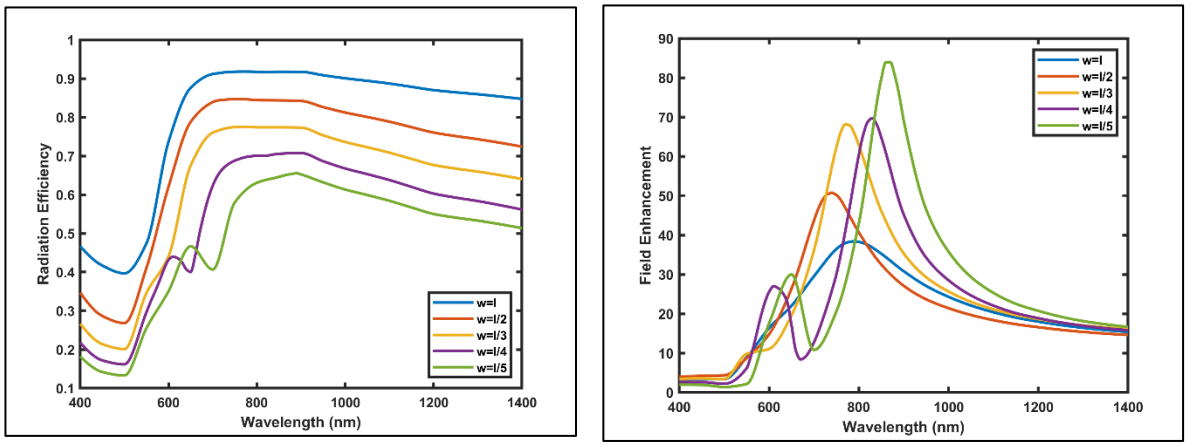

(a) (b)

Figure 2.5 (a) Variation of radiation efficiency and (b) electric field enhancement with wavelength for different width *w* of the petal shaped nanoantenna.

Harvesting efficiency calculated for different values of width *w* has been calculated keeping other parameters constant. Table 2.2 shows the obtained harvesting efficiency for different values of the width *w* of petal shaped nanoantenna. Maximum harvesting efficiency obtained is 0.7450 which corresponds to the design when the width equals to the length of the nanoantenna, which is the case of a nanodisc.

TABLE 2.2. Harvesting efficiency for different values of width *w* of the petal shaped nanoantenna

Width (*w*)	***w= l***	***w= l*/2**	***w= l*/3**	***w= l*/4**	***w=l*/5**
Harvesting Efficiency	0.7450	0.6497	0.5642	0.4874	0.4285

2.2.3.3 Effect of height *h*

The height *h* of the nanoantenna has been varied from 20 nm to 100 nm, keeping *l* = 150 nm and *w*= *l*/2. The variation of radiation efficiency and electric field enhancement with variation of wavelength for different values of *h* has been shown in figure 2.6 (a) and 2.6 (b) respectively.

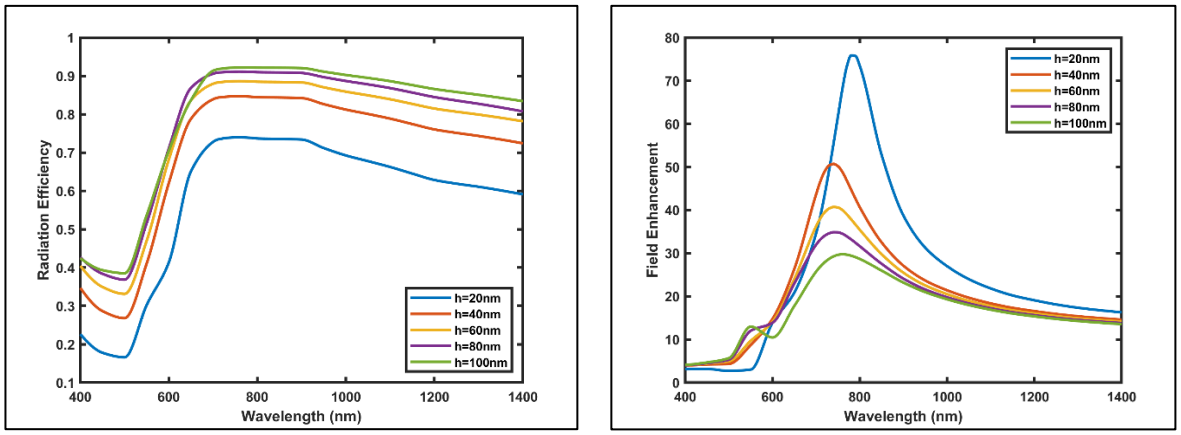

(a) (b)

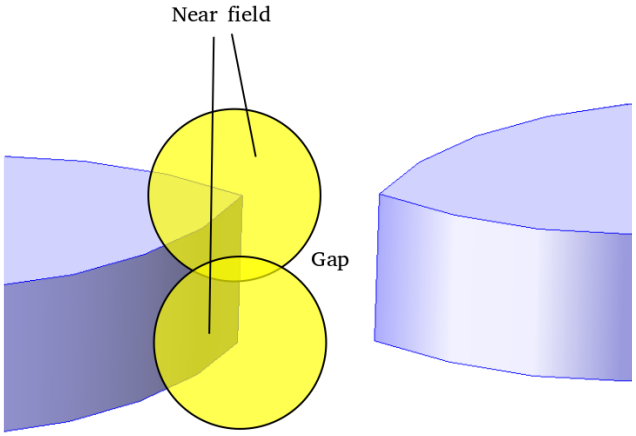

(c)

Figure 2.6 (a) Variation of radiation efficiency and (b) electric field enhancement with respect to wavelength for different value of the height *h* of nanoantenna (c) local field overlap at the corners of single arm of the petal shaped nanoantenna.

A change in height *h* of the nanoantenna not only alters its surface area but also controls the field enhancement by altering the extent of overlap between localized surface plasmons at the top and bottom corners of the antenna tip (as shown in figure 2.6(c)). Hence, as the antenna height *h* increases from 20 nm to 100 nm, though the surface area increases, the overlap of the localized surface plasmons becomes poorer. As a direct consequence, the radiation efficiency increases but field enhancement decreases, substantially.

The value of height *h* of the nanoantenna has been varied and corresponding harvesting efficiency is listed in table 2.3. Maximum harvesting efficiency obtained is 0.7406 which corresponds to the height equal to the 100 nm.

TABLE 2.3. **Harvesting efficiency for different values of height *h* of the petal shaped nanoantenna**

Height (*h*)	**20 nm**	**40 nm**	**60 nm**	**80 nm**	**100 nm**
Harvesting Efficiency	0.5268	0.6497	0.7012	0.7317	0.7406

2.2.3.4 Effect of gap *g*

The gap *g* between the antenna arms is the location of the enhanced electric field, whose magnitude directly depends upon the gap size. Figure 2.7 shows the results of numerical analysis in which gap '*g* has been varied from 5 nm to 40 nm. The smaller the gap is, the better is the overlap between the localized surface plasmons at tips of the two arms (figure 2.7(c)), and hence, greater is the magnitude of the field enhancement obtained. However, since the surface area is not affected by the change in gap size, the radiation efficiency is practically independent of it. While on one hand, the radiation efficiency remains practically unaffected by it, on the other side, a drastic reduction in field enhancement takes place. This is in absolute agreement with expectations based on the reasoning presented above. Harvesting efficiency calculated and has listed in Table 2.4 for different values of gap *g* between two arms of the petal shaped nanoantenna. The value of harvesting efficiency is nearly same in all cases.

TABLE 2.4. **Harvesting efficiency for different values of the gap *g* of the petal shaped nanoantenna**

Gap (*g*)	**5 nm**	**10 nm**	**20 nm**	**30 nm**	**40 nm**
Harvesting Efficiency	0.6351	0.6497	0.6553	0.6552	0.6545

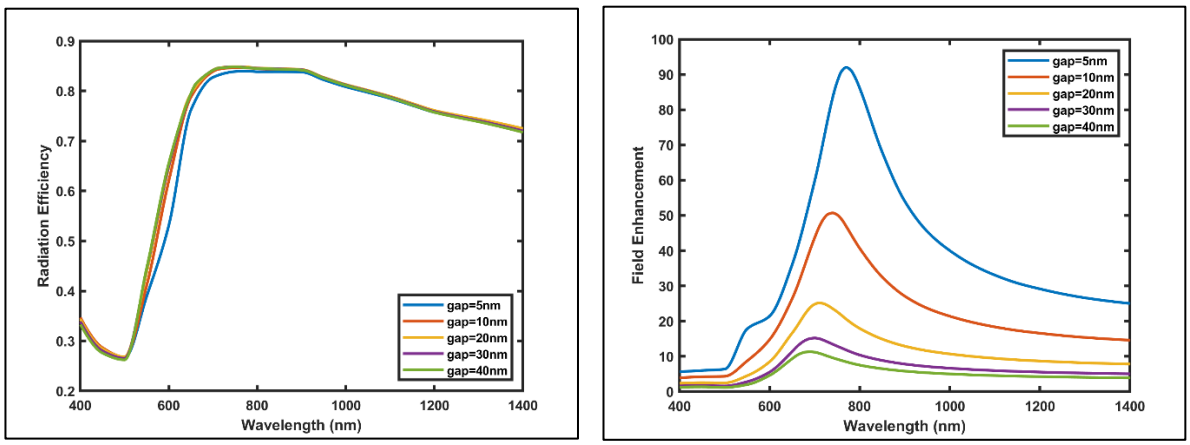

(a) (b)

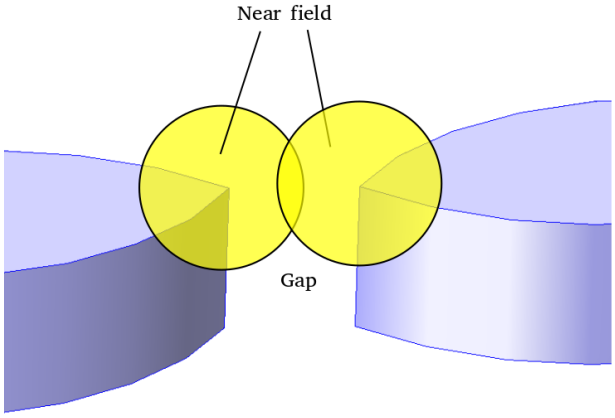

(c)

Figure 2.7 (a) Variation of radiation efficiency and (b) electric field enhancement by varying the tip to tip gap *g* between two nanoantennas (c) local field overlap at the corners of the two arms of the petal shaped nanoantenna.

2.2.3.5 Effect of material

The entire analysis presented above has been aimed at demonstrating the effect of geometrical parameters on the operation and performance of the nanoantenna. Besides the geometry, the choice of the materials also effects the working and performance of the device. In all the computational results presented in the article so far, gold (Au) has been taken as the material of the device. However, there are other highly conductive materials such as silver (Ag), aluminium (Al) and copper (Cu), whose candidature for device fabrication is worth investigation.

For this analysis the length *l*, the width *w*, the height *h* and the gap *g* of the nanoantenna have been taken to be 150 nm, 75 nm (*l*/2), 40 nm and 10 nm respectively. Figure 2.8 (a) and 2.8 (b) shows the variation of radiation efficiency and electric field enhancement with wavelength for Au, Ag, Al and Cu. Along with radiation efficiency and electric field enhancement, harvesting efficiency has also been calculated for the different materials. Table 2.5 shows the value of obtained harvesting efficiency which corresponds to the different constituting material of the nanoantenna.

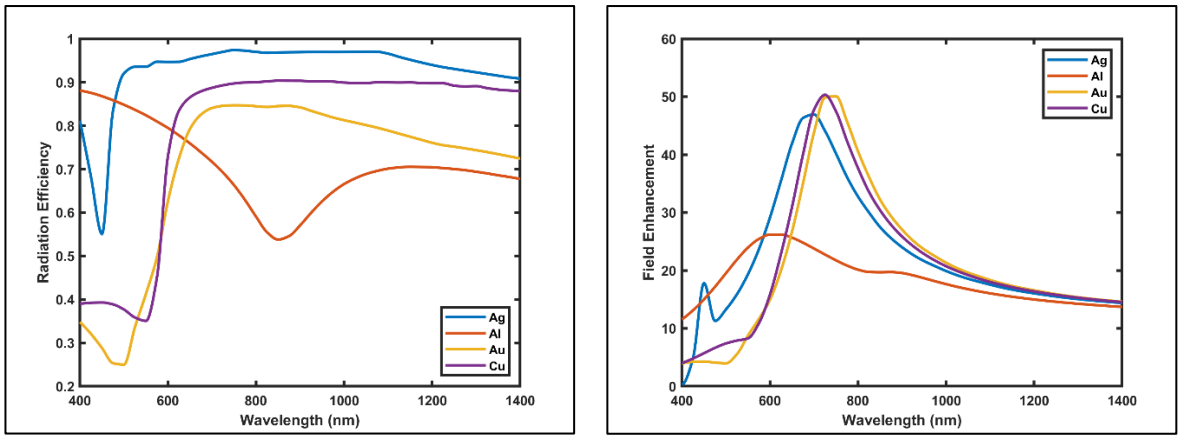

(a) (b)

Figure 2.8 (a) Variation of radiation efficiency and (b) Variation of electric field enhancement with respect to wavelength for different materials for the petal shaped nanoantenna.

The graphs indicate that the silver is the best performer in terms of radiation efficiency. Also, its shows maximum harvesting efficiency i.e. 0.9174. However, its high reactivity makes it unsuitable for longer use. Gold, however is the most popular material for nanoantenna fabrication due to its chemical inertness, falls short in terms of radiation and harvesting efficiencies. Interestingly, copper and aluminium turn out as moderate performers whose radiation and harvesting efficiencies lie in between the other two.

TABLE 2.5. Harvesting efficiency for different materials of the petal shaped nanoantenna

Material	**Ag**	**Al**	**Au**	**Cu**
Harvesting Efficiency	0.9174	0.7312	0.6491	0.7216

2.3 Other Designs of Nanoantenna

2.3.1 Hexameric Flower Shaped Nanoantenna

2.3.1.1 Design

The hexameric flower shaped nanoantenna has six arms with arm's length of 360 nm, the angle between the adjacent arm of 60° and a gap of 10 nm between each of the opposite arms of nanoantenna as shown in figure 2.9. Gold has been used for designing nanoantenna. Drude model has been used for defining permittivity of gold for optical and infrared wavelength.

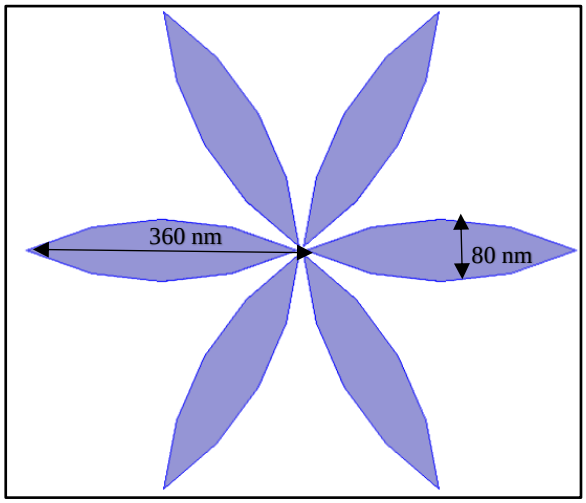

Figure 2.9 The design of hexameric flower shaped nanoantenna

2.3.1.2 Results

The variation of electric field with wavelength has been studied. An input power of 1 V/m has been made incident on the hexameric flower shaped nanoantenna and the distribution of the electric field at the resonant wavelength as illustrated in figure 2.10. The maximum electric field is accumulated at centre as shown in figure 2.10.

The proposed nanoantenna has been investigated over a range of 450 to 850 nm. The resonant wavelength for the reported hexameric flower shaped nanoantenna is 680 nm. At this wavelength reported antenna shows the maximum response for the electric field as shown in Figure 2.11. Radiation efficiency curve with respect to wavelength has been shown in figure 2.12. Maximum radiation efficiency obtained is 72%.

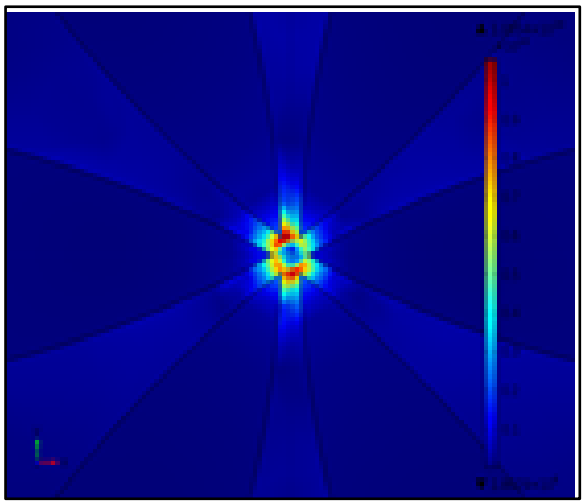

Figure 2.10 Electric field enhancement at the center gap of the hexameric flower shaped nanoantenna at the resonant wavelength.

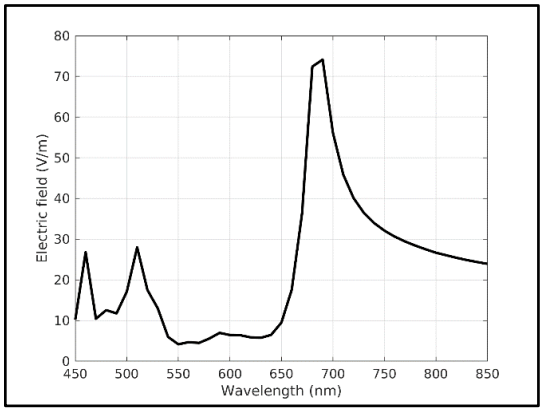

Figure 2.11 Variation of the electric field with a wavelength for the hexameric flower shaped nanoantenna

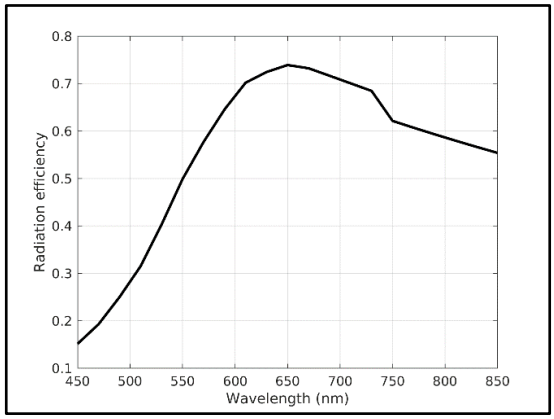

Figure 2.12 Variation of Radiation efficiency with wavelength for the hexameric flower shaped nanoantenna

2.3.2 Arrow shaped nanoantennas

2.3.2.1 Design

The proposed arrow shaped nanoantenna consists of four arms made up of gold in the shape of arrow as shown in figure 2.13. The gap between the two opposite arms of nanoantenna has been taken to be 10 nm. The length of the each arm of nanoantenna 'l' is taken to be 225 nm, height of the antenna 'h' is taken to be 50 nm, tip angle of the proposed nanoantenna theta 'θ' is taken to be 45˚.

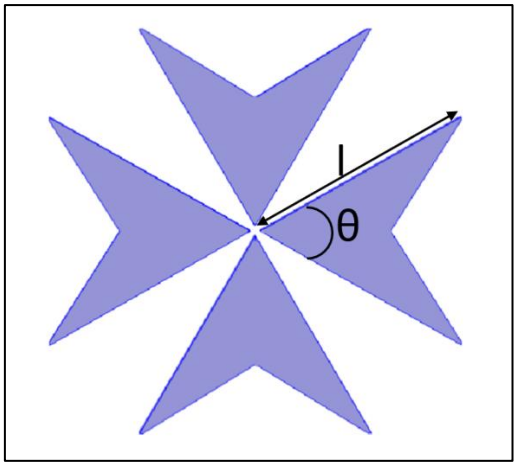

Figure 2.13 Design of the arrow shaped nanoantenna.

2.3.2.2 Numerical Analysis

The electromagnetic radiation is made incident on arrow shaped nanoantenna from the top with electric field along the x-axis, the surface plasmons are observed in the gap region of the nanoantenna. The electric field distribution at the resonance wavelength is shown in figure 2.14. The electric field enhancement with varying wavelength is shown in the figure 2.15. The resonance wavelength is observed at 1088 nm.

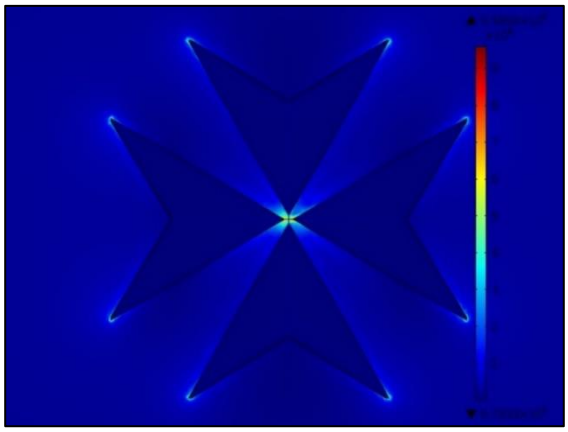

Figure 2.14 Electric field distribution in the gap region of arrow shaped nanoantenna at resonant wavelength.

The variation of radiation efficiency of nanoantenna with respect to wavelength has been shown in figure 2.16. It has been observed from the plot that proposed nanoantenna gives the radiation efficiency more than 80%.

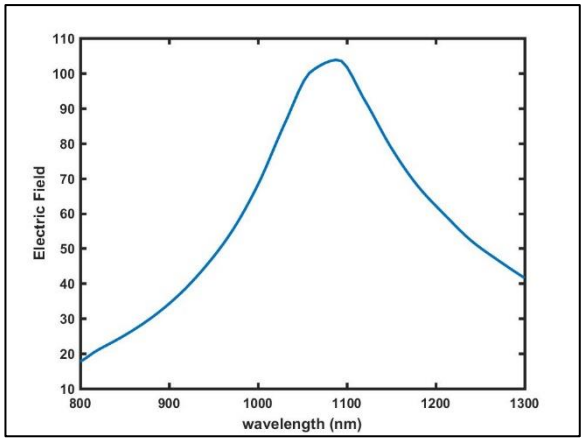

Figure 2.15 Variation of electric field enhancement with wavelength for the arrow shaped nanoantenna

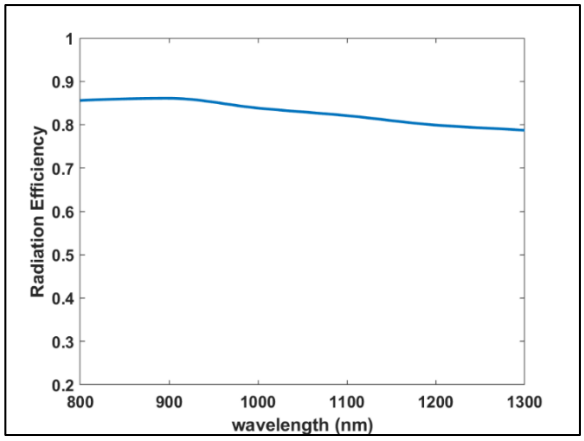

Figure 2.16 Variation of radiation efficiency with wavelength for arrow shaped nanoantenna

2.3.3 Tapered Cone Dipole nanoantenna

2.3.3.1 Design

The proposed antenna has total length of 500 nm, bottom radius is 100 nm, bottom radius of second layer is 58 nm and bottom radius of third layer is 20 nm, smallest radius at the tip is 6 nm. The aperture angle of cone tapered antenna has been taken as 10^0. The schematic diagram of the tapered cone shaped nanoantenna design is shown in figure 2.17.

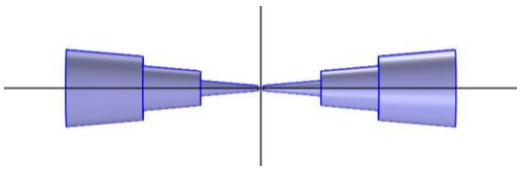

Figure 2.17 Design of tapered cone dipole antenna

2.3.3.2 Numerical analysis

An input power is made incident on the antenna and the surface plasmons are formed in the central gap region of the nanoantenna. The field enhancement in the feed gap at resonant wavelength is observed. The various parameters like electric field distribution in the feed gap of nanoantenna, electric field enhancement, and radiation efficiency have been analyzed. Figure 2.18 shows the electric field distribution in the in the tapered cone dipole nanoantenna.

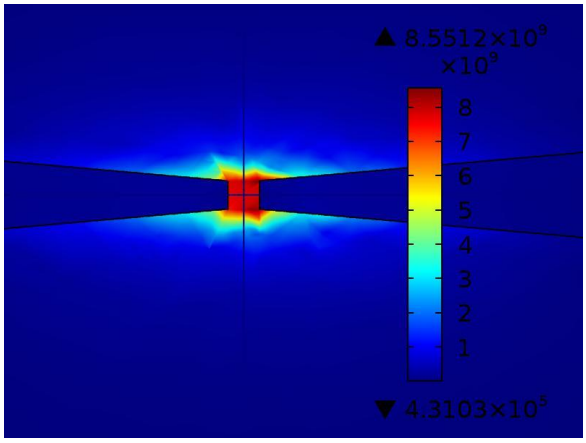

Figure 2.18 Electric field enhancement in the feed gap of the tapered cone dipole nanoantennas.

The electric field enhanced due to nanoantenna has been shown in figure 2.19 with the variation of wavelength. The variation of electric field enhancement and radiation efficiency has been shown in figure 2.19 and figure 2.20 respectively. The structure shows maximum of 94% radiation efficiency beyond 1600 nm wavelength.

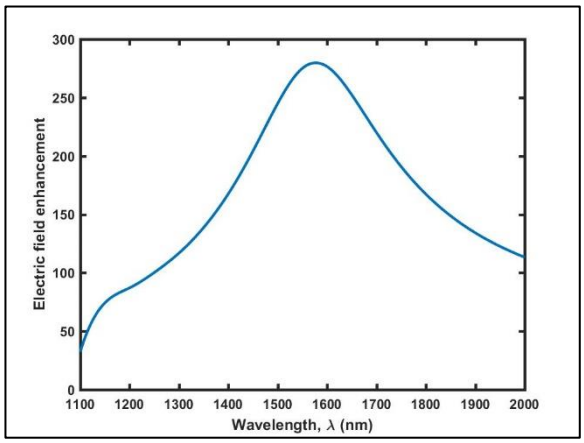

Figure 2.19 Variation of electric field with respect to wavelength for the tapered cone shaped nanoantenna

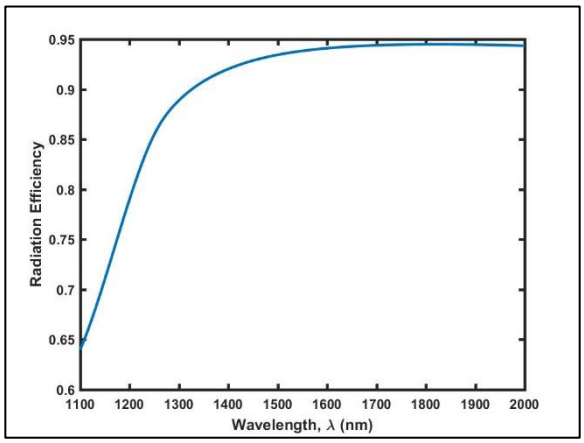

Figure 2.20 Variation of radiation efficiency with respect to wavelength for the tapered cone dipole nanoantenna

2.4 Conclusion

Different types of nanoantennas namely petal shaped nanoantenna, arrow shaped nanoantenna, hexameric flower shaped nanoantenna, and tapered cone dipole antenna have been successfully designed. The two important parameters, radiation efficiency and electric field enhancement, have been studied in detail with respect to all the geometrical and material parameters, which

largely contribute to harvesting solar energy. The electric field get enhanced and confined in the feed gap region between the arms of the proposed nanoantennas. More than 70% radiation efficiency is observed for flower shaped nanoantennas, 80% for arrow nanoantennas, 94% for the tapered cone dipole nanoantenna and 90% for optimized design of petal shaped nanoantennas. Maximum of 74% of harvesting efficiency is obtained for optimized design of petal shaped nanoantennas which makes it suitable candidate for solar energy harvesting. Other than this, the proposed nanoantennas hold a potential in a wide variety of applications such as surface enhanced spectroscopy, sensing and integrated optics.

References

[1] Shankhwar, N., Kalra, Y., & Sinha, R. K. (2017). LiTaO3 based metamaterial perfect absorber for terahertz spectrum. *Superlattices and Microstructures*, *111*, 754-759.

[2] Reena, Kalra, Y., Kumar, A., & Sinha, R. K. (2016). Tunable unidirectional scattering of ellipsoidal single nanoparticle. *Journal of Applied Physics*, *119*(24), 243102.

[3] Rusak, E., Staude, I., Decker, M., Sautter, J., Miroshnichenko, A. E., Powell, D. A., ... & Kivshar, Y. S. (2014). Hybrid nanoantennas for directional emission enhancement. *Applied Physics Letters*, *105*(22), 221109.

[4] Maier, S. A. (2007). *Plasmonics: fundamentals and applications* (Vol. 1, p. 245). New York: springer.

[5] Zheng, P., Kasani, S., & Wu, N. (2019). Converting plasmonic light scattering to confined light absorption and creating plexcitons by coupling a gold nano-pyramid array onto a silica–gold film. *Nanoscale horizons*, *4*(2), 516-525.

[6] Pors, A., Albrektsen, O., Radko, I. P., & Bozhevolnyi, S. I. (2013). Gap plasmon-based metasurfaces for total control of reflected light. *Scientific reports*, *3*(1), 1-6.

[7] Krasnok, A. E., Maksymov, I. S., Denisyuk, A. I., Belov, P. A., Miroshnichenko, A. E., Simovski, C. R., & Kivshar, Y. S. (2013). Optical nanoantennas. *Physics-Uspekhi*, *56(6)*, 539.

[8] Gosciniak, J., & Rasras, M. (2019). High field enhancement between transducer and resonant antenna for application in bit patterned heat-assisted magnetic recording. *Optics Express*, *27*(6), 8605-8611.

[9] Green, M., Dunlop, E., Hohl-Ebinger, J., Yoshita, M., Kopidakis, N., & Hao, X. (2021). Solar cell efficiency tables (version 57). *Progress in photovoltaics: research and applications*, *29*(1), 3-15.

[10] El-Toukhy, Y. M., Hussein, M., Hameed, M. F. O., Heikal, A. M., Abd-Elrazzak, M. M., & Obayya, S. S. A. (2016). Optimized tapered dipole nanoantenna as efficient energy harvester. *Optics Express*, *24*(14), A1107-A1122.

[11] El-Toukhy, Y. M., Hussein, M., Hameed, M. F. O., & Obayya, S. S. A. (2018). Characterization of asymmetric tapered dipole nanoantenna for energy harvesting applications. *Plasmonics*, *13*(2), 503-510.

[12] Grover, S., & Moddel, G. (2013). Metal single-insulator and multi-insulator diodes for rectenna solar cells. In *Rectenna solar cells* (pp. 89-109). Springer, New York, NY.

[13] Mubarak, M. H., Sidek, O., Abdel-Rahman, M. R., Mustaffa, M. T., Mustapa Kamal, A. S., & Mukras, S. M. (2018). Nano-antenna coupled infrared detector design. *Sensors*, *18*(11), 3714.

[14] Neubrech, F., Huck, C., Weber, K., Pucci, A., & Giessen, H. (2017). Surface-enhanced infrared spectroscopy using resonant nanoantennas. *Chemical reviews*, *117*(7), 5110-5145.

[15] Nien, L. W., Lin, S. C., Chao, B. K., Chen, M. J., Li, J. H., & Hsueh, C. H. (2013). Giant electric field enhancement and localized surface plasmon resonance by optimizing contour bowtie nanoantennas. *The Journal of Physical Chemistry C*, *117*(47), 25004-25011.

[16] Gosciniak, J., & Rasras, M. (2019). High field enhancement between transducer and resonant antenna for application in bit patterned heat-assisted magnetic recording. *Optics Express*, *27*(6), 8605-8611.

[17] Shiono, T., Matsuzaki, K., & Furumiya, S. (2013). Near-field recording on phase-change nanoparticles and reflective reproduction from nanoantenna utilizing plasmonic resonance for high-density optical memory. *Optics Express*, *21*(21), 25532-25543.

[18] Bailey, R. L. (1972). A proposed new concept for a solar-energy converter.

[19] Gadalla, M. N. (2013). *Nano Antenna Integrated Diode (Rectenna) For Infrared Energy Harvesting* (Doctoral dissertation).

[20] Gadalla, M. N., Abdel-Rahman, M., & Shamim, A. (2014). Design, optimization and fabrication of a 28.3 THz nano-rectenna for infrared detection and rectification. *Scientific reports*, *4*(1), 1-9.

[21] Ding, W., Bachelot, R., Kostcheev, S., Royer, P., & Espiau de Lamaestre, R. (2010). Surface plasmon resonances in silver Bowtie nanoantennas with varied bow angles. *Journal of Applied Physics*, *108*(12), 124314.

[22] Chen, S. W., Huang, Y. H., Chao, B. K., Hsueh, C. H., & Li, J. H. (2014). Electric field enhancement and far-field radiation pattern of the nanoantenna with concentric rings. *Nanoscale Research Letters*, *9*(1), 1-8.

[23] Hussein, M., Areed, N. F. F., Hameed, M. F. O., & Obayya, S. S. A. (2014). Design of flower-shaped dipole nano-antenna for energy harvesting. *Iet Optoelectronics*, *8*(4), 167-173.

[24] Johnson, P. B., & Christy, R. W. (1972). Optical constants of the noble metals. *Physical review B*, *6*(12), 4370.

[25] Liao, P. F., & Wokaun, A. (1982). Lightning rod effect in surface enhanced Raman scattering. *The Journal of Chemical Physics*, *76*(1), 751-752.

[26] Sturman, B., Podivilov, E., & Gorkunov, M. (2013). Metal nanoparticles with sharp corners: Universal properties of plasmon resonances. *EPL (Europhysics Letters)*, *101*(5), 57009.

[27] Essig, S., Allebé, C., Remo, T., Geisz, J. F., Steiner, M. A., Horowitz, K., ... & Tamboli, A. (2017). Raising the one-sun conversion efficiency of III–V/Si solar cells to 32.8% for two junctions and 35.9% for three junctions. *Nature Energy*, *2*(9), 1-9.

CHAPTER-3

CHAPTER-3

NANOANTENNA AS MAGNETIC DEVICE IN INFRARED FREQUENCY REGION *

3.1 Introduction

In the previous chapter nanoantennas were designed to obtain high electric field [1-6]. In this chapter, we report another interesting application of nanoantennas which is magnetic field enhancement. Ferromagnetic materials are widely used for obtaining strong magnetic field but magnetism cannot be achieved at optical frequency. There are two main reasons for that. One is the effect of magnetic component on permeability is negligible at this range [7]. Another reason that prohibits magnetism in this range is that the energy difference between two magnetic energy levels corresponds to radio frequency rather than visible frequency [8]. Hence, to obtain a magnetic field in the optical regime, other alternatives are required. Optical nanoantennas can serve as one of the alternatives. The enhanced magnetic field can open doors to their potential application in magnetic sensors in the optical range, in surface-enhanced

*****Part of the results reported in this chapter has been published in the journal/conference proceeding

1. "Design of hourglass nanoantenna for magnetic field enhancement." Optics Communications 481, 126511 (2021).

2. "Design of nanoantenna for magnetic field enhancement" Plasmonics: Design, Materials, Fabrication, Characterization, and Applications XVIII. Vol. 11462. SPIE, 2020.

infrared absorption (SEIRA), magnetic imaging and enhanced spectroscopy applications [9, 10].

In 2011, T. Grosjean et. al. proposed a diabolo nanoantenna design, wherein two arms of bowtie nanoantenna were connected by the bridge by using Babinet's principle, for magnetic field enhancement [11]. Later on, in 2012, polarization-independent cross diabolo was introduced by Zhen Gao [12]. As a further improvement, broken diabolo was proposed by Zaihe Yu which confines and enhances both magnetic as well as electric fields simultaneously [13]. Dielectric nanoantennas have also been developed for magnetic field enhancement [14] whose low loss nature is seen as a great advantage. Some applications of the nanoantennas in vortex trapping, optical trapping by nanoparticles have also been demonstrated by some authors [15-18].

In this chapter, we propose two designs of plasmonic nanoantennas namely hourglass shaped nanoantennas and rhombic shape nanoantennas for the magnetic field enhancement. Mechanism for obtaining resonance wavelength and magnetic field is explained in sec 3.2. In sec 3.3, design, working principle and modelling of hourglass shaped nanoantenna is explained. Further, the design has been studied for various geometrical parameters for magnetic field enhancement. Similarly, design and study of results for magnetic field enhancement, obtained by varying geometrical parameters of rhombic shape nanoantennas has been explained in sec 3.4. Finally, the conclusion is drawn in sec 3.5.

3.2 Theory

Ampere's circuital law states that magnetic field is induced around the current carrying conductor and the direction of magnetic field is given by the right hand thumb rule. According to Ampere's circuital law, the line integral of magnetic field along the closed loop is equal to μ_0 times the current passing through the area enclosed by the loop as

$$\int_L B.\, d\ell = \mu_0 \times I \tag{3.1}$$

$$\int_L H.\, d\ell = I \tag{3.2}$$

For a circular loop of radius r, around a straight current carrying wire

$$H = I/2\pi r \tag{3.3}$$

where B is the magnetic field, H is magnetic field intensity, I is the current flowing through the closed-loop. Hence, the magnetic field depends upon two factors, the current flowing through structure and the length of the loop. The magnetic field increases with the net current passing through the loop. It also depends upon the perimeter of loop. As the loop size increases the magnetic field decreases. Also, the magnetic field decreases as the distance from the bridge increases. Hence if the high current is accumulated over a very small area that will to lead to a high magnetic field concentration.

3.3 Hourglass nanoantenna

3.3.1 Design and Modelling

Hourglass shaped nanoantenna design consists of two cones cut into half along the central axis. The two gold half cones are placed on glass substrate facing each other and tips are joined together by a semi-cylindrical bridge. The whole structure when viewed from the upper side, resembles an hourglass shape. The structure can be visualised as a semi-cylinder placed on substrate horizontally, which diverges from both the sides. As shown in figure 3.1 (a-b), the total length of nanoantenna is denoted *L* and angle of each cone by θ, the length and radius of bridge by *l* and *r* respectively. Figure 3.1 (c) shows the three-dimensional view of geometry of hourglass shaped nanoantenna.

The finite element method (FEM) has been used for modeling, design and analysis of the magnetic field response of nanoantenna. The model has been simulated and analysed using COMSOL multiphysics software. The entire calculation is done in a volume of 4 μm x 4 μm x

3 μm. The structure has been considered to be placed on the silica substrate. A plane polarized light is allowed to fall normally on the nanoantenna. The electric field component of magnitude 1 V/m is directed along the x-axis. The refractive index of the substrate is chosen to be 1.5. Perfectly matched layer (PML) has been applied around the boundaries to avoid superfluous reflections. The data for the relative permittivity of different materials has been taken from Rakic [20].

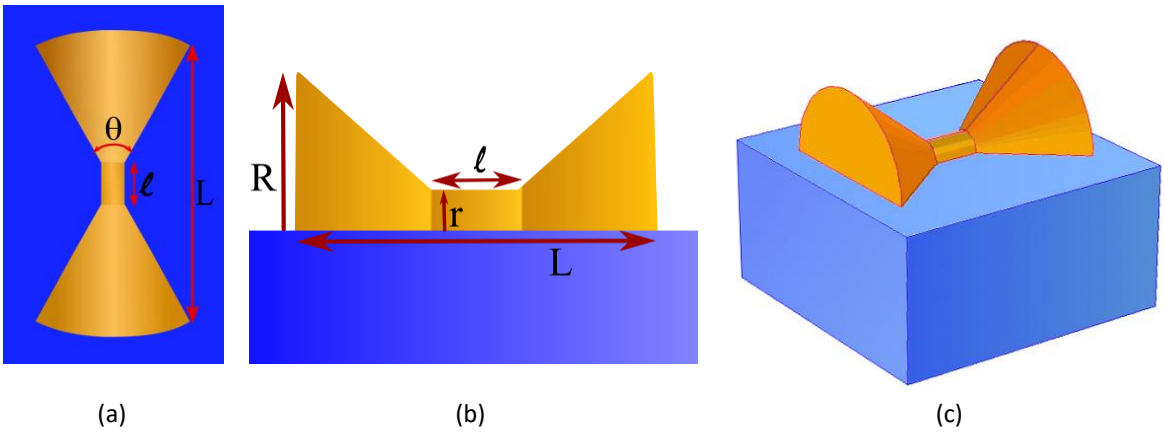

Figure 3.1 Geometry of the hourglass nanoantenna from (a) top view, (b) side view and (c) 3-D view.

The prime aim of the reported design is to enhance the magnetic field in the near infrared region. This structure has technical advantages over other structures, like a simple nanorod which has very small magnetic field accumulation. The surface plasmons tend to accumulate more at the tips [21] and therefore two half cones have been chosen to be placed on both sides of the nanocylinder. This increases the current intensity which further results in the enhancement of magnetic field concentration. The half cones facilitate the charges to funnel through the bridge and in turn enhanced electric field as shown in figure 3.2. Figure 3.2, shows that for a conical structure of nanoantenna, charges get accumulated at the tips, according to the polarization of electric field of incident light. Electric field is then confined and enhanced between the tips. If these tips are connected by a narrow metallic bridge, the charges flow from

one cone to another. The high charge density at the tip is converted into high current intensity through the bridge.

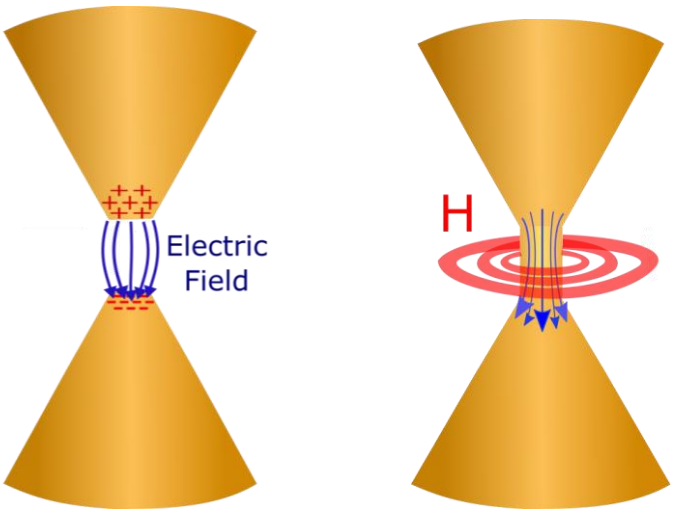

Figure 3.2 Principle of induction of magnetic field in nanoantenna Left: electric field enhancement; right: magnetic field enhancement.

The incident light causes the current to flow along the nanoantenna according to the direction of its electric field. In doing so, current flows from the region of larger cross-sectional area (conical arm) to a region of a smaller cross-sectional area (bridge). As a result, current intensity is extremely high and a highly enhanced magnetic field is achieved around the bridge making it a magnetic hotspot. The high current intensity is the key factor for obtaining a magnetic field. The ratio of the induced magnetic field to the background magnetic field gives the magnetic field enhancement.

3.3.2 Results and discussion

The magnetic field enhancement has been calculated for the proposed hourglass shaped nanoantenna by calculating modulus of magnetic intensity at a point 10 nm above the bridge $|H|^2$ divided by intensity of background magnetic field $|H_b|^2$.

$$\text{Magnetic field enhancement} = \frac{|H|^2}{|H_b|^2} \tag{3.4}$$

Further, the proposed design has been compared with the diabolo nanoantenna. The dimensions of both diabolo and hourglass nanoantenna are taken such that they cover equal area of the substrate. For diabolo nanoantenna the length and the width of the bridge is taken to be 80 nm and 30 nm respectively. The thickness of the whole diabolo antenna is taken to be 24 nm. The length and radius of the semi-cylindrical bridge are taken to be 80 nm and 30 nm respectively so that both designs have comparable cross-sectional area of the bridge. The total length of both nanoantennas is taken to be 300 nm and angle at the tip is taken to be 90˚. The magnetic field enhancement has been obtained for both the nanoantennas and normalized magnetic field intensity enhancement is shown in figure 3.3.

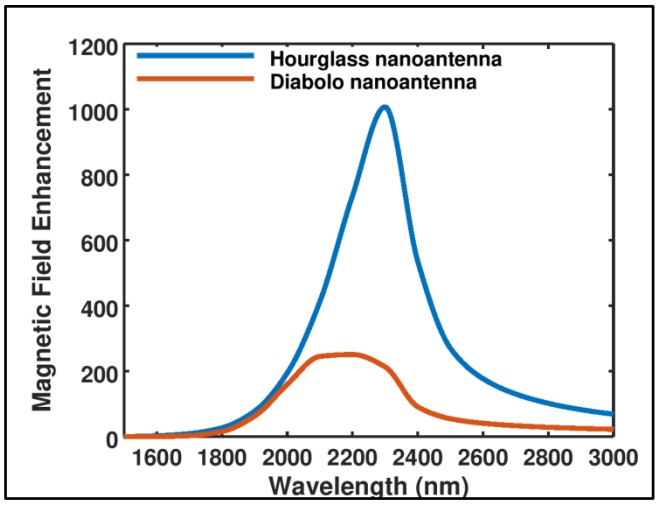

Figure 3.3 Comparison of magnetic field enhancement of hourglass nanoantenna with diabolo nanoantenna having same length and tip angle.

Figure 3.3 shows that the proposed hourglass nanoantenna exhibits five times more enhancement than previously reported diabolo nanoantenna. As the plane polarized light with electric field along the length of nanoantenna is allowed to fall normally on the nanoantenna, charges move along the direction of the electric field. High current density in the bridge induces a high magnetic field around it.

Figure 3.4 (a) shows the current density in the nanoantenna when x-polarized light falls on dit. Figure clearly depicts the high current density in the bridge as current travels from one end

to another. The wavelength of light is chosen to be 2300 nm at which nanoantenna of this configuration resonates. Figure 3.4 (b-d) shows the normalised near field intensity distribution of magnetic field in plane XY, XZ and YZ respectively. XY plane has been taken 10 nm above the bridge and the other two planes are passing through the centre axis.

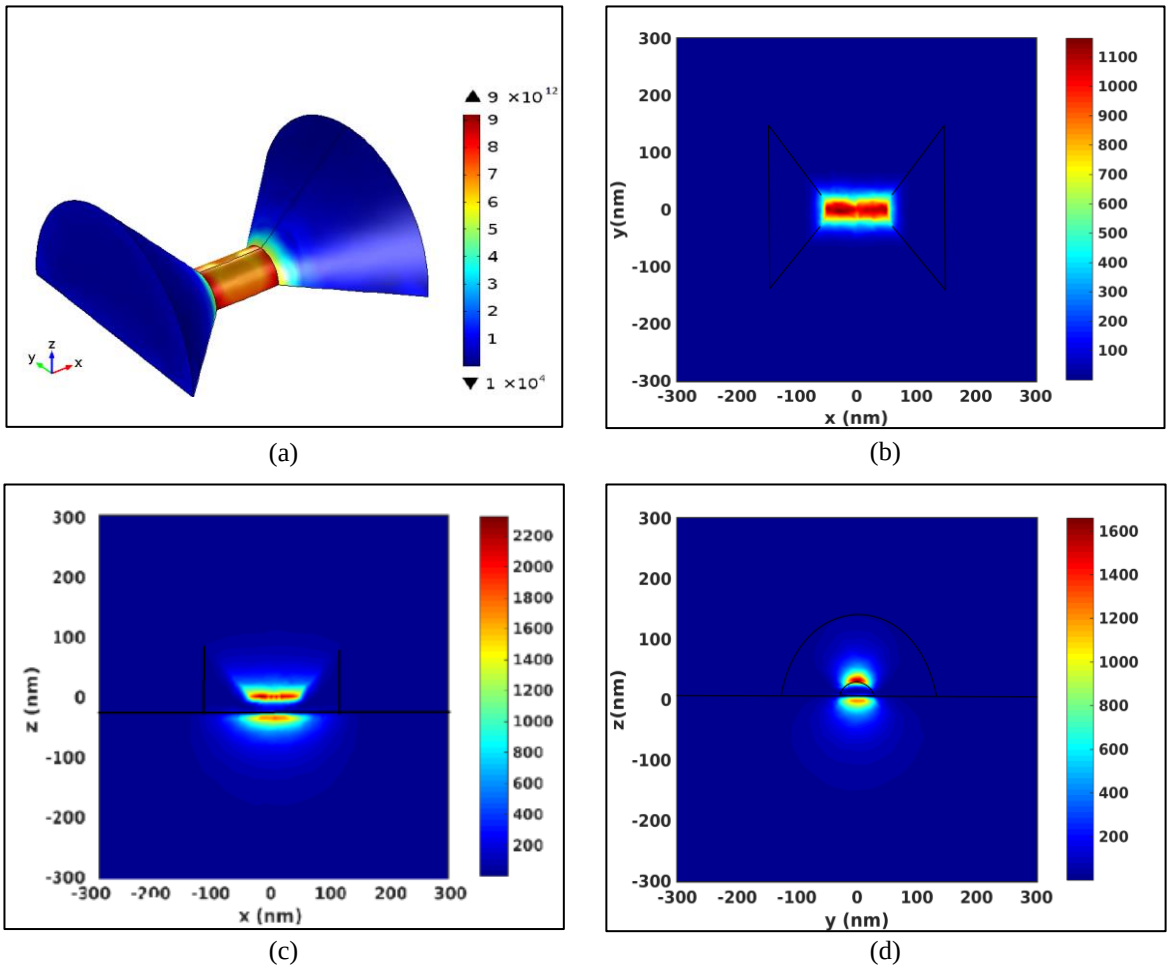

Figure 3.4 (a) Current density, (b) Normalized near-field intensity distribution of magnetic field when excited by linearly polarized light of wavelength 2300 nm along x-axis in XY plane at 10 nm above the bridge, (c) in XZ plane, (d) in YZ plane passing through the center of nanoantenna.

3.3.2.1 Effect of length of the nanoantenna *L*

The variation of magnetic field enhancement for different values of length, *L* of nanoantenna with the variation of wavelength has been obtained as shown in figure 3.5. The angle θ of cone is taken to be 90˚ and radius *r* and length *l* of bridge as 30 nm and 80 nm respectively.

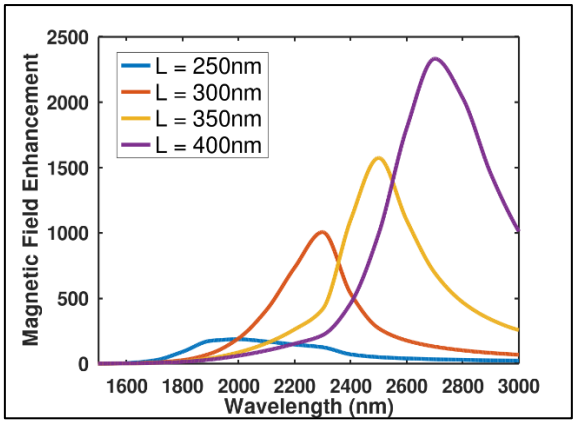

Figure 3.5 Magnetic field enhancement with wavelength for different lengths L of the hourglass nanoantenna.

As the length of the nanoantenna is increased, the surface plasmon resonance wavelength redshifts. Also, with the increase in the length of the nanaoantenna, magnetic field enhancement also increases as evident from figure 3.5. This is because the increase in length leads to the corresponding increase in the area of the cone.

3.3.2.2 Effect of the angle of the cone θ

The magnetic field enhancement for different angles θ of cone keeping the length L of the nanoantenna 300 nm, radius r and length l of bridge 30 nm and 80 nm respectively, with the variation of wavelength has been shown in figure 3.6. Figure 3.6 shows that the magnitude of enhancement increases with the increase in the angle θ of the cone. This is because as the angle of cones increases, the difference in the cross-section area of cones and bridge increases, which contributes to more current intensity in the bridge. Hence more magnetic field is induced around the semi-cylindrical bridge.

It is also observed from the graph that resonance wavelength also redshifts. This may be due to the increase of the slant height of the cone, as the surface plasmons oscillate on the surface of material. The effective length of nanoantenna is not the covering surface of substrate but the distance surface plasmons travel from one cone to another through bridge. With the increase of tip angle the effective length increases that causes the red-shift in the resonance wavelength.

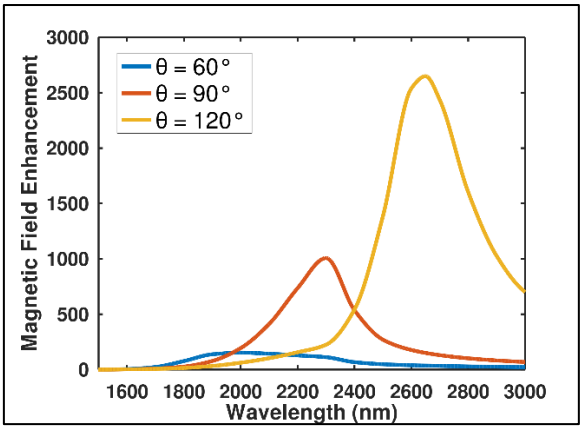

Figure 3.6 Magnetic field enhancement with wavelength for different values of the angle θ of the cone of the hourglass nanoantenna.

3.3.2.3 Effect of the radius *r* of the bridge

Further, the radius r of the semi cylindrical bridge is varied, keeping the length l of bridge 80 nm, total length L of the nanoantenna as 300 nm, and angle θ of cone equal to 90˚. The magnetic field enhancement for various radii r of the bridge with respect to wavelength has been shown in figure 3.7. As the radius r of the bridge decreases, enhancement in the magnetic field increases. This is because the current intensity increases in the bridge as the cross-section area decreases with the decrease in the radius of the bridge. A slight increase in the resonance wavelength is due to an increase of aspect ratio [19].

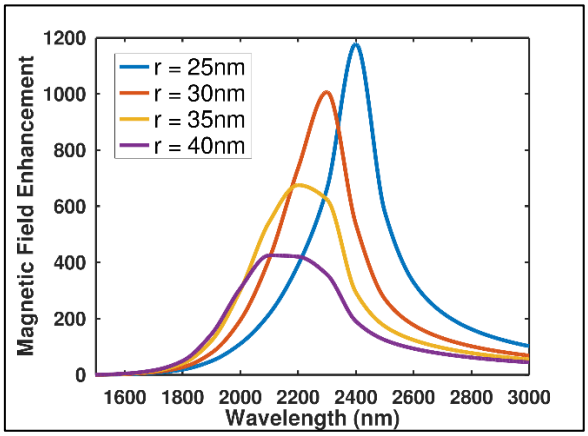

Figure 3.7 Magnetic field enhancement with wavelength for different radius r of bridge of the hourglass nanoantenna.

3.3.2.4 Effect of the length of the bridge, *l*

The magnetic field enhancement has been calculated for various lengths *l* of the semi-cylindrical bridge, by keeping the radius *r* of the bridge 30 nm, total length *L* of the nanoantenna 300 nm, and angle θ of cone equal to 90˚. The magnetic field enhancement for different values of length of the bridge has been shown in figure 3.8. Also, with the increase in the length *l* of the nanoantenna, magnetic field enhancement also increases as evident from figure 3.5. This is because the increase in length leads to the corresponding increase in the area of the cone. There is a slight increase in the magnetic field enhancement with the decrease in the length *l*, of the bridge. As the total length of the antenna is fixed, decrease in the bridge length, leads to the simultaneous increase in the length of the cones. This small increment in the antenna length, increases the cross-section area of cones, leading to the increased current intensity in the bridge and hence, enhanced magnetic field.

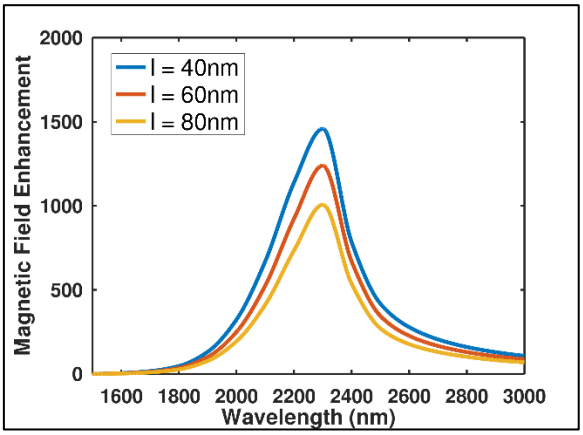

Figure 3.8 Magnetic field enhancement with wavelength for different lengths *l* of bridge of the hourglass nanoantenna.

3.3.2.5 Effect of the material

The performance of nanoantenna depends on the conductivity of the material. Therefore, the designed structure has been studied for different constituting materials and magnetic field enhancement has been calculated. The enhancement in the magnetic field with different materials gold, silver, copper, and aluminium has been obtained as shown in figure 3.9. It can be observed that Silver gives the maximum enhancement in the magnetic field and Aluminium

gives the lowest enhancement among these materials. Copper gives comparable results with gold. Copper and silver can be the alternative candidates for the proposed design if corrosion is not an issue. The analysis of the effect of the various geometrical parameters as well as the effect of the different materials can prove helpful in the modelling, design and optimisation of the various application specific nanoantennas.

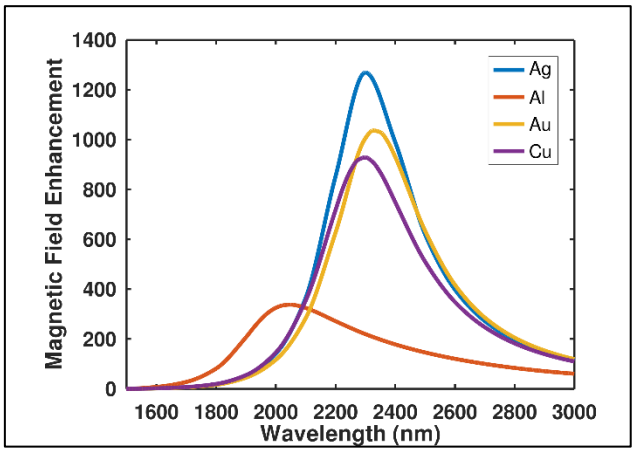

Figure 3.9 Variation of magnetic field enhancement with wavelength for materials taken for the hourglass nanoantenna.

3.4 Rhombic Nanoantenna

3.4.1 Design and Modelling

The rhombic nanoantenna is made up of gold, consisting of a pair of rhombuses facing each other at tips, connected through a square bridge has been designed for magnetic field enhancement. The designed nanoantenna has been numerically analyzed using finite element method (FEM) via COMSOL Multiphysics. The perfectly matched layer has been used around the nanoantenna to avoid superficial reflection. The value of permittivity for gold has been taken from experimental data [20].

Figure 3.10 shows the design of the nanoantenna with the sides of rhombus *L*, sides of central square *G*, and height or thickness of structure *H*. The geometrical parameters have been varied to analyze the enhancement of the magnetic field using COMSOL Multiphysics software. When plane polarized light is allowed to fall on the nanoantenna, the electric

current thus induced travels from one rhombus to another through the narrow bridge. Because of high current density in the bridge, high magnetic field is induced around it.

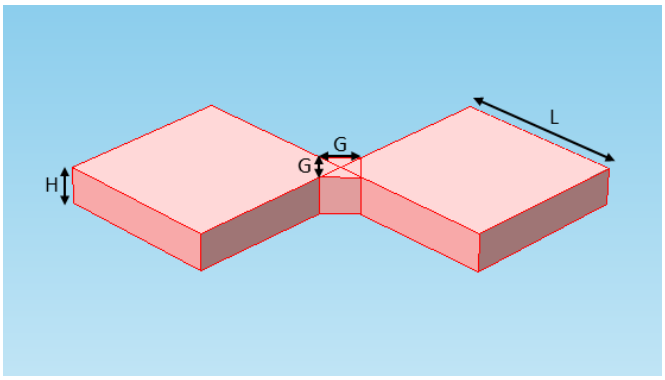

Figure 3.10 Design of the rhombic nanoantennas.

3.4.2 Results and discussion

When a plane polarized electromagnetic light wave polarized along x-axis is made incident on the structure, the induced current travels from one arm to the other, through the central bridge inducing strong magnetic field around it. Figure 2.11 shows the current density distribution in the volume of nanoantenna when illuminated by the resonant wavelength of 2300 nm and the white arrow shows the direction of current. The structure parameters are taken as L= 225 nm, G= 50 nm, H = 50 nm.

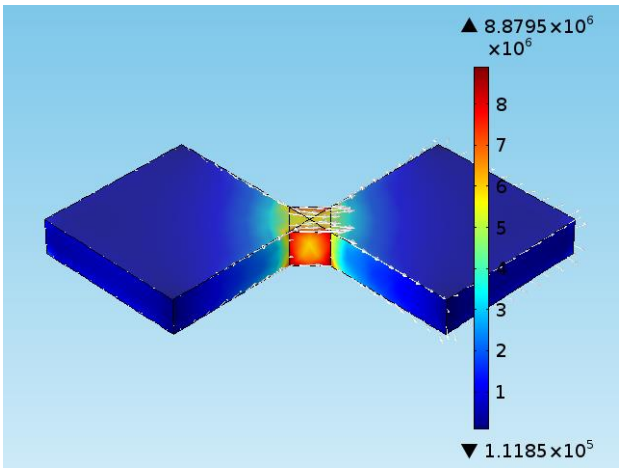

Figure 3.11 Current density distribution in the rhombic nanoantenna at resonant wavelength. White arrow shows the direction of flow of current when plane polarized light polarized along x-axis, falls vertically on it.

For the same dimensions, the near-field distributions of the magnetic-field enhancement generated by the proposed nanoantenna at a wavelength of 2300 nm have been shown figure

3.12. Figure 3.12 (a) shows magnetic field enhancement in the x-y plane at 10 nm above the surface of bridge. Figure 3.12 (b) and 3.12 (c) shows magnetic field distribution in x-z plane and y-z plane respectively passing through the central axis of symmetry.

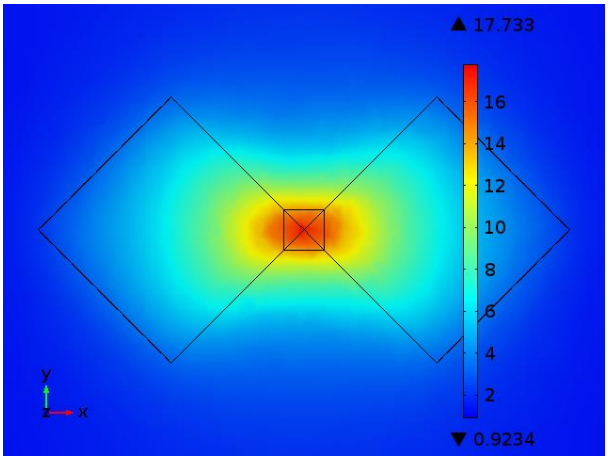

(a)

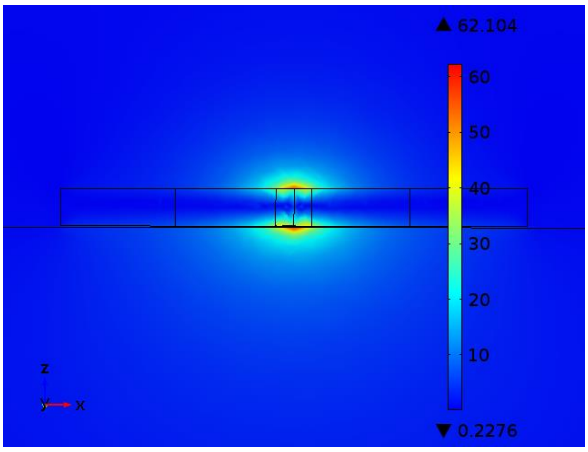

(b)

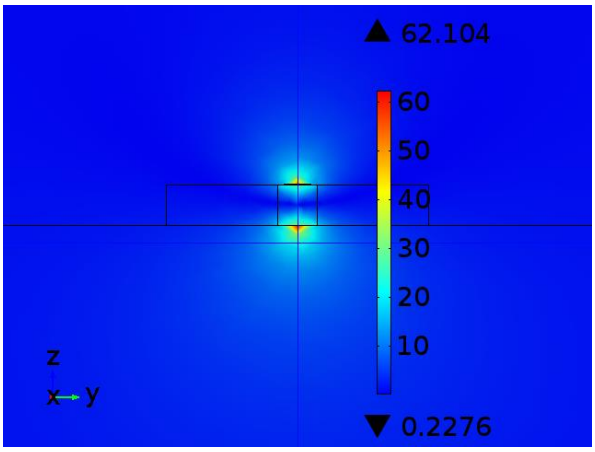

(c)

Figure 3.12 Near-field enhancement of magnetic field at resonant wavelength (a) in x-y plane at 10 nm above the surface of nanoantenna (b) in x-z plane (c) in y-z plane passing through the center of the rhombic nanoantenna

3.4.2.1 Variation in magnetic field enhancement with variation of side length *L*

Keeping the other parameters constant, the length of the sides *L* of the nanoantenna has been changed and its effect on magnetic field enhancement has been observed as shown in the figure 3.13. Height *H* and *G* has been taken to be 50 nm. Figure 3.13 shows that as the length of nanoantenna increases, the resonant peak observed shifts to higher wavelengths. This is because localized surface plasmon resonance shifts to higher wavelength as the nanoparticle

size increases. Also, there is increase in the field enhancement with increase in sides *L* of the nanoantenna.

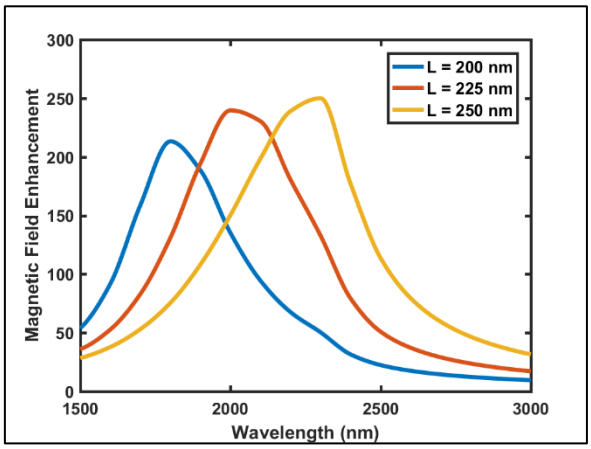

Figure 3.13 Variation magnetic field enhancement with wavelength for side length *L* of the rhombic nanoantenna

3.4.2.2 Variation in magnetic field enhancement with variation of height *H*

Further, by keeping length *L* of the antenna arm 225 nm and bridge length *G* equal to 50 nm, the height *H* of the antenna has been varied and the magnetic field enhancement observed with the change in wavelength is shown in Figure 3.14. It has been observed from the figure that with the increase in height of nanoantenna field enhancement decreases and the resonant wavelength gets blue shifted.

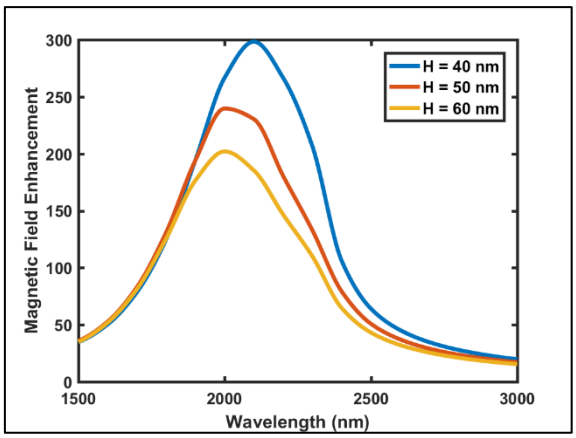

Figure 3.14 Variation of magnetic field enhancement with wavelength for different height *H* of the rhombic nanoantenna.

3.4.2.3 Variation in magnetic field enhancement with variation of bridge length *G*

Further, by keeping the length *L* and height *H* of nanoantenna fixed at 225 nm and 40 nm respectively, length *L* of bridge has been varied. The magnetic field enhancement for different values of *G* has been shown in figure 3.15. As the length of the bridge increases, enhancement of magnetic field decreases. The enhancement depends on the cross-sectional area of the bridge. Smaller the cross-section area, higher is the current density, hence the magnetic field around it.

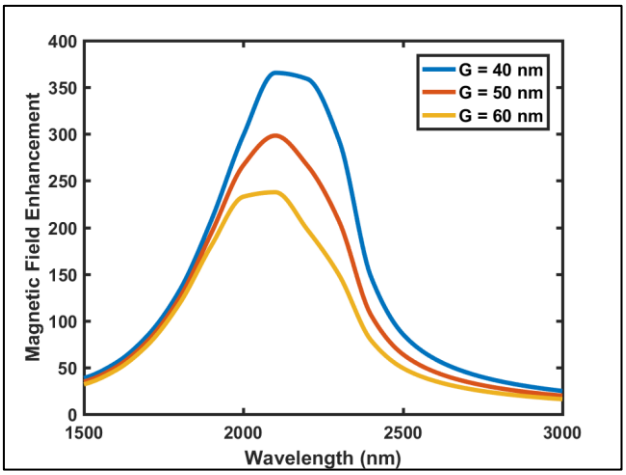

Figure 3.15 Variation of magnetic field enhancement with wavelength for different value of the bridge length *G* of the rhombic nanoantenna.

3.4.2.4 Variation in magnetic field enhancement for different materials

Further, by keeping all geometrical parameters constant, material of the rhombus shaped nanoantenna has been varied and corresponding enhancement in magnetic field is calculated. The length *L*, height *H* and gap *G* of nanoantenna fixed at 225 nm, 40 nm and 40 nm respectively. The magnetic field enhancement for different constituting material of the proposed nanoantenna has been shown in figure 3.16. The silver shows the maximum magnetic field enhancement while the aluminum shows the lowest among all materials.

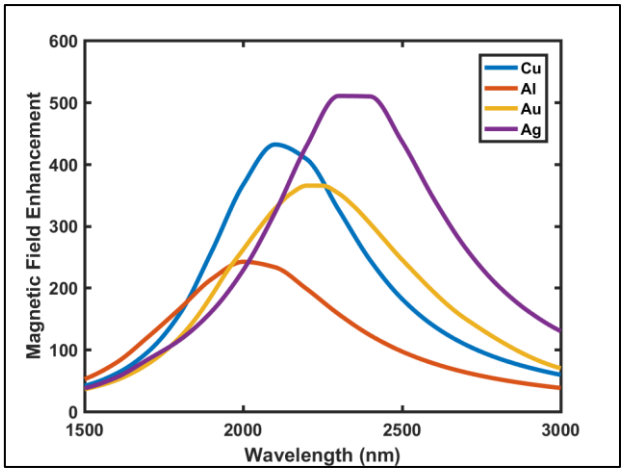

Figure 3.16 Variation of magnetic field enhancement with wavelength for different constituting material of the rhombic nanoantenna.

3.5 Conclusion

The hourglass shaped nanoantenna and rhombic shaped nanoantenna have been successfully designed and analysed for magnetic field enhancement. The variation of magnetic field enhancement with wavelength by changing geometrical and material parameters has been calculated. The magnetic field enhancement increases and red-shifts with increasing length of nanoantenna. The magnetic field also increases with decrease in the cross-sectional area of central bridge. The hourglass shaped nanoantenna has been compared with existing design of diabolo nanoantenna and was found to be a better candidate for magnetic field enhancement at higher frequencies. The advantage of the work is that it suggests a mechanism to achieve high magnetic field enhancement in the optical spectrum, which is not possible using commonly known ferromagnetic materials. Further both the designed antennas are tunable, hence, can be tuned to resonate at different wavelengths by changing the geometrical parameters.

References

[1] Krasnok, A. E., Maksymov, I. S., Denisyuk, A. I., Belov, P. A., Miroshnichenko, A. E., Simovski, C. R., & Kivshar, Y. S. (2013). Optical nanoantennas. *Physics-Uspekhi*, *56(6)*, 539.

[2] Bakker, R. M., Permyakov, D., Yu, Y. F., Markovich, D., Paniagua-Domínguez, R., Gonzaga, L. ... & Kuznetsov, A. I. (2015). Magnetic and electric hotspots with silicon nanodimers. *Nano Letters*, *15*(3), 2137-2142.

[3] Ding, W., Bachelot, R., Kostcheev, S., Royer, P., & Espiau de Lamaestre, R. (2010). Surface plasmon resonances in silver Bowtie nanoantennas with varied bow angles. *Journal of Applied Physics*, *108*(12), 124314.

[4] Ranga, R., Kalra, Y., & Kishor, K. (2020). Petal shaped nanoantenna for solar energy harvesting. *Journal of Optics*, *22*(3), 035001.

[5] Dregely, D., Taubert, R., Dorfmüller, J., Vogelgesang, R., Kern, K., & Giessen, H. (2011). 3D optical Yagi–Uda nanoantenna array. *Nature communications*, *2*(1), 1-7.

[6] Reena, Kalra, Y., Kumar, A., & Sinha, R. K. (2016). Tunable unidirectional scattering of ellipsoidal single nanoparticle. *Journal of Applied Physics*, *119*(24), 243102.

[7] L.D. Landau, E.M. Liftshitz, L.P. Pitaevskii, Electrodynamics of Continuous Media, second ed., Pergamon Press, 1984 (chapter 79).

[8] Cai, W., Chettiar, U. K., Yuan, H. K., de Silva, V., Kildishev, A. V., Drachev, V. P., & Shalaev, V. M. (2007). Optical magnetism: from Red to Blue. *arXiv preprint physics/0701020*.

[9] Yi, N., Liu, Z., Sun, S., Song, Q., & Xiao, S. (2015). Mid-infrared tunable magnetic response in graphene-based diabolo nanoantennas. *Carbon*, *94*, 501-506.

[10] Mivelle, M., Grosjean, T., Burr, G. W., Fischer, U. C., & Garcia-Parajo, M. F. (2015). Strong modification of magnetic dipole emission through diabolo nanoantennas. *ACS Photonics*, *2*(8), 1071-1076.

[11] Grosjean, T., Mivelle, M., Baida, F. I., Burr, G. W., & Fischer, U. C. (2011). Diabolo nanoantenna for enhancing and confining the magnetic optical field. *Nano letters*, *11*(3), 1009-1013.

[12] Gao, Z., Shen, L., Li, E., Xu, L., & Wang, Z. (2011). Cross-diabolo nanoantenna for localizing and enhancing magnetic field with arbitrary polarization. *Journal of lightwave technology*, *30*(6), 829-833.

[13] Yu, Z., Gao, Z., & Wang, Z. (2015). Broken-diabolo nanoantenna for co-enhancing and-confining optical electric and magnetic field. *Optics Communications*, *346*, 34-37.

[14] Darvishzadeh-Varcheie, M., Kamandi, M., Albooyeh, M., & Capolino, F. (2019). Optical magnetic field enhancement at nanoscale: a nanoantenna comparative study. *Optics Letters*, *44*(20), 4957-4960.

[15] Hameed, N., Nouho Ali, A., & Baida, F. I. (2017). Optical manipulation of nanoparticles by simultaneous electric and magnetic field enhancement within diabolo nanoantenna. *Scientific reports*, *7*(1), 1-10.

[16] Kang, J. H., Kim, K., Ee, H. S., Lee, Y. H., Yoon, T. Y., Seo, M. K., & Park, H. G. (2011). Low-power nano-optical vortex trapping via plasmonic diabolo nanoantennas. *Nature communications*, *2*(1), 1-6.

[17] Shankhwar, N., Kalra, Y., & Sinha, R. K. (2017). Split-nanotube-based negative index metamaterial for midinfrared wavelengths. *Journal of Nanophotonics*, *11*(2), 026014.

[18] Hameed, N. M., & Al Lethawe, M. A. (2020). Geometrical optimization study of diabolo nanoantenna. *Optik*, *201*, 163534.

[19] Cao, J., Sun, T., & Grattan, K. T. (2014). Gold nanorod-based localized surface plasmon resonance biosensors: A review. *Sensors and actuators B: Chemical*, *195*, 332-351.

[20] Rakić, A. D., Djurišić, A. B., Elazar, J. M., & Majewski, M. L. (1998). Optical properties of metallic films for vertical-cavity optoelectronic devices. *Applied optics*, *37*(22), 5271-5283.

[21] Babadjanyan, A. J., Margaryan, N. L., & Nerkararyan, K. V. (2000). Superfocusing of surface polaritons in the conical structure. *Journal of Applied Physics*, *87*(8), 3785-3788.

CHAPTER-4

CHAPTER-4

NANOANTENNA AS PERFECT ABSORBER AND REFRACTIVE INDEX SENSOR*

4.1 Introduction

Plasmonic materials have attracted much attention in recent years for varying applications. In previous chapters, different application of plasmonic nanoantennas have been presented in solar energy harvesting and generating magnetic field in infrared region using properties like electric field enhancement and magnetic field enhancement. On account of being made of metals, plasmonic nanoantennas exhibit substantial Ohmic loss, which facilitates their utilisation for absorption of light. By choosing a suitable design and optimising geometrical parameters one can obtain absolute absorption in a range of frequencies, which can be very useful in some applications such as in biosensors [1,2], optical filters [3,4], and photodetectors [5]. In this chapter, plasmonic nanoantenna has been designed for perfect absorption which is then utilized for refractive index sensing.

Absorbers can be categorized into broadband and narrowband on the basis of bandwidth. Broadband absorbers can be used in solar panels utilized in solar energy harvesting [7, 8].

*Part of the results reported in this chapter has been published in Journal: "Ultra-narrow band perfect absorber for sensing applications in the visible region." The European Physical Journal D 77.3, 42 (2023).

Narrowband absorbers can be used in sensing [9-11], thermal radiation tailoring [12], filters [13] etc. The first absorber was proposed and demonstrated experimentally by Lardy et al. in 2008 for sensing application in the infrared region [14]. In this design like most of the previous designs, triple layers of metal-dielectric-metal (MDM) have been chosen where a dielectric spacer enables strong plasmonic coupling between the top resonator and bottom metal film [15-17]. The above-mentioned absorbers can be considered as resonators coupled to a transmission line with a dielectric spacer region, whose thickness influences the radiative damping rates and resonance frequency. However, due to strong radiative damping and inherent metal loss, the bandwidth of the absorbers is relatively broad (> 40 nm). Sensitivity and Figure of Merit (FOM) are the two important parameters to specify the performance of sensors. Sensitivity is measure of change in the output quantity with respect to change in the input quantity. The term "bulk sensitivity" refers to the shift in the resonance wavelength with respect to the surrounding refractive index that is used to calculate the sensitivity of the presented plasmonic sensors [18–20]. Higher FOM indicates a high ability to sense changes in the environment. It is defined by the ratio of the sensitivity to the bandwidth at half maxima of the peak. Therefore, attempts have been made to reduce the absorption bandwidth in order to increase the corresponding figure of merit (FOM). In 2016, Z. Yong et al. proposed a narrow band absorber for sensing application of FWHM 7.5 nm in the near IR region with FOM 110/RIU [21]. Many absorbers from UV to near IR have been demonstrated till now [16, 22–24]. However, narrowband absorbers in visible range have not been studied much. Most of them show resonance in a broad range of wavelengths and have a very low FOM [11, 25, 26]. Much work has been done by researchers practically and experimentally to obtain high FOM in the visible range. In 2014, Emiko and Tetsu experimentally studied localised surface plasmon resonance sensors based on spectral dips [27]. G. Liu et al. in 2016 proposed theoretically a network type plasmonic nanostructure with multiple reflection bands reaching

full width at half maximum of 3 nm and FOM of 68.57/RIU [28]. In 2017, Wu et al. proposed grating absorbers with nanoribbons in between metal dielectric metal (MDM) having sensing applications in the visible range and FOM equal to 233.5/RIU [29]. In 2020, a narrow band perfect absorber of Al_2O_3 based on dielectric dielectric- metal configuration was proposed by M. Pan et al. having a sensitivity of 108 nm/RIU reaching FOM up to 240.7/RIU [30].

In this Chapter, the design of all metallic plasmonic narrowband absorber has been proposed. The designed structure confines and enhances electric as well as magnetic field at a single hot spot and shows a narrow absorption peak of full width at half maximum (FWHM) less than 2 nm in the visible wavelength. The design shows the sensitivity of 680 nm/RIU and FOM of 348.72/RIU, which is higher than the earlier reported results in the visible wavelength [25, 30–33]. Further, the performance of the absorber has been investigated by varying geometrical parameters and the design is optimised for maximum absorption and high FOM.

4.2 Design and modelling

The geometry comprises of four cuboids of silver, facing each other at tips, placed over a silver layer of thickness *t* of 100 nm. The whole structure is placed on a glass substrate and surrounded by air on top. The design and geometrical parameters are demonstrated in figure 4.1. Length and width of cuboids have been taken as *a* and height has been taken as *h*. The gap 'g' between the tips of the opposite cuboid has been taken as 30 nm.

The set of four cuboids has been arranged in the form of an array of periodicity *p*. Silver has been chosen as the material because of its high reflectivity. The thickness of the silver layer has been chosen such that no light is transmitted through this layer and the maximum absorption takes place at resonance wavelength. The value of relative permittivity for silver has been taken from literature [32].

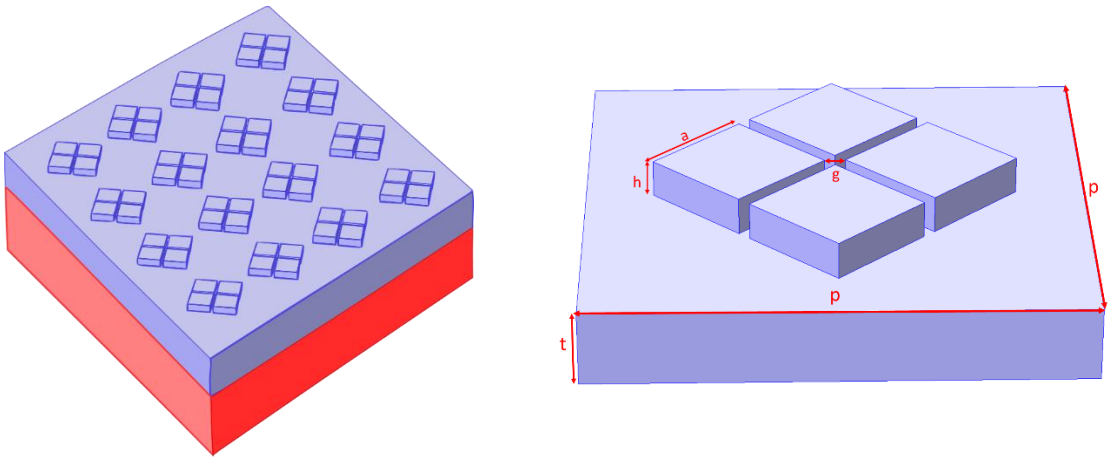

(a) (b)

Figure 4.1 (a) Schematic of the proposed metallic absorber (b) unit cell with geometrical parameters.

The transverse magnetic (TM) light, polarised along x-direction is allowed to fall on the surface of the structure from the top. The distance between light source and the structure is taken more than half of resonant wavelength. The simulation is performed on single unit enclosed in a cuboid having dimensions of periodicity *p* along x and y axis. The periodic boundary conditions have been applied along x and y plane on the boundary of cuboid enclosing unit cell to represent as infinite array in x–y plane. The refractive index of glass substrate is taken to be 1.5. The maximum mesh size is taken as 10 nm. The reflection coefficient has been calculated using the finite element method via COMSOL Multiphysics. The absorption coefficient has been obtained by using the relationship A = 1 − R. The resonance wavelength of plasmonic structures depends upon shape, size, geometry, constituting material as well as the surrounding medium. This property of changing resonance wavelength with refractive index can be used in sensing applications. The sensors are characterised by their sensitivity and FOM. Sensitivity, S for refractive index sensor is defined by the ratio of the spectral shift with the change of refractive index of the surrounding medium and FOM is the ratio of sensitivity to the FWHM [22–24].

$$S = \frac{\Delta\lambda}{\Delta n} \qquad FOM = \frac{S}{FWHM}$$

4.3 Results and Discussion

Absorption and reflection spectra for the structure has been shown in figure 4.2. As the thickness of the silver film is greater than the skin depth, the absorption is reduced to A = 1-R. The absorption spectrum shows an absorption peak at 692 nm of which the full width at half maxima is 1.95 nm, which is much narrower than the previously reported design in the visible range [10, 15, 29–31]. A maximum of 99.45% absorption is obtained at the resonance wavelength. Further, the quality factor Q given by the ratio of the resonance wavelength to the FWHM of resonance peak ($\lambda_{res}/\Delta\lambda$) which comes out to be 354.87 is much higher than previously reported designs [21, 27-30].

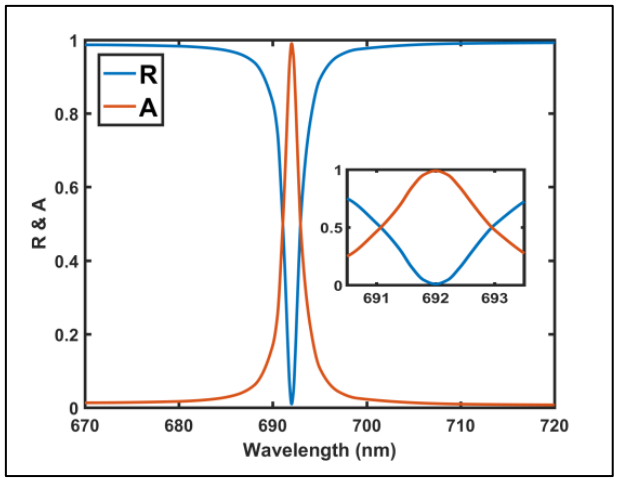

Figure 4.2 Reflection and absorption coefficient for *a* = 140 nm, *h* = 30 nm and *p* = 650 nm showing resonance at 692 nm and FWHM = 1.95 nm.

4.3.1 Effect of dimensions of the nanopillars

4.3.1.1 Effect of height *h*

The study of dependence of the size of cuboidal pillars on the absorption peak has been studied. First, the height of the silver cuboids *h* has been varied, and the periodicity *p* and sides *a* of cuboids have been fixed at 650 nm and 160 nm respectively. The plot showing the variation of absorption coefficient and FWHM with the variation of height from 25 to 45 nm in the step of 5 nm, has been depicted in figure 4.3(a) and the variation of resonance wavelength with height has been shown in figure 4.3(b). As there is a vertical waveguide in between four silver pillars,

the increment in the height eventually increases the length of the waveguide. Therefore, the resonance shifts toward longer wavelengths, as seen in figure 4.3(b). Although FWHM decreases with a decrease in the height of silver pillars, but below 30 nm height, the absorption decreases. Hence, the height has been fixed at 30 nm.

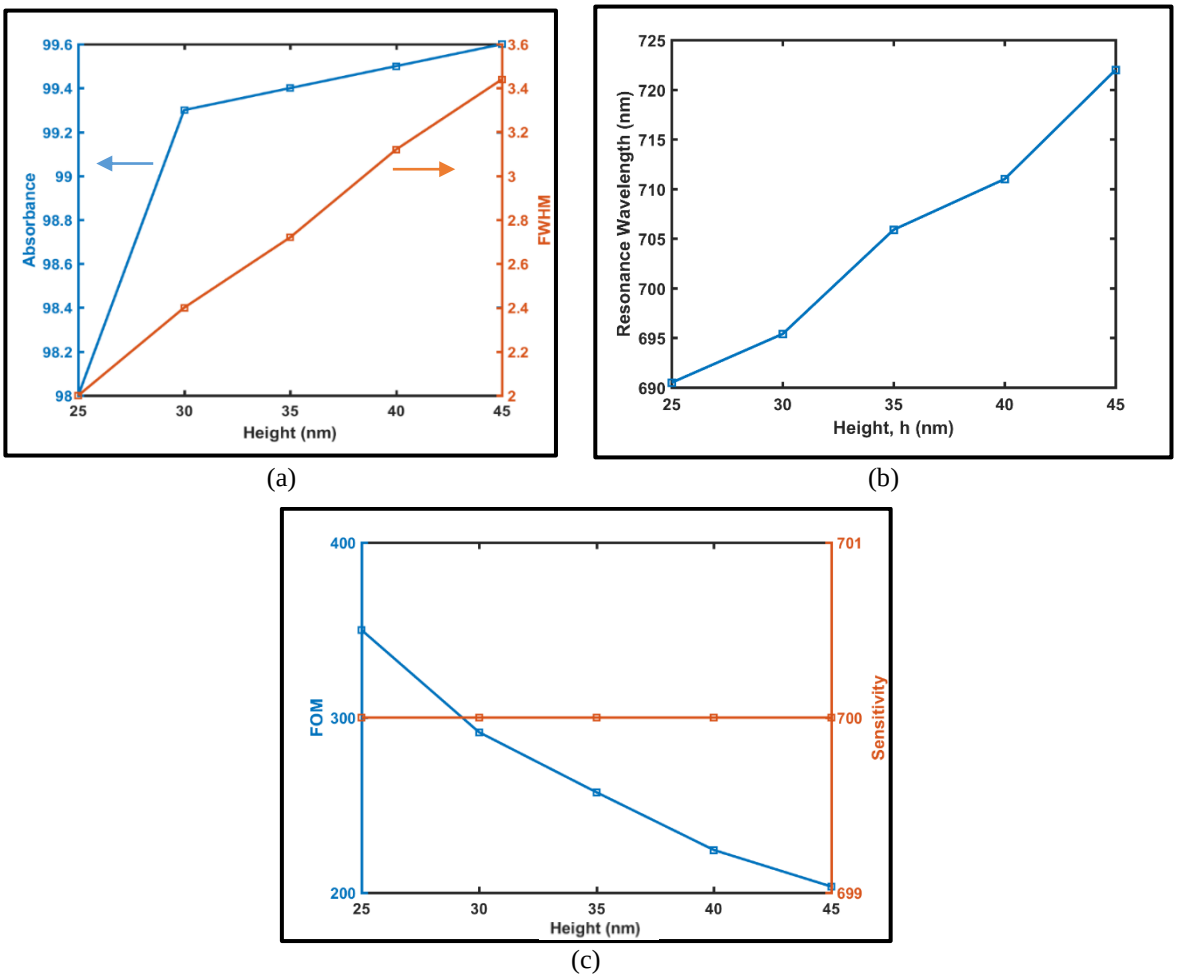

Figure 4.3 Variation of (a) Absorption coefficient and FWHM (b) Resonance wavelength and (c) FOM and sensitivity with the variation of height, *h*.

Further, the effect of height of the pillars on the sensitivity has been studied by keeping all other parameters same as above and corresponding FOM has been calculated. The graph showing the variation of the sensitivity and FOM of the structure with the variation in height of the nanopillars of the nanoantennas has been shown in figure 4.3(c). It has been observed from the figure that there is no effect of height of the nanopillars on the sensitivity of structure but there is fall in the FOM of the structure with increase in the height because of increase in

the value of FWHM with the height of nanopillars. An increase in the value of parameter *h* increases the absorption. The increase in the value of *h* increases the volume of cuboidal pillars on the silver layer. This increases the regions of high E-field alongside the wall of the cuboidal pillars. The increase in the high E-field regions increases the shift in the plasmon resonance wavelength as shown in the figure 4.3(b). However, a higher value of *h* also reduces the probability of coupling surface plasmons on top of the cuboid pillars as the evanescent tail of the plasmon will no longer be able to reach the top surface [19]. This may reduce the values of sensitivity. To achieve higher absorption, sensitivity and FOM, the height *h* was adopted as 30 nm.

4.3.1.2 Effect of Side length, *a*

Further, the sides of silver cubes *a* have been varied from 120 to 160 nm in the step size of 10 nm, keeping the periodicity *p* and height *h* of cuboids at 650 nm and 30 nm respectively. The effect of varying the sides of cubes on absorption coefficient and FWHM has been shown in figure 4.4(a) and the shift in the resonance wavelength has been shown in figure 4.4 (b). It has been observed that with the increase in *a*, there is a slight redshift in the resonance wavelength, and full width at half maxima decreases. Red shift in the resonance wavelength with the increase in side length *a* can be understood in analogy to a half-wave dipole antenna whose resonant wavelength is directly proportional to the antenna length, given by,

$$\lambda_{res} = 2 \times \text{length}$$

As the length of the dipole increases so does the resonant wavelength [31]. In fact, it can be established as a general truth for all the antenna designs that increase in the size of the resonant components results in increase or red shift in the resonant wavelength. Hence, in the reported design the resonant wavelength increases with increase in side length *a*. A small value of FWHM can lead to high FOM for sensing applications which can be achieved by decreasing the side lengths of pillars. But if side length is reduced below 140 nm, absorption decreases.

The effect of sides of nanopillars, *a* on the sensitivity and FOM of the structure has been illustrated in figure 4.4 (c). The sensitivity of the structure increases with increase in *a* while FOM decreases with increase in *a*. This is because increase in the value of FWHM is more than the increase in the value of sensitivity with *a*.

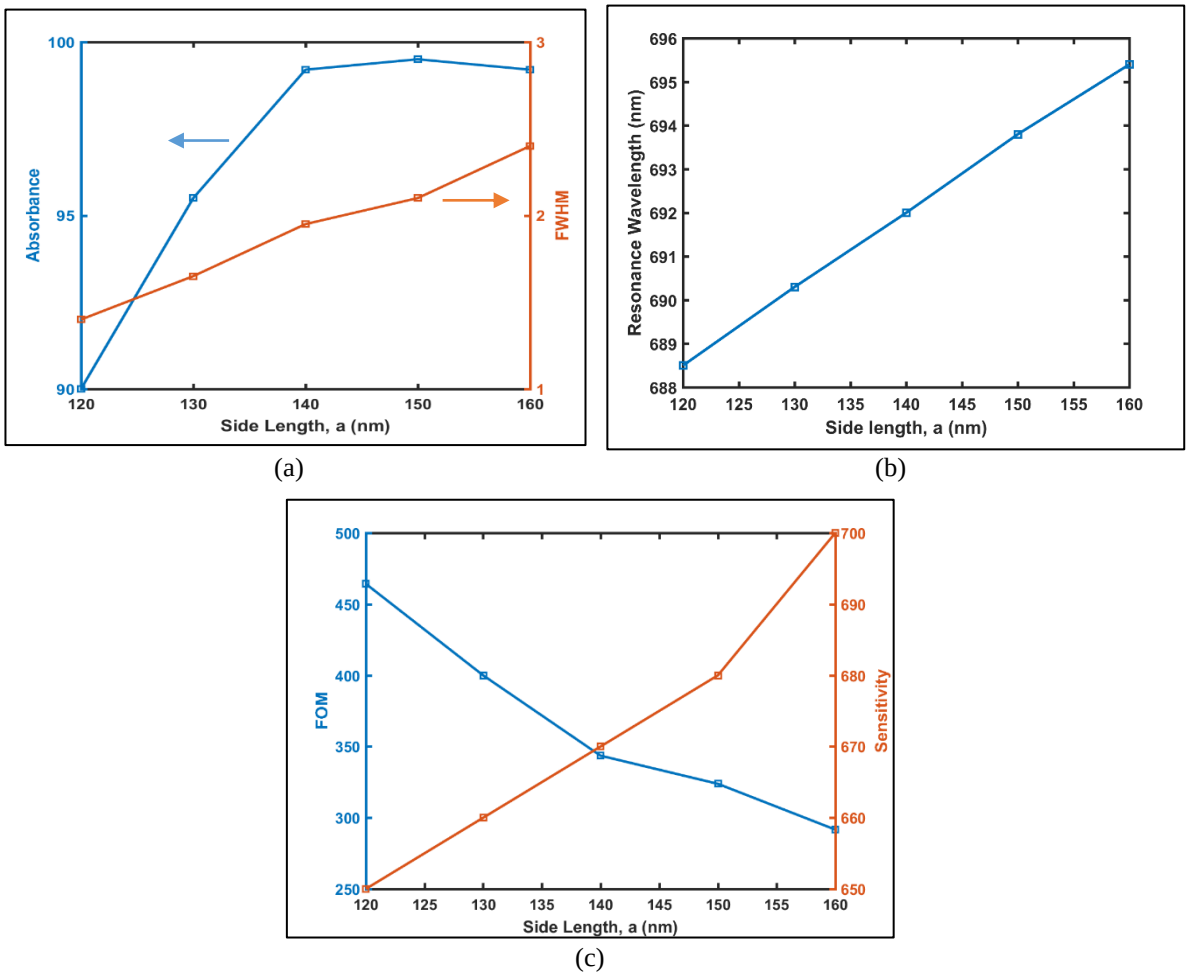

(a) (b)

(c)

Figure 4.4 Variation of (a) Absorption coefficient and FWHM (b) Resonance wavelength and (c) FOM and sensitivity with the variation of sides of pillars, *a*.

4.3.2 Effect of Periodicity *p*

Keeping *a* and *h* constant at 140 nm and 30 nm respectively, the periodicity of the structure has been varied from 600 nm to 800 nm in the step size of 50 nm, and absorbance and FWHM have been recorded. The variation of maximum absorption and FWHM with the variation of periodicity *p* has been shown in figure 4.5 (a). It has been observed from the figure that FWHM decreases with an increase in periodicity and the absorption coefficient first

increases and then starts decreasing with a further increase in the periodicity. Also, there is a linear shift in the resonance wavelength with an increase in periodicity as shown in figure 4.5 (b).

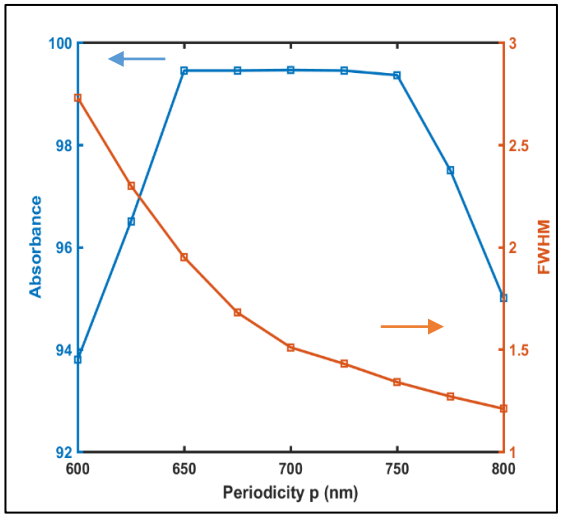

(a)

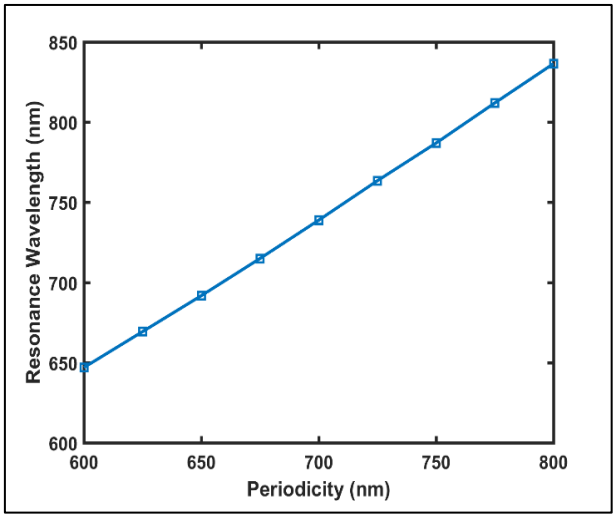

(b)

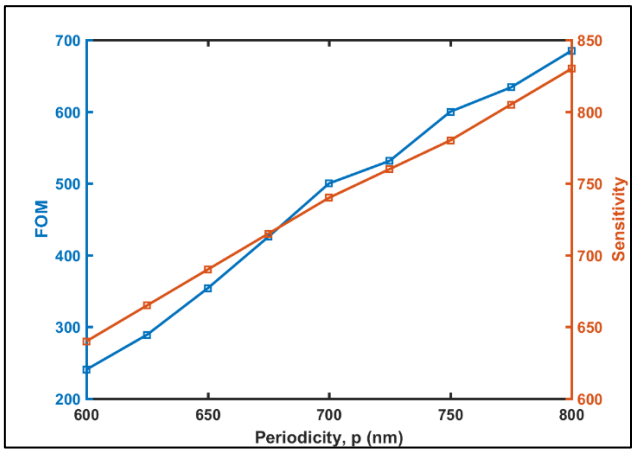

(c)

Figure 4.5 Variation of (a) Absorption coefficient and FWHM (b) Resonance wavelength and (c) FOM and sensitivity with the variation of periodicity *p*.

The design is optimised at a wavelength of 692 nm to operate in the visible spectrum. The value of the sensitivity and the FOM has been calculated and plotted in figure 4.5 (c). It can be clearly shown from the figure 4.5 (c) that both the sensitivity and FOM increase with increase in periodicity *p*. The shifting of the resonance wavelength with the variation of a period can be explained by using LC model. When the period decreases, the gap between adjacent unit cells

decreases and then the electric field enhancement capacitance between adjacent unit cells increases. So, the resonance wavelength shifts towards a higher value [6, 19, 33, 34].

4.3.3 Effect of gap *g*

Keeping *a* and *h* constant at 140 nm and 30 nm respectively and the periodicity *p* of the structure at 650 nm, the gap *g* between the opposite two pillars has been varied from 20 to 60 nm in the step of 10 nm. The absorbance and FWHM has been calculated and plotted in figure 4.6 (a). It is seen from the figure that there is maximum absorption at the gap of 30 nm while there is no effect of gap *g* on the FWHM.

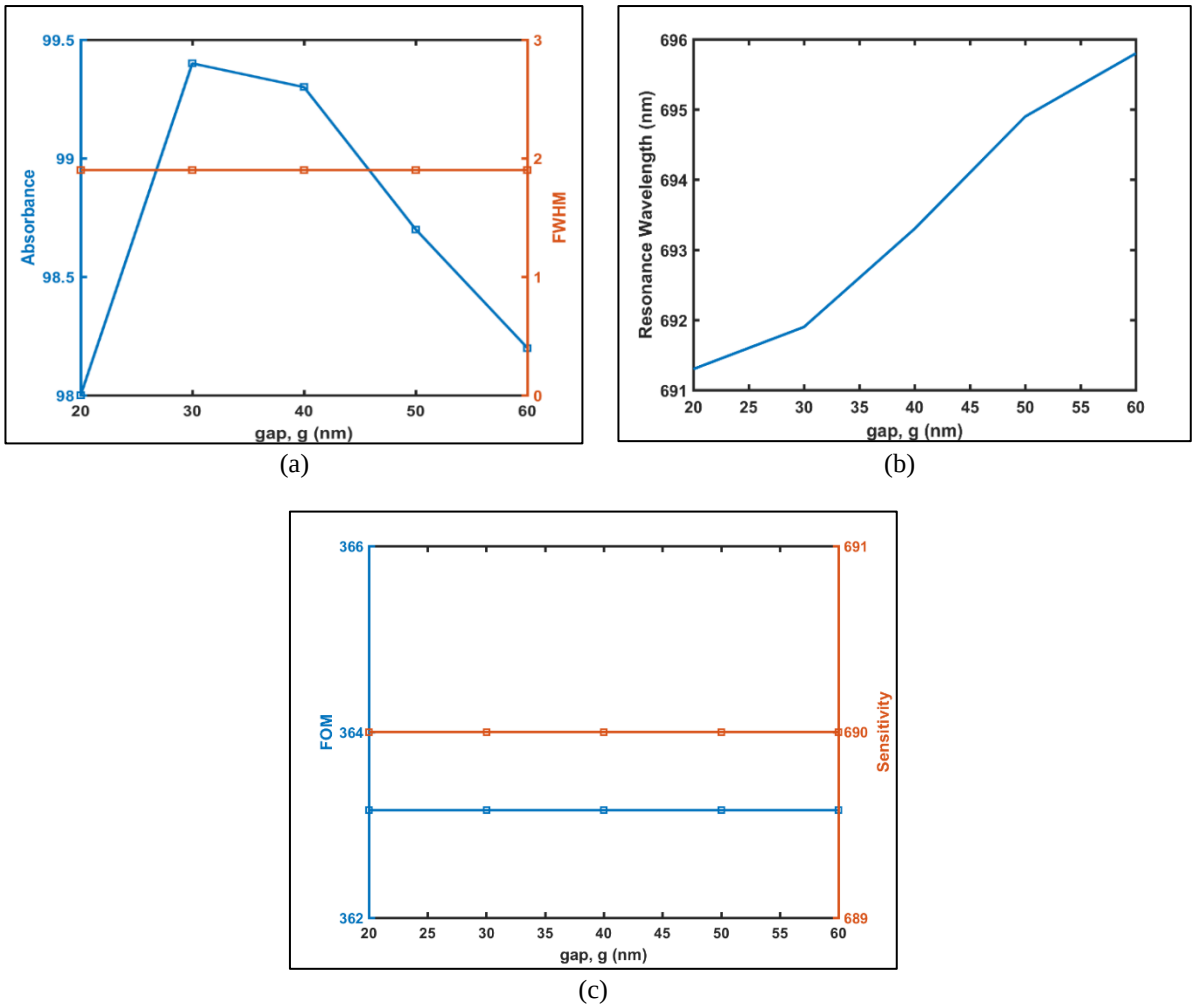

(a) (b)

(c)

Figure 4.6 Variation of (a) Absorption coefficient and FWHM (b) Resonance wavelength and (c) FOM and sensitivity with the variation of gap, *g* between opposite pillars.

There is slight shift in the resonance wavelength with the gap *g* as observed from figure 4.6 (b). The variation of the sensitivity and FOM with gap *g* is shown in figure 4.6 (c). It can be

stated that there is no effect on sensitivity of the structure with the gap between the opposite pillars. Therefore, FOM remains unaltered with the gap g as both the sensitivity and FWHM remain constant with the gap g.

4.4 Mechanism

To better understand the mechanism of absorption, electric and magnetic field spatial distribution plots have been drawn. Here geometrical parameters are set as a = 140 nm, h = 30 nm, g = 30 nm and p =650 nm. The plane polarized light of wavelength 692 nm is allowed to fall on the absorber from the top. The corresponding electric field and magnetic field distribution has been drawn in the xy and xz plane respectively and shown in figure 4.7 (a, b).

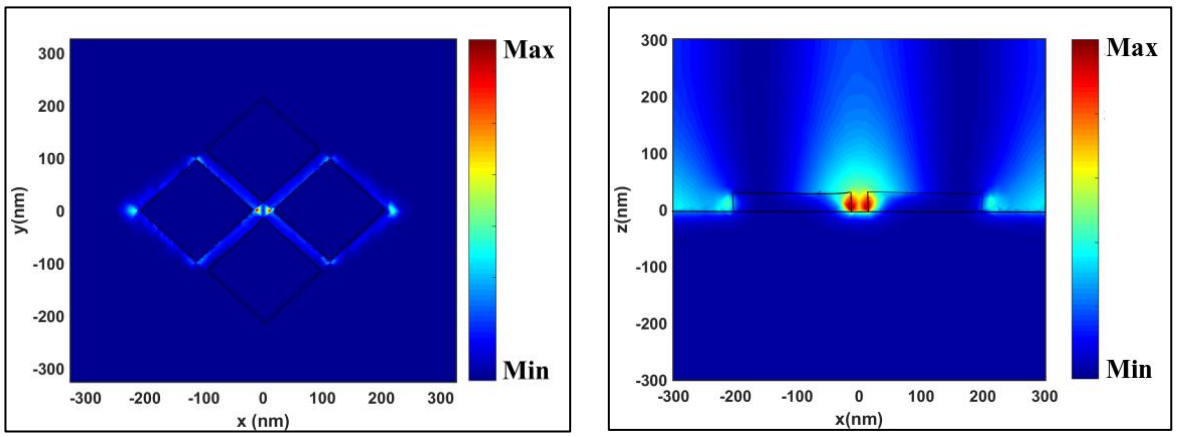

(a) (b)

Figure 4.7 (a) Distribution of electric field intensity along x-y plane (b) distribution of magnetic field intensity along xz plane.

It has been observed from the figure that the structure is not only a perfect absorber but also enhances the electric field intensity which is desirable in bio-sensors. The figure 4.7 (a) and (b) show that electric and magnetic fields are concentrated at the central gap. The electric field is observed due to the formation of localised surface plasmons. Localised surface plasmons tend to accumulate at the tip or the edges, that's why they are concentrated at the upper part more than the base of the cuboids. Electric field enhancement is more at the gap rather than the other edges. Two opposite silver pillars and the connecting silver base together act as a split ring resonator. The charges accumulated at the edges flow through the conducting base, exhibiting

a current carrying loop type configuration, which results in the induction of the magnetic field in the central gap. Therefore, the magnetic field is mainly concentrated at the center of the vertical gap. Figure 4.7(a) shows the electric field intensity distribution profile from the top view and figure 4.7 (b) shows the magnetic field intensity distribution from the side view. Both electric, as well as magnetic fields, are concentrated at the same hot spot.

Figure 4.8 shows the electric field and magnetic field enhancement for the same configuration as mentioned above at the center of the four pillars at height of 30 nm from the silver layer. Both the curves exhibit narrow resonance peak.

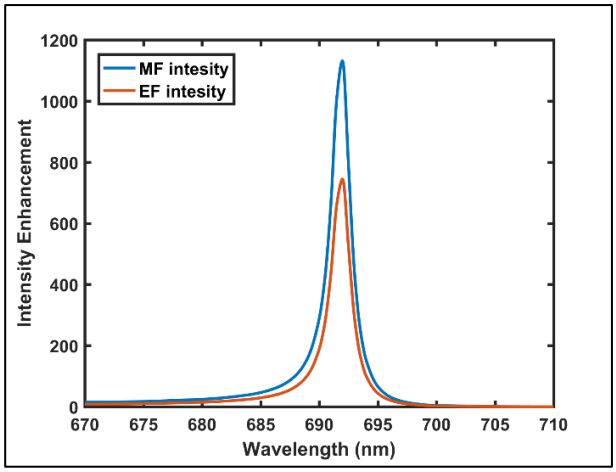

Figure 4.8 Electric and magnetic field intensity enhancement at the central gap at a height of 30 nm above the silver film.

4.5 Plasmonic sensing capability

As discussed, the resonance wavelength of plasmonic structures depends upon shape, size, geometry, constituting material as well as the surrounding medium. This property of changing resonance wavelength with refractive index can be used in sensing applications. The sensors are characterised by their sensitivity and FOM. Sensitivity, S for refractive index sensor is defined by the ratio of the spectral shift with the change of refractive index of the surrounding medium, and FOM is the ratio of sensitivity to the FWHM [18-20].

$$S = \frac{\Delta\lambda}{\Delta n} \qquad FOM = \frac{S}{FWHM}$$

Moreover, the change of intensity is also considered for sensing as the refractive index of the surrounding environment changes. S* is defined by the maximum change of intensity of reflected light with a unit change in refractive index. I is the absolute intensity of reflected light at resonance wavelength. FOM* is defined by the maximum S*/ I ratio.

$$S^* = \frac{\Delta I}{\Delta n} \qquad FOM^* = \left[\frac{S^*}{I}\right]_{max}$$

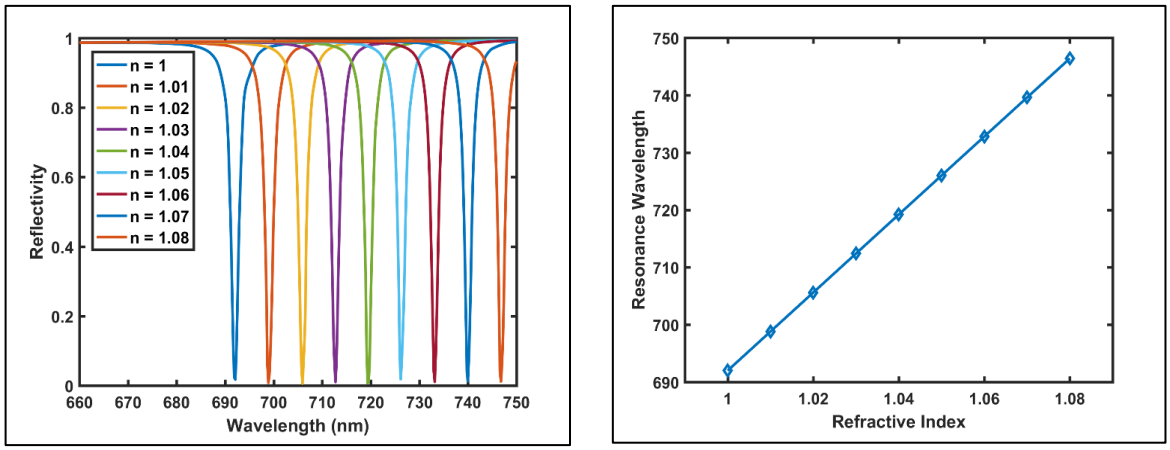

(a) (b)

Figure 4.9 (a) Reflection spectrum of the proposed all metallic absorber with the variation of wavelength for different values of refractive index varying from 1 to 1.08 (b) Shift in resonance wavelength with variation of refractive index.

Air like reflective index sensors with values ranging from 1 to 1.08 are most commonly used in gas sensors [6]. The optimized design has been investigated for air-like refractive index sensor for different values of refractive index. The refractive index of the surroundings has varied from 1 to 1.08 and corresponding absorption spectra were recorded. The reflection spectrum for different values of refractive index varying from 1 to 1.08 has been shown in figure 4.9 (a). The variation in resonance wavelength with the variation of the refractive index of the surrounding medium has been shown in figure 4.9 (b). There is a redshift in the resonance wavelength with an increase in the refractive index of the surrounding. The sensitivity and FOM comes out to be 680 nm/RIU and 348.72/RIU. The value of S* and FOM* as calculated at 692 nm wavelength comes out to be 99.68 and 17,580.

4.6 Conclusion

Ultra narrow-band perfect absorber structure has been designed and optimised. Further, this ultra-narrowband absorber has been studied in refractive index sensing applications. The structure offers 99.45% absorption and has a very narrow peak at resonance wavelength. The mechanism of absorption has been revealed via observing electric and magnetic field distribution. The structure offers a high-quality factor of 354.87 with a sensitivity of 680 nm/RIU and high figure of merit of 348.72/RIU. With these parameters the proposed structure can be used as refractive index sensor, photodetector and optical filter.

References

[1] Chou Chao, C. T., Chou Chau, Y. F., & Chiang, H. P. (2021). Biosensing on a plasmonic dual-band perfect absorber using intersection nanostructure. *ACS omega*, *7*(1), 1139-1149.

[2] Shrivastav, A. M., Cvelbar, U., & Abdulhalim, I. (2021). A comprehensive review on plasmonic-based biosensors used in viral diagnostics. *Communications biology*, *4*(1), 70.

[3] Baitha, M. N., & Kim, K. (2022). Polarization Switchable Enhanced Photonic Spin Hall Effect for Optical Switch and Filters. *IEEE Photonics Technology Letters*, *34*(24), 1329-1332.

[4] Ji, C., Lee, K. T., Xu, T., Zhou, J., Park, H. J., & Guo, L. J. (2017). Engineering light at the nanoscale: structural color filters and broadband perfect absorbers. *Advanced Optical Materials*, *5*(20), 1700368.

[5] Dorodnyy, A., Salamin, Y., Ma, P., Plestina, J. V., Lassaline, N., Mikulik, D., ... & Leuthold, J. (2018). Plasmonic photodetectors. *IEEE Journal of Selected Topics in Quantum Electronics*, 24(6), 1-13.

[6] Pevec, S., & Donlagic, D. (2018). Miniature fiber-optic Fabry-Perot refractive index sensor for gas sensing with a resolution of $5x10^{-9}$ RIU. *Optics express*, *26*(18), 23868-23882.

[7] Wang, Y., Sun, T., Paudel, T., Zhang, Y., Ren, Z., & Kempa, K. (2012). Metamaterial-plasmonic absorber structure for high efficiency amorphous silicon solar cells. *Nano letters*, *12*(1), 440-445.

[8] Fei Guo, C., Sun, T., Cao, F., Liu, Q., & Ren, Z. (2014). Metallic nanostructures for light trapping in energy-harvesting devices. *Light: Science & Applications*, *3*(4), e161-e161.

[9] Li, Y., Su, L., Shou, C., Yu, C., Deng, J., & Fang, Y. (2013). Surface-enhanced molecular spectroscopy (SEMS) based on perfect-absorber metamaterials in the mid-infrared. *Scientific reports*, *3*(1), 1-8.

[10] Jamali, A. A., & Witzigmann, B. (2014). Plasmonic perfect absorbers for biosensing applications. *Plasmonics*, *9*(6), 1265-1270.

[11] Zhou, W., Li, K., Song, C., Hao, P., Chi, M., Yu, M., & Wu, Y. (2015). Polarization-independent and omnidirectional nearly perfect absorber with ultra-thin 2D subwavelength metal grating in the visible region. *Optics express*, *23*(11), A413-A418.

[12] Liu, X., Tyler, T., Starr, T., Starr, A. F., Jokerst, N. M., & Padilla, W. J. (2011). Taming the blackbody with infrared metamaterials as selective thermal emitters. *Physical review letters*, *107*(4), 045901.

[13] Lee, K. T., Seo, S., & Guo, L. J. (2015). High-Color-Purity Subtractive Color Filters with a Wide Viewing Angle Based on Plasmonic Perfect Absorbers. *Advanced Optical Materials*, *3*(3), 347-352.

[14] Landy, N. I., Sajuyigbe, S., Mock, J. J., Smith, D. R., & Padilla, W. J. (2008). Perfect metamaterial absorber. *Physical review letters*, *100*(20), 207402.

[15] Li, Q., Li, Z., Xiang, X., Wang, T., Yang, H., Wang, X., ... & Gao, J. (2019). Tunable perfect narrow-band absorber based on a metal-dielectric-metal structure. *Coatings*, *9*(6), 393.

[16] Becker, J., Trügler, A., Jakab, A., Hohenester, U., & Sönnichsen, C. (2010). The optimal aspect ratio of gold nanorods for plasmonic bio-sensing. *Plasmonics*, *5*(2), 161-167.

[17] Huang, C., Ye, J., Wang, S., Stakenborg, T., & Lagae, L. (2012). Gold nanoring as a sensitive plasmonic biosensor for on-chip DNA detection. *Applied Physics Letters*, *100*(17), 173114.

[18] Agrawal, A. K., Ninawe, A., & Dhawan, A. (2021). Enhanced SPR-based localized and bulk sensing using a plasmonic nanopillar array with spacer. *IEEE Sensors Journal*, *22*(7), 6491-6508.

[19] Agrawal, A. K., Suchitta, A., & Dhawan, A. (2022). Nanostructured plasmonic chips employing nanopillar and nanoring hole arrays for enhanced sensitivity of SPR-based biosensing. *RSC advances*, *12*(2), 929-938.

[20] Agrawal, A. K., Ninawe, A., & Dhawan, A. (2021). Non-uniform narrow groove plasmonic nano-gratings for SPR sensing and imaging. *IEEE Access*, *9*, 10136-10152.

[21] Yong, Z., Zhang, S., Gong, C., & He, S. (2016). Narrow band perfect absorber for maximum localized magnetic and electric field enhancement and sensing applications. *Scientific reports*, *6*(1), 1-7.

[22] Liu, N., Mesch, M., Weiss, T., Hentschel, M., & Giessen, H. (2010). Infrared perfect absorber and its application as plasmonic sensor. *Nano letters*, *10*(7), 2342-2348.

[23] Wu, D., Liu, Y., Li, R., Chen, L., Ma, R., Liu, C., & Ye, H. (2016). Infrared perfect ultra-narrow band absorber as plasmonic sensor. *Nanoscale research letters*, *11*(1), 1-9.

[24] Luo, S., Zhao, J., Zuo, D., & Wang, X. (2016). Perfect narrow band absorber for sensing applications. *Optics express*, *24*(9), 9288-9294.

[25] Agarwal, P., Kishor, K., & Sinha, R. K. (2022). Ultrasensitive dual-band terahertz metasurface sensor based on all InSb resonator. *Optics Communications*, *522*, 128667.

[26] Cho, S. Y., Briscoe, J. L., Hansen, I. A., Smith, J. K., Chang, Y., & Brener, I. (2013). Label-free plasmonic immunosensing for plasmodium in a whole blood lysate. *IEEE Sensors Journal*, *14*(5), 1399-1404.

[27] Kazuma, E., & Tatsuma, T. (2014). Localized surface plasmon resonance sensors based on wavelength-tunable spectral dips. *Nanoscale*, *6*(4), 2397-2405.

[28] Liu, G., Yu, M., Liu, Z., Pan, P., Liu, X., Huang, S., & Wang, Y. (2016). Multi-band high refractive index susceptibility of plasmonic structures with network-type metasurface. *Plasmonics*, *11*(2), 677-682.

[29] Wu, D., Li, R., Liu, Y., Yu, Z., Yu, L., Chen, L., ... & Ye, H. (2017). Ultra-narrow band perfect absorber and its application as plasmonic sensor in the visible region. *Nanoscale research letters*, *12*(1), 1-11.

[30] Pan, M., Su, Z., Yu, Z., Wu, P., Jile, H., Yi, Z., & Chen, Z. (2020). A narrowband perfect absorber with high Q-factor and its application in sensing in the visible region. *Results in Physics*, *19*, 103415.

[31] Krasnok, A. E., Maksymov, I. S., Denisyuk, A. I., Belov, P. A., Miroshnichenko, A. E., Simovski, C. R., & Kivshar, Y. S. (2013). Optical nanoantennas. *Physics-Uspekhi*, *56(6)*, 539.

[32] Johnson, P. B., & Christy, R. W. (1972). Optical constants of the noble metals. *Physical review B*, *6*(12), 4370.

[33] Ma, Z., & Ding, F. (2012, November). Ultra-broadband metamaterial absorber in Terahertz regime. In *2012 Asia Communications and Photonics Conference (ACP)* (pp. 1-3). IEEE.

[34] Wang, B. X., Zhai, X., Wang, G. Z., Huang, W. Q., & Wang, L. L. (2015). A novel dual-band terahertz metamaterial absorber for a sensor application. *Journal of Applied Physics*, *117*(1), 014504.

CHAPTER-5

CHAPTER-5

OPTICAL TRAPPING OF DIELECTRIC NANOPARTICLE USING SEMI-CONICAL SHAPED NANOANTENNAS *

5.1 Introduction

Light has energy and carries momentum [1]. When light is incident on material, it imparts momentum to it. This causes the material to experience some force. For bulk material this force is very less but for smaller particle this force cannot be neglected. With the help of this force smaller particles can be trapped and is known as optical trapping. The instrument which can trap and manipulate nanoparticles is known as optical tweezer.

In 2018, Arther Askin won the Nobel prize for his contribution in the field of optical trapping. In the first paper published by him in 1970, he showed the deflection of neutral atom by the central force induced by the radiation pressure [2]. In 1971, he demonstrated that micron size particle could levitate in both air and water by optical forces [3]. Latter a series of papers were published by him in this area. In 1986, he was finally able to trap nanoparticle using single beam gradient which is called as optical tweezer [4].

*****Part of the results reported in this chapter has been accepted in the conference proceedings: "Optical trapping of dielectric nanoparticle using semi-conical shaped nanoantennas" International Conference on Atomic, Molecular, Material, Nano and Optical Physics with Applications (ICAMNOP-2023) held at Delhi Technological University, Delhi on 20-22 Dec 2023, PP-105.

However, conventional optical tweezers have certain limitations. Firstly, size of the trapped particle is diffraction limited. Secondly, the high power lasers are required for trapping, which can damage the biological nanoparticles. Plasmonic optical tweezers overcome these limitations. In plasmonic optical tweezers, plasmons formed generate high electric field by using low power laser. Low power laser is required and there will be less damage to the particle. Also plasmonic nanoantenna confine electric field in subwavelength region that break the diffraction limit. The nanoparticles can be easily trapped using these types of tweezers. In recent years, many structures of plasmonic materials have been utilised for optical trapping of nanoparticles, these include photonic crystals [5], optical waveguides [6], nanoapertures [7] and nanoantennas [8-10]. Plasmonic nanoantennas in particular can be used to increase and restrict optical fields with a deep subwavelength range, resulting in improved optical forces and potential energy as well as strong light–matter interaction [11]. Further, plasmonic nanoantennas are also used because they are simple to integrate with other photonic waveguides for nanoscale optical information processing [12].

Apart from trapping nanoparticle, efforts are also being undertaken to trap particle with high trapping stiffness using low power laser, so that, smaller particle can easily be trapped without gettting damaged by the high power intensity of light. For designing optical tweezers, force on the particle from linear momentum transfer should be greater than 10 fN [7, 13]. Since the early demonstration of the optical trapping of 200 nm polystyrene beads in water using pair of gold nanopillars in 2008 [14], numerous theoretical and experimental works have been conducted with various nanoantenna geometries, including gap dipole antennas [8], bowtie antennas [9], pairs of nanocylinders with outer rings [13], V-shaped antennas [10], T-shaped antennas [15] and many more [16]. Numerous nanoparticles such as magnetic nanoparticles [17], proteins [18], λ-DNA [19], gold nanoparticles [20], and polystyrene and silica beads [21],

have been trapped using optical tweezers and their interactions with confined field have also been thoroughly examined.

In this chapter, semi conical nanoantenna has been proposed and optimised at wavelength of 1064 nm to trap the polystyrene nanoparticle using a low power laser. Further, the force has been calculated by integrating Maxwell stress tensor.

5.2 Working

There are two types of forces acting on particle by the light, with one being the scattering force and second is the lateral force. The scattering force is applied along the direction of light and the lateral force acts along the high intensity of light. When light falls on the particle, photons transfer momentum to the particle. In case of a dielectric particle, light is refracted both when it enters and exits the particle. This means the direction of emitted light is different from that of incident light. Now the particle moves in the opposite direction to conserve the momentum. Figure 5.1 explains the mechanism by ray diagram considering two cases. The first case is the one in which the intensity gradient increases and the second in which high intensity at the centre. The net momentum on the particle forces it to move towards the high intensity in the first case and in the second case net momentum forces the particle backwards towards the intensity of the light. When the intensity of light is isotropic only a scattering force is applied to the particle. To stabilise the particle, the lateral force should neutralise scattering force. This is the basic principle of the conventional optical tweezers.

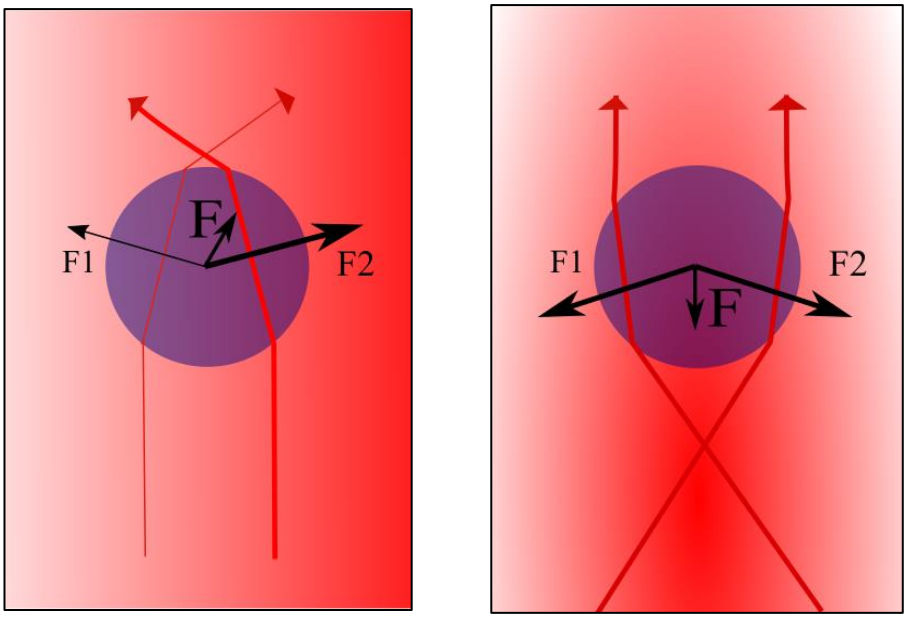

(a) (b)

Figure 5.1: (a) Intensity of light increases from left to right (b) radial intensity gradient of light with focus slightly below the nanoparticle. The larger intensity cause large momentum transfer which cause resultant force applied on particle in the direction of maximum intensity.

5.3 Formula used

Trapping force on the nanoparticle has been calculate by

$$F = \oint \langle T \rangle . \, dS \tag{5.1}$$

where, the integration is performed over a closed surface that encloses the particle and ⟨T⟩ is the time averaged Maxwell stress tensor given by

$$\langle T \rangle = \tfrac{1}{2} \, \mathrm{Re} \, [\varepsilon \, EE^* + \mu \, HH^* - 1/2(\varepsilon |E|^2 + \mu |H|^2) \tag{5.2}$$

where E is the electric field, H is the magnetic field

Trapping stiffness has been calculated by

$$K_i = \frac{dF_i}{dX_i} \tag{5.3}$$

where, F_i is the force in the direction X_i.

5.4 Design and modelling of semi conical shape nanoantenna

The structure consists of two cones (supposed to be cut into half through axis passing through the centre) facing each other through tips as shown in figure 5.2. The length *l* of each cone is taken to be 200 nm. Inner radius of taken to be 15 nm and the outer radius of the cone is taken to be 100 nm. The material of nanoantenna is taken as gold. The gap *g* between the opposite semi-cones is taken to be 30 nm. The nanoantenna is placed on the glass substrate and is surrounded by water from above. Polystrene nanoparticle that has to be trapped is suspended in the water, having diameter of 20 nm. The refractive index of polystyrene nanoparticle is taken to be 1.6. The refractive index of the glass is taken to be 1.5 and that of water is 1.33. The size of the nanoparticle is chosen because most of the biomolecules are having size in this range. The design is optimized at wavelength 1064 nm because biomolecules have negligible absorption at this range of wavelength. The value of permittivity of the gold at wavelength 1064 nm is −48.45−3.6i. The plane polarized light having electric field along the x direction is allowed to fall from the top of the nanoantenna. The surrounding environment of the nanoantenna is enclosed by a perfectly matched layer (PML). The intensity of the laser has been taken as 17 mW/μm^2 to minimize the damage of the biomolecules due to heating effect.

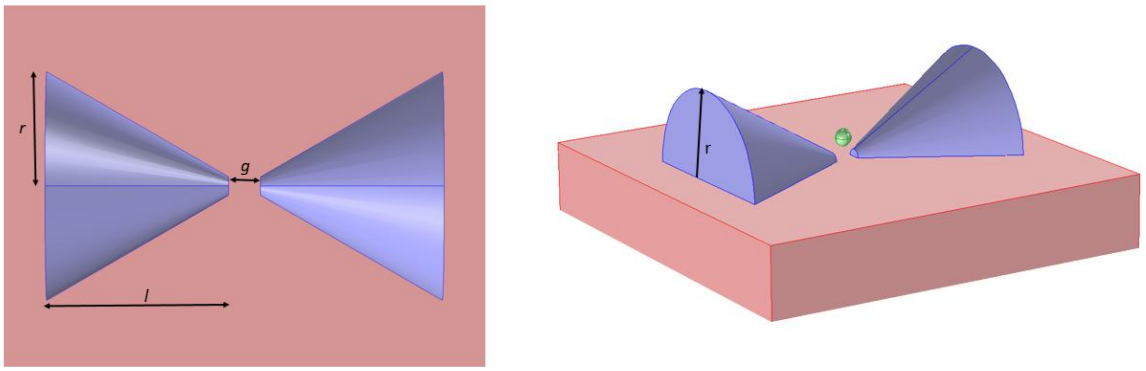

(a) (b)

Figure 5.2: Geometry of nanoantenna along with geometrical parameters (a) from the top view (b) 3D view, with semi conical shaped nanoantenna shown in blue colour; silica substrate shown in brown colour, nanoparticle of diameter 20 nm to be trapped shown in green colour.

5.5 Results and discussion

The electric field is accumulated between the gap regions of the nanoantenna and the field profile is shown in figure 5.3.

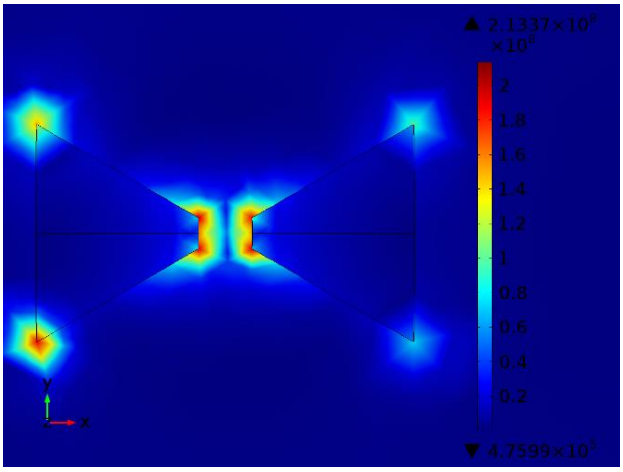

Figure 5.3 Electric field distribution profile of semi cone shaped nanoantenna at wavelength of 1064 nm.

The nanoparticle is allowed to move along the x, y and z direction. The force on the nanoparticle due to electric field is then calculated by using equation 5.1.

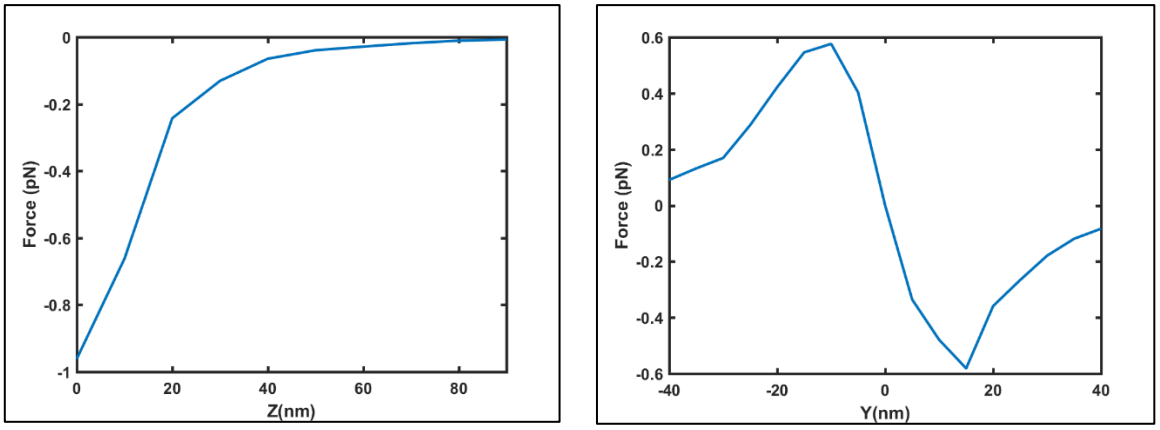

(a) (b)

Figure 5.4 (a) force exerted on bead along z-direction when particle is moved from the upper surface of the nanoantenna to the 90 nm above the centre of the nanoantenna, (b) force exerted on bead when along y-direction when moved along y-axis from -40 nm to 40 nm.

The particle is set at the centre of the nanoantenna and then allowed to move in the upward direction. The position of the particle is taken as the coordinates of the centre of the particle. As clear from the figure 5.4 (a), the maximum force exerted on the bead at the centre of the nanoantenna is 0.9 pN. The negative sign indicates that the force exerted in the –z direction i.e.

toward the nanoantenna. As the nanoparticle moves upward the force decreases and diminishes when move further from 80 nm.

Then the nanoparticle is allowed to move in the y direction from -40 nm to 40 nm, taking bottom of the nanoparticle touching the surface of glass substrate. It can be observed from the figure 5.4 (b) that the force is exerted in the +y direction when the particle is in the –y axis and vice versa. The force exerted on the nanoparticle is towards the centre of the nanoantenna where the nanoantenna with maximum force at the $\pm$ 15 nm i.e. at the edges of the nanoantenna, where electric filed is maximum. Force along y direction diminishes at the centre of the nanoantenna and beyond $\pm$ 40 nm.

The stiffness along the y and z direction were calculated for a particle positioned at the centre of the nanoantenna using equation 5.3. For a 20 nm particle, the trapping stiffness for the proposed semi conical shaped nanoantenna were found to be 21 $fNnm^{-1}W^{-1}$ and 19 $fNnm^{-1}W^{-1}$ in the y and z directions respectively. Thus, the dielectric nanoparticle was easily be trapped by the proposed nanoantenna.

5.6 Conclusion

In this chapter, nanoantenna design has been utilized for optical trapping application by means of generating high electric field. The design is optimized such that low power intensity of the laser is sufficient to generate high electric field at the hot spot. Forces on the nanoparticle along y-axis and z-axis have been calculated by integrating Maxwell stress tensor over the surface of nanoparticle. The trapping stiffness was found to be 21 $fNnm^{-1}W^{-1}$ and 19 $fNnm^{-1}W^{-1}$ in the y and z directions respectively. Thus, the proposed nanoantenna is able to trap a dielectric particle of size as small as 20 nm using a laser intensity 17 $mW/\mu m^2$.

References

[1] Ashkin, A. (1970). Acceleration and trapping of particles by radiation pressure. *Physical review letters*, *24*(4), 156.

[2] Ashkin, A. (1970). Atomic-beam deflection by resonance-radiation pressure. *Physical Review Letters*, *25*(19), 1321.

[3] Ashkin, A., & Dziedzic, J. M. (1971). Optical levitation by radiation pressure. *Applied Physics Letters*, *19*(8), 283-285.

[4] Ashkin, A., Dziedzic, J. M., Bjorkholm, J. E., & Chu, S. (1986). Observation of a single-beam gradient force optical trap for dielectric particles. *Optics letters*, *11*(5), 288-290.

[5] Serey, X., Mandal, S., & Erickson, D. (2010). Comparison of silicon photonic crystal resonator designs for optical trapping of nanomaterials. *Nanotechnology*, *21*(30), 305202.

[6] Yang, A. H., Moore, S. D., Schmidt, B. S., Klug, M., Lipson, M., & Erickson, D. (2009). Optical manipulation of nanoparticles and biomolecules in sub-wavelength slot waveguides. *Nature*, *457*(7225), 71-75.

[7] Xu, Z., Song, W., & Crozier, K. B. (2018). Direct particle tracking observation and Brownian dynamics simulations of a single nanoparticle optically trapped by a plasmonic nanoaperture. *Acs Photonics*, *5*(7), 2850-2859.

[8] Ploschner, M., Mazilu, M., Krauss, T. F., & Dholakia, K. (2010). Optical forces near a nanoantenna. *Journal of Nanophotonics*, *4*(1), 041570.

[9] Roxworthy, B. J., Ko, K. D., Kumar, A., Fung, K. H., Chow, E. K., Liu, G. L., ... & Toussaint Jr, K. C. (2012). Application of plasmonic bowtie nanoantenna arrays for optical trapping, stacking, and sorting. *Nano letters*, *12*(2), 796-801.

[10] Jin, R. C., Li, J. Q., Li, L., Dong, Z. G., & Liu, Y. (2019). Dual-mode subwavelength trapping by plasmonic tweezers based on V-type nanoantennas. *Optics Letters*, *44*(2), 319-322.

[11] Juan, M. L., Righini, M., & Quidant, R. (2011). Plasmon nano-optical tweezers. *Nature photonics*, *5*(6), 349-356.

[12] Li, Z., Kim, M. H., Wang, C., Han, Z., Shrestha, S., Overvig, A. C., ... & Yu, N. (2017). Controlling propagation and coupling of waveguide modes using phase-gradient metasurfaces. *Nature nanotechnology*, *12*(7), 675-683.

[13] Xu, Z., Song, W., & Crozier, K. B. (2018). Optical trapping of nanoparticles using all-silicon nanoantennas. *ACS Photonics*, *5*(12), 4993-5001.

[14] Grigorenko, A. N., Roberts, N. W., Dickinson, M. R., & Zhang, Y. J. N. P. (2008). Nanometric optical tweezers based on nanostructured substrates. *Nature Photonics*, *2*(6), 365-370.

[15] Li, R., Zhao, Y., Li, R., Liu, H., Ge, Y., & Xu, Z. (2021). Plasmonic optical trapping of nanoparticles using T-shaped copper nanoantennas. *Optics Express*, *29*(7), 9826-9835.

[16] Kotsifaki, D. G., & Chormaic, S. N. (2019). Plasmonic optical tweezers based on nanostructures: fundamentals, advances and prospects. *Nanophotonics*, *8*(7), 1227-1245.

[17] Xu, H., Jones, S., Choi, B. C., & Gordon, R. (2016). Characterization of individual magnetic nanoparticles in solution by double nanohole optical tweezers. *Nano Letters*, *16*(4), 2639-2643.

[18] Pang, Y., & Gordon, R. (2012). Optical trapping of a single protein. *Nano letters*, *12*(1), 402-406.

[19] Shoji, T., Saitoh, J., Kitamura, N., Nagasawa, F., Murakoshi, K., Yamauchi, H., ... & Tsuboi, Y. (2013). Permanent fixing or reversible trapping and release of DNA micropatterns on a gold nanostructure using continuous-wave or femtosecond-pulsed near-infrared laser light. *Journal of the American Chemical Society*, *135*(17), 6643-6648.

[20] Zhang, W., Huang, L., Santschi, C., & Martin, O. J. (2010). Trapping and sensing 10 nm metal nanoparticles using plasmonic dipole antennas. *Nano letters*, *10*(3), 1006-1011.

[21] Kang, J. H., Kim, K., Ee, H. S., Lee, Y. H., Yoon, T. Y., Seo, M. K., & Park, H. G. (2011). Low-power nano-optical vortex trapping via plasmonic diabolo nanoantennas. *Nature communications*, *2*(1), 582.

CHAPTER-6

CHAPTER-6

CONCLUDING REMARKS AND FUTURE RESEARCH SCOPE

This chapter includes concluding remarks about the work incorporated in this thesis and the future perspective of the present work of the thesis. In this thesis, various designs of nanoantennas have been proposed and their analysis has been done for different kinds of applications like electric field enhancement, magnetic field enhancement, solar energy harvesting, spectroscopy, sensing and.

In chapter 2, different types of nanoantennas have been designed whose aim is to enhance electric field at hot spot in near infrared frequency region. Nanoantennas have been studied for various properties such as electric field enhancement, radiation efficiency and harvesting efficiency. These nanoantennas can be tuned to various frequencies. The aim is to achieve resonance in wavelength range of 500 nm to 700 nm. At this frequency range of spectrum, solar radiation is maximum. Hence, nanoantennas can be utilised in solar energy harvesting. More than 70% radiation efficiency is observed for flower shaped nanoantennas, 80% for arrow nanoantennas and 90% for optimised design of petal shaped nanoantennas. Maximum of 74% of harvesting efficiency is obtained for optimised design of petal shaped nanoantennas which makes it suitable candidate for solar energy harvesting.

In chapter 3, nanoantennas resolve the shortcoming of obtaining magnetism at higher frequency by suggesting a mechanism as magnetism is not possible at near IR region by using commonly known ferromagnetic materials. Nanoantennas have been studied for the magnetic

field enhancement for various geometrical parameters and different materials. It has been observed that resonance frequency can be tuned with changing geometrical parameters. The hourglass shaped nanoantenna has been compared with existing designs of diabolo nanoantenna and has found to be a better candidate for magnetic field enhancement at higher frequencies. The hourglass shaped nanoantennas gives 1000 times enhancement at resonance wavelength of 2200 nm.

In chapter 4, Ultra narrow-band perfect absorber structure has been designed and optimised. The work utilises the fact that ohmic losses are inevitable in metals, which facilitates their utilisation in absorption of light. The structure offers 99.45% absorption and has a very narrow peak, less than 2 nm at resonance wavelength. The mechanism of absorption has been revealed via observing electric and magnetic field distribution. The structure offers a high-quality factor of 354.87. The structure shows a good sensing capability with a sensitivity of 680 nm/RIU and high figure of merit of 348.72/RIU. The proposed design holds great potential for sensing and near-field optics.

In chapter 5, semi-conical shaped nanoantenna for optical trapping has been proposed and optimised at 1064 nm. A dielectric nanoparticle was allowed to move in y and z direction keeping initial position at the centre of the gap between two arms of semi-conical shaped nanoantenna. The force on the particle has been calculated by integrating Maxwell stress tensor. Trapping stiffness was then calculated at equilibrium position. The structure offers high trapping stiffness i.e. 21 $fNnm^{-1}W^{-1}$ and 19 $fNnm^{-1}W^{-1}$ in the y and z directions respectively. Thus, the dielectric nanoparticle of size 20 nm proposed design was easily trappped using intensity of 17 mW/um^2.

In this thesis, different types of nanoantenna designs have been discussed for various applications. However, the designs and their practical applications are not limited to the existing work and can be further expanded as follows:

- Nanoantenna can be converted into rectenna by placing a diode in between two metallic arms of nanoantennas.
- The enhanced magnetic field can open doors to their potential application in magnetic sensors in the optical range, in surface-enhanced infrared absorption (SEIRA), magnetic imaging, enhanced spectroscopy applications and magnetic sensors in optical region.
- The narrowband perfect absorber can also be used in absorption filters and near-field optics.
- The nanoantennas can be used for study of bio cells such as DNA. It can utilized for trapping of the atoms other than nanoparticles.